The Geothermal Hydrology of Southern Grass Valley, Pershing County, Nevada

By F.H. Olmsted, Alan H. Welch, M.L. Sorey, and D.H. Schaefer

U.S. GEOLOGICAL SURVEY
Water Resources Investigations Report 96-4139

Menlo Park, California
1997

U.S. DEPARTMENT OF THE INTERIOR
BRUCE BABBITT, Secretary

U.S. GEOLOGICAL SURVEY
GORDON P. EATON, Director

For additional information
write to:

F.H. Olmsted
U.S. Geological Survey
345 Middlefield Rd., MS 439
Menlo Park, CA 94025

Copies of this report can be
purchased from:

U.S. Geological Survey
Branch of Information Services
Box 25286
Denver, Colorado 80225-0286

CONTENTS

FIGURES

TABLES

CONVERSION FACTORS, VERTICAL DATUM, AND ISOTOPE UNITS

Multiply	By	To Obtain
	Mass	
gram (g)	0.03527	ounce (oz)
kilogram (kg)	2.205	pounds (lb)
	Length	
millimeter (mm)	0.03937	inch (in.)
meter (m)	3.281	feet (ft)
kilometer (km)	0.6214	mile (mi)
	Area	
square meter (m^2)	10.76	square feet (ft^2)
hectare (ha)	2.471	acres
square kilometer (km^2)	0.3861	square mi (mi^2)
square kilometer (km^2)	247.1	acres
	Volume	
cubic centimeter (cm^3)	0.06102	cubic inch (in^3)
liter (L)	0.03531	cubic foot (ft^3)
liter (L)	0.2642	gallon (gal)
cubic meter (m^3)	8.107×10^{-4}	acre-foot (acre-ft)
cubic meter (m^3)	35.31	cubic feet (ft^3)
cubic kilometer (km^3)	0.2399	cubic mile (mi^3)
	Density	
gram per cubic centimeter (g/cm^3)	62.43	pound per cubic feet ($lb/ft^{3)}$
kilogram per liter (kg/L)	62.43	pound per cubic feet ($lb/ft^{3)}$

Multiply	By	To Obtain
	Fluid Flow	
liter per second (L/s)	15.85	gallon per minute (gal/min)
liter per second (L/s)	25.58	acre-foot per year (acre-ft/yr)
kilogram per second (kg/s)	7,938	pound per hour (lb/h)
cubic hectometer per year (hm^3/yr)	810.7	acre-foot per year (acre-ft/yr)
	Energy	
joule (J)	0.2390	calorie (cal)
joule (J)	9.480×10^{-4}	British thermal unit (Btu)
	Power	
watt (W)	1	joule per second (J/s)
watt (W)	0.2390	calorie per second (cal/s)
watt (W)	1.341×10^{-3}	horsepower (hp)
megawatt (mW)	1,341	horsepower (hp)
	Enthalpy	
joule per gram (J/g)	0.2390	calorie per gram (cal/g)
	Thermal conductivity	
W/m K	2.390	thermal conductivity units (tcu)
W/m K	2.390	mcal/cm.s.°C
	Heat flow	
milliwatt per square meter (mW/m^2)	2.390×10^{-2}	heat-flow unit (hfu)
milliwatt per square meter (mW/m^2)	2.390×10^{-2}	$\mu cal/cm^2.s$

Water-Quality Units

	Concentration	
microgram per liter (µg/L)	5.841×10^{-5}	grain per gallon
milligram per liter (mg/L)	5.841×10^{-2}	grain per gallon

Specific conductance

microsiemen per centimeter @ 25°C (µS/cm @ 25°C) =1 micromho per centimeter @ 25°C (µmho/cm @ 25°C)

1 millisiemen per meter @ 25°C (mS/m @ 25°C) =1 millimho per meter @ 25°C (mmho/m @ 25°C)

pH

$pH = -\log_{10}$ hydrogen-ion activity

Temperature

Degrees Celsius (°C) = 5/9 (degrees Fahrenheit - 32)

0°C = 273.15 Kelvin (K)

Temperature gradient

1°C/km = 5.486 x 10^{-2} °F/100 ft

Stable isotopes: Stable isotopes evaluated are oxygen-18, relative to oxygen-16 ($^{18}O/^{16}O$), and deuterium (hydrogen-2), relative to hydrogen-1 ($^{2}H/^{1}H$). Each ratio is determined for a sampled water and is then related mathematically to the comparable ratio for a standard of known isotopic composition. By convention, the computed results are expressed as "delta oxygen-18" ($\delta\ ^{18}O$) and "delta deuterium" (δ D), with the units of measure "per mil" (‰). A negative delta value indicates that the sampled water is isotopically lighter than the standard--that is, the sampled water has a smaller proportion of oxygen-18 or deuterium relative to oxygen-16 or hydrogen-1 than the standard.

Sea level: In this report, "sea level" refers to the National Geodetic Vertical Datum of 1929 (NGVD of 1929, formerly called "Sea-Level Datum of 1929), which is derived from a general adjustment of the first-order leveling networks of the United States and Canada.

The Geothermal Hydrology of Southern Grass Valley, Pershing County, Nevada

By F.H. Olmsted, Alan H. Welch, M.L. Sorey, and D.H. Schaefer

ABSTRACT

Leach Hot Springs, 45 kilometers south of Winnemucca, Nevada, is within southern Grass Valley, part of a Cenozoic structural basin containing fill locally more than 1,800 meters thick. The hot springs discharge 9 liters per second of water at near-boiling temperatures at the base of a scarp associated with a northeast-trending fault zone having a throw of more than 800 meters. The spring discharge probably constitutes less than one-fourth of the total discharge of water, both thermal and nonthermal, from southern Grass Valley. The springs represent the surface expression of a high-temperature hydrothermal system with characteristics similar to those of other hydrothermal systems in the northern Basin and Range province.

The Paleozoic and Mesozoic basement enclosing the fill in southern Grass Valley consists of slightly to moderately metamorphosed, intensively deformed sedimentary, volcanic, and plutonic rocks having low primary porosity and permeability. Basin and Range faults are associated with steeply dipping zones of low permeability within the fill that act as partial barriers to ground-water flow as well as conduits for rising thermal water, as at Leach Hot Springs.

Sodium and bicarbonate are dominant in thermal water at Leach Hot Springs and also in wells near the hot springs and in a test well 5 kilometers to the south-southwest, but nonthermal water has no dominant constituent. Chloride concentrations in nonthermal water are greater than in thermal water, but thermal water contains more of the minor constituents fluoride, lithium, and boron than nonthermal water.

The thermal aquifer or aquifers in the Leach Hot Springs hydrothermal system are at temperatures of 150-180°C or possibly higher on the basis of quartz, cation, and sulfate-water-isotope geothermometers. Stable-isotope data indicate that the thermal water was recharged when the climate was cooler and probably wetter than at present; such conditions existed during the period 10,000-40,000 years before the present. Radiocarbon data and modeling results also indicate an age greater than 10,000 years for the thermal water.

The southern Grass Valley area lies within the Battle Mountain heat-flow high, a region typified by heat flow greater than 120 milliwatts per square meter. Temperature measurements in more than 70 shallow wells define several areas of anomalously high near-surface conductive heat flow in southern Grass Valley associated with rising thermal water. However, only one deep well has been drilled into the system, 1.2 kilometers northwest of Leach Hot Springs. The well reached a maximum temperature of 125°C at a depth of 2,600 meters.

Numerical modeling of heat and fluid flow in simplified conceptual models has delineated important aspects of the Leach Hot Springs hydrothermal system and other similar systems in the northern Basin and Range Province, including relations between spring flow, depth and areal extent of fluid circulation, and the maximum temperature attained within the flow system. The absence of magmatic heat sources for such systems requires relatively deep fluid circulation and (or) laterally extensive reservoirs in order to capture sufficient heat to attain fluid temperatures near 180°C.

INTRODUCTION

Grass Valley, south of Winnemucca, Nevada, lies within a region of abnormally high conductive heat flow referred to by Sass and others (1971) as the "Battle Mountain high". The study area, which encompasses the southern half of Grass Valley and parts of the adjacent East, Sonoma, and Tobin Ranges (fig. 1), contains at least three and possibly five near-surface heat-flow anomalies associated with one or more hydrothermal systems[1]. The largest and most intense anomaly is centered at Leach Hot Springs, hereinafter abbreviated LHS, the only surface discharge of thermal water in the study area. Adjacent valleys also contain hot springs associated with active hydrothermal systems, and a fossil hydrothermal system is mined for mercury in the Goldbanks Hills at the south end of Grass Valley (fig. 1).

The hydrothermal system associated with LHS has been assumed to be similar to several other active systems in the northern Basin and Range province in terms of the size and temperature of the underlying fluid reservoir (see, for example, Brook and others, 1979, p. 52-53 and Hose and Taylor, 1974). In this study, the characteristics of the hydrothermal system or systems in southern Grass Valley (SGV) are interpreted from geologic, hydrologic, geochemical, and geophysical studies. These studies included the drilling of more than 100 test wells during the middle to late 1970s for measurements of heat flow and in some cases for collection of data on hydraulic head and water chemistry. Most of the wells were less than 170 m deep, but several penetrated consolidated bedrock beneath the valley-fill deposits. Unlike many other geothermal areas in the northern Basin and Range province, where deep drilling by private industry has provided data on reservoir conditions and has led to electric-power development in several cases, only one deep (2.6-km) hole has been drilled in southern Grass Valley.

Purposes of the Study

The purposes of the study are to summarize and interpret information gathered to date by the Geological Survey and others and to develop a conceptual model of the LHS hydrothermal system in SGV. Numerical simulations of heat and fluid flow in hypothetical geometric configurations of the system are used to estimate limiting cases of reservoir size and depth.

Some of the interpretations in an earlier report on this study (Welch and others, 1981) are now revised substantially. The revisions are

[1] As used in this report, the term "hydrothermal system" refers to a ground-water flow system that comprises a source of heat, circulating fluid (chiefly water but locally including steam in some systems), and sufficient permeability to allow the circulating fluid to descend to depths, then rise, to either discharge at the surface or flow laterally at shallow depths.

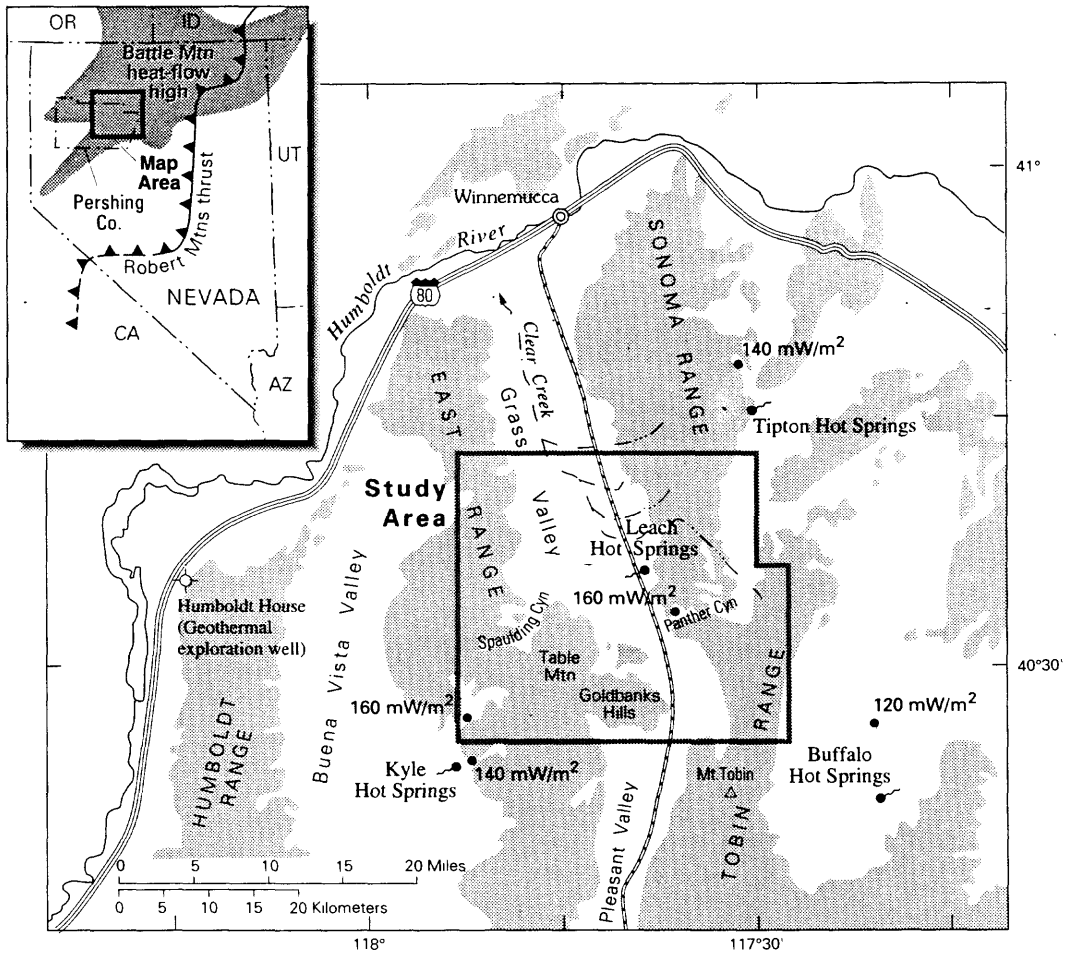

Figure 1. Location of southern Grass Valley study area. Inset map in upper left corner shows the location of the leading edge of the Roberts Mountain thrust, with sawteeth on upper plate, the extent of the Battle Mountain heat-flow high, and the outline of Pershing County. Values of conductive heat flow reported by Sass and others (1978) are shown for wells drilled in Grass Valley and adjacent areas.

based on (1) more recent data in releases by the University of Utah Research Institute (UURI, 1981a-h), (2) re-interpretation of gravity data from two sources, (3) new geochemical data, and (4) subsurface geologic and temperature data obtained from the deep test well drilled in 1980 by Aminoil 1.2 km northwest of LHS.

Previous Work

Leach Hot Springs were first mentioned by Clarence King in his report on the 40th parallel survey (King, 1878). Russell (1885) and Jones (1915) later examined the fault scarp at the springs. Dreyer (1940) described the springs briefly and listed a chemical analysis of the spring water and temperatures. Cohen (1964) briefly appraised the water resources of Grass Valley and estimated ground-water recharge on the basis of an empirical relation of recharge to altitude zones developed by Maxey and Eakin (1949). Waring (1965) included limited data from LHS in his list-

ing of thermal waters in the United States.

Studies designed to appraise the geothermal-resource potential of SGV and to test the applicability of various geophysical techniques for finding geothermal resources were done chiefly in the 1970s. Work by the Geological Survey began with a compilation of a source list of data for evaluation of the geothermal-resource potential of selected hydrothermal systems (including that at LHS) in the central and northern Basin and Range province (Olmsted and others, 1973). A reconnaissance study of some of these systems, again including that at LHS (Olmsted and others, 1975, p. 176-205), followed this compilation. The work included drilling eleven shallow ($\leq$50 m) test wells used, in part, to define the thermal anomaly surrounding the hot springs, geologic mapping of an 88-km^2 area including the anomaly, hydrochemical sampling, and related hydrogeologic studies.

Concurrently with the studies of Olmsted and others (1975), a geologic and a hydrochemical reconnaissance of hydrothermal systems in the central and northern Basin and Range province were conducted by Hose and Taylor (1974) and Mariner and others (1974), respectively. Hose and Taylor (1974) were among the first to suggest that hydrothermal systems like that at LHS result from convective rise of water along fault-controlled conduits in a region of high regional geothermal gradient, rather than from convection induced by local magmatic heat sources. Mariner and others (1974) analyzed water collected from one of the hotter orifices at LHS and applied chemical geothermometers to estimate thermal-aquifer or reservoir temperatures.

Partly on the basis of these studies, Renner and others (1975, p. 16-17), in the first assessment of the geothermal resources of the United States by the U.S. Geological Survey, estimated the subsurface extent, thickness, volume, temperature, and heat content of the presumed reservoir in the LHS hydrothermal system. Brook and others (1979, p. 52-53), in the second national geothermal-resources assessment, slightly modified the earlier estimates. Mariner and others (1983a) interpreted the low-temperature thermal water near LHS as leakage from the high temperature system.

The work by the Geological Survey in the early 1970s was later augmented by geophysical surveys by the Lawrence Berkeley Laboratory (Beyer and others, 1976a,b) and by test drilling and heat-flow determinations done jointly by the Geological Survey and Lawrence Berkeley Laboratory (Sass and others, 1977).

Beyer and others (1976) reviewed the methods employed and the results from the geophysical experiments and surveys. The purpose of these studies was to compare and evaluate geophysical techniques used in exploration and delineation of geothermal reservoirs. The various techniques employed and the types of information sought are summarized below.

Some of these techniques were particularly useful in delineating major faults and determining the configuration of the Cenozoic structural basin. For example, seismic-reflection profiling identified major faults, some of which extend into basement beneath the valley fill (Majer, 1978; Zoback and Anderson, 1983). Gravity surveys, supplemented by data from electrical-resistivity and seismic-refraction and -reflection experiments have been the primary basis for interpreting the configuration of the structural basin and the

Method: reference(s)	Information
Gravity: Erwin (1974): Goldstein and Paulsson (1977; 1978); UURI (1981b)	Thickness of fill; structure
Seismic refraction and reflection: Majer (1978); UURI (1981b); Zoback and Anderson (1983)	Thickness of fill; structure; stratigraphy
Seismic noise: Liaw (1977)	Movement of magma or thermal fluid
Microearthquakes and P-wave delay and attenuation: Majer (1978)	Presence of crustal magma or cemented zones in fill
Dipole-dipole resistivity: Dey and Morrison (1977)	Thickness of fill; stratigraphy; zones of low- and high-resistivity fill; thermal anomalies within fill
Telluric and direct-current resistivity: Beyer (1977)	Geologic structure; zones of high- or low-resistivity fill; thermal anomalies within fill
Self-potential (SP): Corwin (1976)	Vertical movement of thermal and nonthermal waters
Electromagnetic: Wilt and others (1980)	Thickness of fill; stratigraphy
Magnetotelluric: Gamble and others (1977; Morrison and others (1979)	Thickness of fill; stratigraphy
Aeromagnetic: U.S. Geol. Survey (1973); Zietz and others (1978)	Thickness of fill; structure; magnetic anomalies within basement

thickness of Cenozoic valley fill. Most earlier estimates of fill thickness have been shown to be too small on the basis of results from the deep Aminoil well. These results, which necessitated major revision of one of the early interpretations, are discussed further in the section, "Thickness of Valley Fill".

Heat-flow studies in SGV include those of Sass and others (1971; 1976; 1977), Olmsted and others (1975), and Welch and others (1981). Sass and others (1971, p. 6407-6411) described regional heat flow in the Basin and Range province and first identified the "Battle Mountain high," which includes SGV. Their interpretations were necessarily generalized and tentative because of sparse data, but the high regional heat flow has been confirmed by later measurements. Olmsted and others (1975, p. 205-206) estimated heat discharge from the area of the LHS thermal anomaly and obtained limited heat-flow data from shallow test wells drilled outside the anomaly. Welch and others (1981, p. 148) estimated regional heat flow on the basis of a heat budget for a polygonal area occupying part of SGV and estimated heat discharge from thermal anomalies at LHS, Panther Canyon, and two other places in SGV.

Geologic investigations related to geothermal resources in SGV include those of Olmsted and others (1975), Noble (written communication, 1975), Noble and others (1975), Beyer and others (1976a), UURI (1981c, g), Brogan and Birkhahn (1981), and Welch and others (1981). Wollenberg (1974) used the mass of spring deposits at LHS estimated from gravity data and spring-water

chemistry to calculate the age of the hydrothermal system.

Although there are several sources of hydrochemical data, comprehensive studies of the aqueous geochemistry of the area are lacking. Dreyer (1940), Waring (1965), and Sanders and Miles (1974) reported some analyses of LHS waters. Mariner and others (1974; 1975; 1983a) presented chemical, isotopic, and gas analyses for samples from the thermal springs. Bowman and others (1976), Wollenberg and others (1977), and UURI (1981a) reported major, minor, and trace-element analyses of the thermal and some nonthermal waters. Bliss (1983) compiled most of the published and some unpublished data. O'Connell and Kaufmann (1976), Wollenberg (1974), and Wollenberg and others (1977) studied the radioactivity at LHS and several other northern Nevada geothermal areas. Nehring and others (1979) and Nehring and Mariner (1979) discussed the sulfate-water isotope geothermometry of thermal water in the northern Basin and Range province. Welch and others (1981, p. 67-98) presented and interpreted additional hydrochemical data; these data are included in the present report.

Results of numerical simulation of the LHS hydrothermal system are reported by Welch and others (1981), Wheatcraft (1983), Pottorff (1988), and Lopez and others (1994). The work of Welch and others (1981) was modified only slightly during the present study and forms the basis for the section, "Models of Basin and Range hydrothermal systems." Wheatcraft (1983) examined a horizontal-flow conceptual model, using a two-dimensional numerical code developed by Faust and Mercer (1977). Pottorff (1988) and Lopez and others (1994) used three-dimensional models to simulate vertical and horizontal groundwater flow from the Sonoma Range to LHS. Their results are discussed in "Models of Basin and Range hydrothermal systems", and are also summarized by Sorey and Olmsted (1994).

Methodology

Test wells were drilled with hydraulic- (mud-) rotary equipment and were completed with steel casing, generally of 32-, 38-, or 51-mm (1-1/4-, 1-1/2-, and 2-in.) nominal inside diameter. Wells used for water-level measurements or collection of water samples for chemical analysis were fitted at the bottom with well points or screens. Other wells, used primarily for temperature measurements, were capped at the bottom and filled with water. A few wells, originally completed for temperature measurement, were later perforated for water-level measurement. In all wells, the annulus between the casing and the drill-hole walls was filled with either neat cement or drill cuttings and surface materials to minimize or prevent hydraulic interconnection between aquifers. Information about these wells is given in table A1 in the appendix.

Borehole geophysical logs were made in many wells to refine interpretation of the lithology and to define the physical characteristics of the materials penetrated. The logs included single-point resistivity, spontaneous-potential, caliper (hole-diameter), natural-gamma, gamma-gamma, neutron, and temperature. Final temperature measurements were made with thermistors lowered into the wells on cables. In addition to drill cuttings collected throughout the drilling process, core samples were taken at selected intervals, and several physical parameters were measured on these samples in the laboratory. The measure-

ments included density, porosity, and thermal conductivity.

Heat flow was calculated for zones penetrated by wells that exhibited linear temperature gradients by multiplying the gradient by the measured or assumed thermal conductivity. Meaningful results were obtained from relatively shallow wells completed in the study area because the generally low vertical permeability of the basin-filling sediments precluded significant convective heat transfer. A heat budget for the study area was computed from measurements and estimates of conductive, convective, advective, and radiative components. The average heat flow computed in this way can be compared with other estimates obtained from regional heat-flow studies.

Hydrochemical sampling of wells and springs included the analysis of selected unstable constituents and properties in the field (pH, temperature, specific conductivity, and alkalinity) and sample preservation. Before sampling, each well was pumped and (or) bailed several times during a period of several months. During pumping and bailing, the total discharge was recorded, and samples were collected for determination of specific conductance. These data were used to determine whether the water quality was reasonably constant after at least several well-bore volumes of water had been removed. Final sampling for laboratory analysis began only after the specific conductance remained virtually constant in several successive samples.

Field determinations of pH and alkalinity were made using the methods of Wood (1976, p. 12-18). The water was filtered through a 0.45-μm pore-size membrane filter (142-mm diameter), and samples collected for cation analysis were acidified. Unacidified filtered samples were collected for anion and isotopic analysis. Samples for silica analysis were diluted with distilled water to prevent polymerization where oversaturation with respect to quartz was suspected. Plastic bottles washed with acid were used for all samples collected for chemical analysis, and glass bottles with polyseal caps were used for samples collected for isotopic analysis.

Numerical simulations were performed of heat and fluid flow in simplified generic models that may represent limiting cases of hydrothermal systems associated with Basin and Range hot springs. Applications of modeling results to the LHS hydrothermal system, together with results obtained from other investigations, provide constraints on the depth and lateral extent of deep fluid circulation in SGV.

Acknowledgments

Sunoco Energy Development Co. greatly facilitated this study by permitting access to several wells. The writers benefited from discussions with John Sass, Robert Fournier, and Alfred Truesdell of the U.S. Geological Survey and Michael Wilt of the Lawrence Berkeley Laboratory. The manuscript was improved by reviews by S.E. Ingebritsen, D.R. Plouff, R.H. Mariner, and Colin Williams.

GEOLOGY

Physical Features

Grass Valley, like many valleys in the northern part of the Basin and Range province as de-

fined by Fenneman (1931), is bounded by north-trending mountain blocks and has ephemeral surface drainage. Altitudes in the SGV drainage basin range from 1,360 m above sea level on the valley floor at the northern boundary of the study area to 2,695 m at China Mountain. in the northern Tobin Range to the southeast (fig. 2).

Grass Valley is bounded on the east by the Sonoma Range, on the southeast by the Tobin Range, on the west by the East Range, on the southwest by Table Mountain and the Goldbanks Hills, on the north by the Humboldt River (20-25 km north of the study area), and is separated from Pleasant Valley to the south by an inconspicuous drainage divide.

Leach Hot Springs are on a fault that is part of a fault set having an aggregate throw of more than 800 m. Other significant features in SGV include Spaulding and Sheep Ranch Canyons (the probable sites of significant ground-water recharge), Panther Canyon (near the mouth of which is a prominent thermal anomaly associated with a possibly separate hydrothermal system), and a third thermal anomaly in the south-central part of the valley, about 6 km south-southwest of LHS.

Major Rock Groups

The rocks within the SGV drainage basin comprise two major groups: Paleozoic and Mesozoic basement, and Cenozoic valley fill. The basement underlies the valley fill and is exposed in the adjacent mountains. Most of the valley fill is within the valley, although the mountains contain small exposures of Cenozoic sedimentary and volcanic rocks.

Paleozoic and Mesozoic Basement

The Paleozoic and Mesozoic basement consists of slightly to moderately metamorphosed sedimentary, volcanic, and plutonic rocks. Most of these rocks are complexly folded and faulted. They are well consolidated and probably have low primary porosity and permeability. The several basement rock units shown in figure 2 are described briefly in table 1. The log of deep test well Aminoil USA 11-36 shows the character of the basement and the overlying valley fill northwest of LHS (table 2).

Cenozoic Valley Fill

The Cenozoic valley fill ranges from unconsolidated alluvium to consolidated volcanic rocks, chiefly basalt and rhyolite. Most of the fill is undeformed or slightly deformed, but it is tilted and faulted near Basin and Range faults.

The Cenozoic basalt and rhyolite resemble the Paleozoic and Mesozoic basement in most physical characteristics (table 1). Basalt and minor rhyolite about 12-15 Ma (million years before present) (Miocene) are exposed in the Table Mountain and Goldbanks Hills area (Noble, 1975). The small exposure of basalt 1.5 km southeast of LHS may be associated with this Miocene basalt, as indicated by isotopic age dating, lithology, and trace-element abundance (Noble, 1975). Noble (1975) believed the basalt to be a dike. However, poor exposures obscure the nature of the contact of the basalt and pre-alluvial sediments; we believe it is equally likely that the basalt is a flow rock faulted against Quaternary alluvium to the west. Rhyolite of probable Tertiary age crops out in a small area northeast of

TABLE 1. Physical and hydrologic properties of major geologic map units.

Erathem	Map unit	Rock types[1]	Degree of deformation and lithification	Hydrologic characteristics
CENOZOIC	Quaternary alluvium	Unconsolidated fluvial deposits ranging from clay to gravel; sorting poor to moderate; locally silicified	Relatively undisturbed except near zones of active faulting along valley margins; unconsolidated except where silicified by hydrothermal alteration	Permeability moderate to low, with a high ratio of horizontal to vertical permeability because of horizontal stratification; permeability moderate to high
	Quaternary-Tertiary alluvium	Coarse- to fine-grained deposits including tuff and volcaniclastic sediments		Similar to the overlying alluvium, but porosity and permeability are lower because of compaction and lithification. Minor vertical fractures may allow more vertical ground-water movement than in the Quaternary alluvium
	Tertiary sedimentary rocks	Semiconsolidated deposits ranging from ash and tuff to mudstone, sandstone, and siltstone	Locally these deposits have been faulted, tilted, and eroded after deposition	
	Tertiary volcanic rocks	Vesicular olivine basalt flows and shallow intrusive rhyolite		
MESOZOIC	Granodiorite	Granodiorite	Extensively folded and faulted during several periods of tectonism. Metamorphism of sedimentary and volcanic rocks ranges from low to high grade	Low primary porosity and permeability with secondary permeability related to fractures and solution cavities in the limestone and dolomite. Vertical fractures allow downward movement of ground water which may in part recharge the geothermal system. Extensional faulting may create zones of relatively high permeability
	Sedimentary and metasedimentary rocks	Limestone, dolomite, sandstone, and fine-grained clastic rocks		
	Koipato Group	Altered porphyritic andesite, rhyolite, and tuffaceous sedimentary rocks		
	Leucogranite	Fine- to medium-grained granite		
PALEOZOIC	Sedimentary and metamorphic rocks	Sandstone, conglomerate, chert, argillite, quartzite, limestone, greenstone, siltstone, and minor schist		

[1] From Johnson (1977).

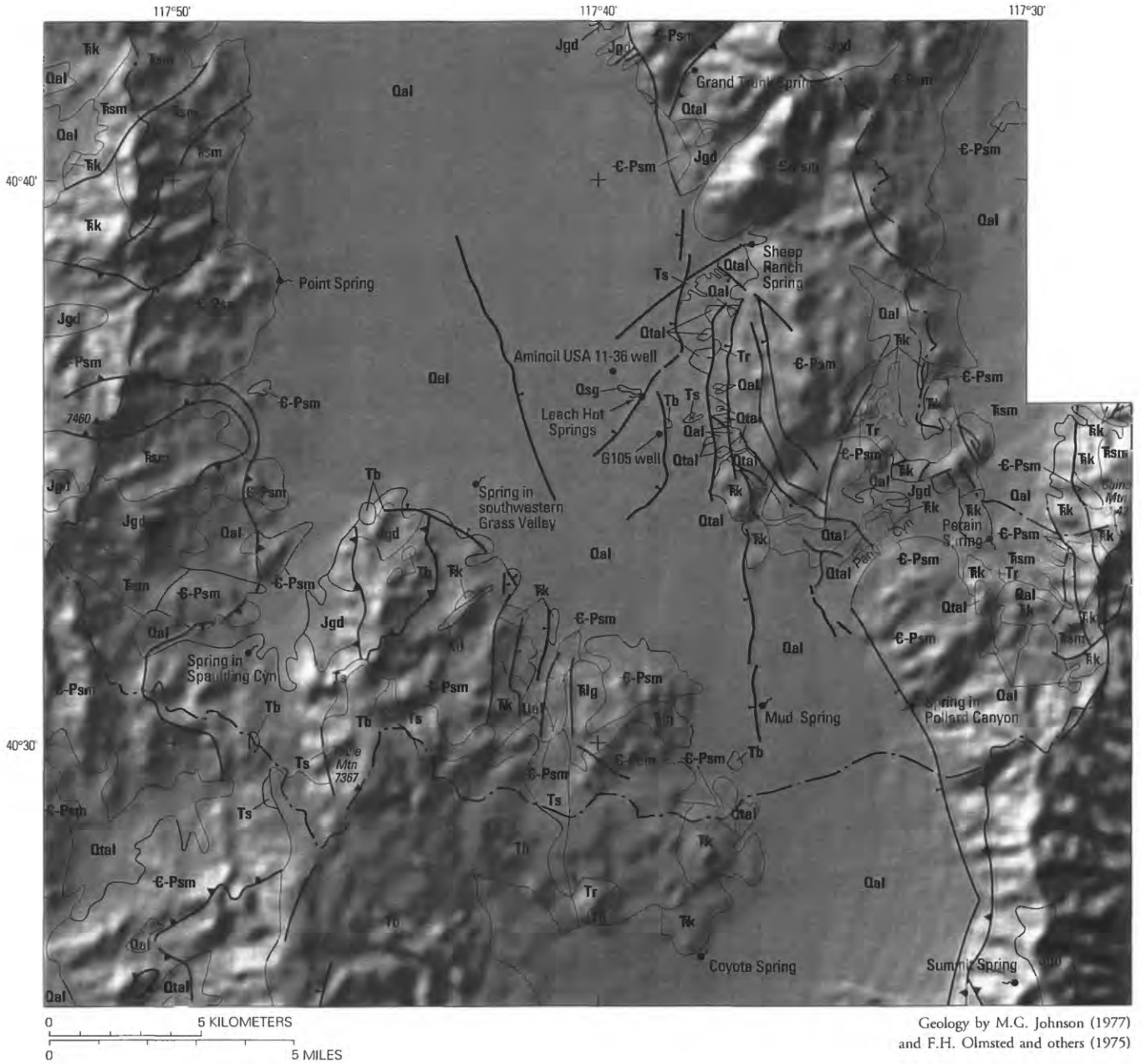

Figure 2. Generalized geologic map of southern Grass Valley area.

EXPLANATION

Contact

Normal fault—Dashed where uncertain. Bar and ball on downthrown side

Thrust fault—Dashed where uncertain. Sawteeth on upper plate

Drainage divide

Spring

CORRELATION OF MAP UNITS

Qal	Qsg	Pleistocene and Holocene	QUATERNARY
	Qtal	Pliocene and Pleistocene	
	Ts	Miocene and Pliocene	TERTIARY
	Tb/Tr	Oligocene and Miocene	
	Kd		CRETACEOUS(?)
	Jgd	Middle Jurassic	JURASSIC
	Trsm	Middle and Upper Triassic	TRIASSIC
	Trk	Lower Triassic	
	Trlg		
	€-Psm		CAMBRIAN TO PERMIAN

DESCRIPTION OF MAP UNITS

Qal ALLUVIUM – Unconsolidated fluvial deposits ranging from clay to gravel

Qsg SINTER GRAVEL – Opaline and chalcedonic sinter near Leach Hot Springs

Qtal QUATERNARY-TERTIARY ALLUVIUM – Coarse- to fine-grained deposits including tuff and volcaniclastic sediments

Ts SEDIMENTARY ROCKS – Semiconsolidated deposits ranging from ash and tuff to mudstone, sandstone, and siltstone

Tb/Tr VOLCANIC ROCKS – Vesicular olivine basalt (Tb) and shallow intrusive rhyolite (Tr)

Kd DIABASE DIKE – Fine-grained diabase

Jgd GRANODIORITE – Intrusive granodiorite

Trsm SEDIMENTARY AND METASEDIMENTARY ROCKS – Limestone, dolomite, sandstone, and fine-grained clastic rocks

Trk KOIPATO GROUP – Altered porphyritic andesite, rhyolite, and tuffaceous sedimentary rocks

Trlg LEUCOGRANITE – Fine- to medium-grained granite

€-Psm SEDIMENTARY AND METAMORPHIC ROCKS – Sandstone, conglomerate, chert, argillite, quartzite, limestone, greenstone, siltstone, and minor schist of Paleozoic age

TABLE 2. Generalized log of Aminoil USA 11-36 test well.

[Well is 500 ft S, 500 ft E of NW corner of section 36, T. 32 N., R. 38 E., Mt. Diablo baseline and meridian; altitude of land surface 1,393.9 m above sea level. Drilled May 15-July 2, 1980 by R.B. Montgomery Drilling Co.; logged by Walter R. Wilde of GeothermEx, Inc. Lithologic description summarized and stratigraphic interpretation modified by F.H. Olmsted.]

Material	Thickness (m)	Depth (m)
Quaternary alluvium:		
Heterogeneous deposits ranging from silt and clay to coarse sand and gravel; soft, poorly sorted, tan	427	427
Tertiary and Quaternary alluvium:		
Siltstone, mudstone, and claystone; some gravel and sand; soft to moderately indurated, green, brown, and pink	564	991
Tertiary sedimentary rocks:		
Similar to Tertiary and Quaternary alluvium but includes abundant tuff	464	1,455
Tertiary volcanic rocks:		
Chiefly altered lavas of mafic to intermediate composition; some silicic lavas	77	1,532
Silicic tuffs and tuffaceous sediments	93	1,625
Pre-Tertiary metamorphic and igneous rocks:		
Rhyolite, white, cryptocrystalline; upper 25-30 m stained with iron oxides or hydroxides. Interpreted by Wilde and Koenig (UURI, 1981g) to be part of Triassic Koipato Formation	118	1,743
Granite	40	1,783
Heterogeneous metavolcanic rocks; diabase dikes, pervasively altered	466	2,249
Altered granite; diabase dikes	241	2,490
Amphibolite	121	2,611

LHS; similar rock was penetrated at depths of 323-360 m at the bottom of well G105, about 0.5 km southwest of the basalt exposure described above (fig. 2).

Most of the overlying valley fill consists of, in ascending order: (1) Tertiary sedimentary rocks, which include tuff, especially in the lower part; (2) Tertiary and Quaternary alluvium, which ranges from silt and clay to coarse sand and gravel, and which is unconsolidated to slightly consolidated; and (3) Quaternary alluvium, presumably of late Pleistocene and Holocene age, which is less consolidated than the Tertiary and Quaternary alluvium (table 2). Subsurface bound-

aries of these units are ill-defined. The average density and degree of consolidation probably increase, and the porosity decreases, with depth.

Physical Properties of Rock Materials

Table 1 summarizes the physical and hydrologic properties of the rock units in southern Grass Valley, and table 3 summarizes the physical properties of the valley-fill deposits, as measured on core samples from test wells by the Geothermal Laboratory of the U.S. Geological Survey in Menlo Park, California, and the Hydrologic Laboratory of the Geological Survey in Lakewood, Colorado. All samples are from depths of less than 165 m and therefore represent only the uppermost part of the valley fill. However, several samples from wells near the margins of the valley represent older deposits, probably of Tertiary age. Properties measured in the laboratory included grain density, dry bulk density, and saturated bulk thermal conductivity. Saturated bulk density, porosity, and grain thermal conductivity (table 3) are calculated from other properties measured in the laboratory.

Porosity, ϕ, is calculated as

$$\phi = \frac{\rho_s - \rho_d}{\rho_s} \qquad (1)$$

where ρ_s = grain density and ρ_d = dry bulk density.

Saturated bulk density, ρ_a, is calculated as

$$\rho_a = \rho_s(1 - \phi) + \phi \qquad (2)$$

Grain thermal conductivity, K_s, is calculated as

$$K_s = \exp\frac{\ln K_a - \phi \ln K_f}{1 - \phi} \qquad (3)$$

where K_s = saturated bulk thermal conductivity and K_f = thermal conductivity of pore fluid (water = 0.60 W/m.K at 20°C).

Also measured for some samples were porosity and particle-size distribution. These measurements generally were made on different parts of the core sample from that used for the measurements of grain density, dry bulk density, and saturated bulk thermal conductivity. Because of the small-scale heterogeneity of the deposits, large differences in porosity were observed within the same core sample. In order to avoid discrepancies that would result from measurements on different parts of the core samples, saturated bulk density and grain thermal conductivity are based on calculated rather than measured porosities.

Because the fill is derived chiefly from Paleozoic and Mesozoic rocks adjacent to and underlying SGV, the values of grain density in table 3 indicate the probable range in density of these basement rocks. The lowest values, less than 2,500 kg/m^3, probably represent silicic volcanic and metavolcanic rocks; the highest values, nearly 2,800 kg/m^3, may represent mafic igneous or dolomitic rocks. The average, 2,670 kg/m^3, corresponds to the value commonly used for basement rocks in gravity computations, as discussed later.

Well-log data indicate that 57 percent of the near-surface valley fill is coarse-grained (chiefly sand and gravel), 38 percent is fine-grained (defined as having a median grain size of 0.06 mm or less and consisting chiefly of clay and silt), and 5 percent is tuff and tuffaceous sediments. On the basis of these percentages, the weighted-

TABLE 3. Summary of physical properties of core samples of shallow valley-fill deposits from southern Grass Valley.

[For each sample, saturated bulk density and porosity were calculated from grain density and dry bulk density; grain thermal conductivity was calculated from saturated bulk thermal conductivity and porosity. Fine-grained deposits are defined as having a median grain size of 0.06 mm or less, coarse-grained deposits as having a median grain size of more than 0.06 mm. Measurements were made by U.S. Geological Survey Geothermal Laboratory in Menlo Park, CA, and Hydrologic Laboratory in Lakewood, CO.]

Property	Range	Harmonic mean	Arithmetic mean	Standard deviation
Coarse-grained deposits (13 samples):				
Grain density (kg/m^3)	2,600-2,780	------	2,690	50
Saturated bulk density (kg/m^3)	1,920-2,330	------	2,180	80
Porosity (percent)	20.9-38.7	------	29.4	4.6
Grain thermal conductivity (W/m.K)	2.13-3.71	------	2.81	.50
Saturated bulk thermal conductivity (W/m.K)	1.40-2.18	1.75	------	------
Fine-grained deposits (23 samples):				
Grain density (kg/m^3)	2,530-2,760	------	2,670	60
Saturated bulk density (kg/m^3)	1,680-2,240	------	1,930	150
Porosity (percent)	26.8-58.0	------	44.2	7.8
Grain thermal conductivity (W/m.K)	1.81-4.18	------	2.61	.57
Saturated bulk thermal conductivity (W/m.K)	1.09-1.59	1.33	------	------
Tuff and tuffaceous sediments (5 samples):				
Grain density (kg/m^3)	2,420-2,660	------	2,490	100
Saturated bulk density (kg/m^3)	1,440-1,610	------	1,540	70
Porosity (percent)	57.4-69.7	------	63.4	5.2
Grain thermal conductivity (W/m.K)	1.43-3.42	------	2.51	.81
Saturated bulk thermal conductivity (W/m.K)	0.78-1.26	0.99	------	------
All deposits (assuming 57 percent are coarse-grained, 38 percent are fine grained, and 5 percent are tuff and tuffaceous sediments):				
Grain density (kg/m^3)	2,420-2,780	------	2,670	60
Saturated bulk density (kg/m^3)	1,440-2,330	------	2,050	110
Porosity (percent)	20.9-69.7	------	36.7	5.8
Grain thermal conductivity (W/m.K)	1.81-4.18	------	2.72	.54
Saturated bulk thermal conductivity (W/m.K)	0.78-2.18	1.51	------	------

average saturated bulk density of the fill sampled by the wells is 2,050 kg/m^3 (table 3).

As discussed in the section, "Thickness of valley fill," the average saturated bulk density of all the valley-fill deposits probably is significantly greater than the average of 2,050 kg/m^3 computed for the core samples. Correlation of gravity and deep-well data suggests that the average for all the fill may be about 2,350 kg/m^3. This greater density probably is reflected in some of the other properties as well: the average bulk thermal conductivity is also greater, and the average porosity is less, for all the fill than for the near-surface deposits represented by the core samples. The wide range of saturated bulk densities reflects the wide range in porosity of the sediments. The lowest densities, less than 1,500 kg/m^3, represent highly porous tuff of probable Tertiary age; the highest densities, more than 2,300 kg/m^3, represent partly indurated deposits of low porosity.

Calculated porosity of 41 core samples ranges from about 21 to nearly 70 percent (table 3). Sass and others (1977, p. 37), reported a bimodal distribution for a larger number of samples, with peaks between 20 and 30 percent representing coarse deposits and between 45 and 55 percent representing fine deposits. The weighted-average porosity of all the deposits sampled is about 37 percent (table 3). However, the average porosity of all the fill probably is substantially less: it may be only 19 percent on the basis of an average grain density of 2,670 kg/m^3 and an average saturated bulk density of 2,350 kg/m^3.

Like grain density, values of grain thermal conductivity of the valley fill are assumed to represent those of the source basement rocks. Except for silicic tuff of probable Tertiary age (in which grain thermal conductivities range as low as 1.43 W/m.K), shale has the lowest thermal conductivity, 1.81 W/m.K; quartzose or dolomitic rocks have the highest, 4.18 W/m.K. The arithmetic mean, 2.72 W/m.K (table 3), probably represents average basement adjacent to and underlying SGV.

Saturated bulk thermal conductivities of 41 core samples of valley fill range from 0.78 to 2.18 W/m.K (table 3). As with porosity, the values of bulk thermal conductivity have a bimodal distribution; the higher peak (harmonic mean, 1.75 W/m.K)[2] represents coarse-grained deposits, and the lower peak (harmonic mean, 1.33 represents fine-grained deposits. The harmonic mean for all the deposits sampled (assuming the proportions of coarse, fine, and tuffaceous deposits used earlier) is 1.51 W/m.K (table 3). However, on the basis of an average porosity of 19 percent and an average grain thermal conductivity of 2.72 W/m.K, the average saturated bulk thermal conductivity of all the fill is 2.04 W/m.K.

Structure

Pre-Cenozoic History

Pre-Cenozoic deformation in the region that includes southern Grass Valley occurred primarily during the Antler orogeny (Roberts, 1951), the Sonoma orogeny (Silberling and Roberts, 1962), and the Nevadan orogeny (Roberts, 1968). The Antler orogeny consisted of the eastward movement of thick sequences of siliceous and volcanic rocks over an assemblage of Paleozoic carbonate rocks. The eastward displacement of the upper

[2] The harmonic mean, rather than the arithmetic mean, is used because the valley-fill deposits are stratified horizontally, approximately normal to the direction of conductive heat flow.

plate (allochthon) amounted to about 140 km along the Roberts Mountains thrust (Roberts and others, 1958; Stewart and Poole, 1974; Smith and Ketner, 1977). The timing of the orogeny has been variously dated as Late Devonian and Early Mississippian or simply Early Mississippian (Speed and Sleep, 1982, p. 815-818). Near Grass Valley, the lower Paleozoic Harmony and Valmy Formations of the allochthon are complexly faulted and folded (Johnson, 1977), which probably has imparted significant secondary permeability to these rocks.

The lower plate (autochthon) of the Roberts Mountains thrust contains calcareous rocks of Cambrian through Devonian age which are exposed in windows and horsts across most of the width of the allochthon (Stewart, 1980, fig. 22). However, because the rocks beneath the thrust are not exposed locally, their nature is speculative. In the Goat and Horse Mountain windows about 65 km southeast of LHS, the autochthon consists of quartzite, limestone, and shale (Stewart and McKee, 1977, p. 53). Significant interbasin movement of ground water could occur through solution openings in the limestone if these exposures represent the composition of the autochthon in the Grass Valley area.

The Sonoma orogeny of Late Permian and Early Triassic age (Speed, 1971; Silberling, 1973) was comparable in scope to the preceding Antler orogeny and followed the deposition of the Havallah and Pumpernickel Formations (Silberling and Roberts, 1962). As in the Antler orogeny, deep-water sedimentary rocks were thrust eastward along the Golconda thrust over previously deformed lower Paleozoic rocks.

After the Sonoma orogeny, Triassic and Jurassic marine and nonmarine rocks were deposited unconformably on the older, deformed units. As summarized by Johnson (1977, p. 40), the Jurassic and Cretaceous Nevadan orogeny affected all the pre-Cenozoic rocks. This orogeny is manifested in the Grass Valley region by westward movement of the upper plate of several kilometers, northeasterly folds, and low-grade regional metamorphism. The orogeny culminated in the intrusion of granodiorite into metasedimentary rocks, resulting in contact metamorphism and minor local folding and faulting.

Cenozoic History

The earliest block faulting in the northern Basin and Range province may have begun as early as 40-35 Ma (late Eocene to early Oligocene) (Nolan, 1943, p. 183; Gilluly, 1963; Hamilton and Myers, 1966, p. 527; Eaton, 1982, p. 412). However, extensional tectonism and associated widespread volcanism in the region that includes SGV began in Miocene time, perhaps 20-15 Ma (Proffett, 1977, p. 258; Christiansen and McKee, 1978, p. 286; Davis, 1979, p. 43; Eaton, 1982, p. 412). The Tertiary volcanic rocks in the study area were deposited during this episode. The onset of extensional faulting may have been related to a change in plate-tectonic regime when the North American plate began to interact with the northwest-moving Pacific plate along the San Andreas fault system (Coney, 1978, p. 4546). The normal faulting responsible for the present configuration of basins and ranges in the north-central Great Basin probably was initiated still later (Louderback, 1924, p. 5-38; Nielsen, 1965, p. 1306; Gilbert and Reynolds, 1973, p. 2508; Stewart, 1983, p. 34), and it has locally continued to the present, as evidenced by sizable

offsets in 1915 along the Pleasant Valley fault south of the study area (Page, 1935).

Basin and Range Faults

Noble (1975) separated a complex set of faults that offset basin-filling sediments in SGV into an east-side system, a central-graben system, and a transverse system (fig. 3). The east-side system resulted from uplift of the southern Sonoma Range. Tertiary rocks exposed east of LHS were rotated to dips of as much as 30-50°E. LHS are in one of the prominent transverse fault zones near its intersection with one of the faults of the east-side system. A warm spring 650 m southwest of the hot springs is on the same transverse

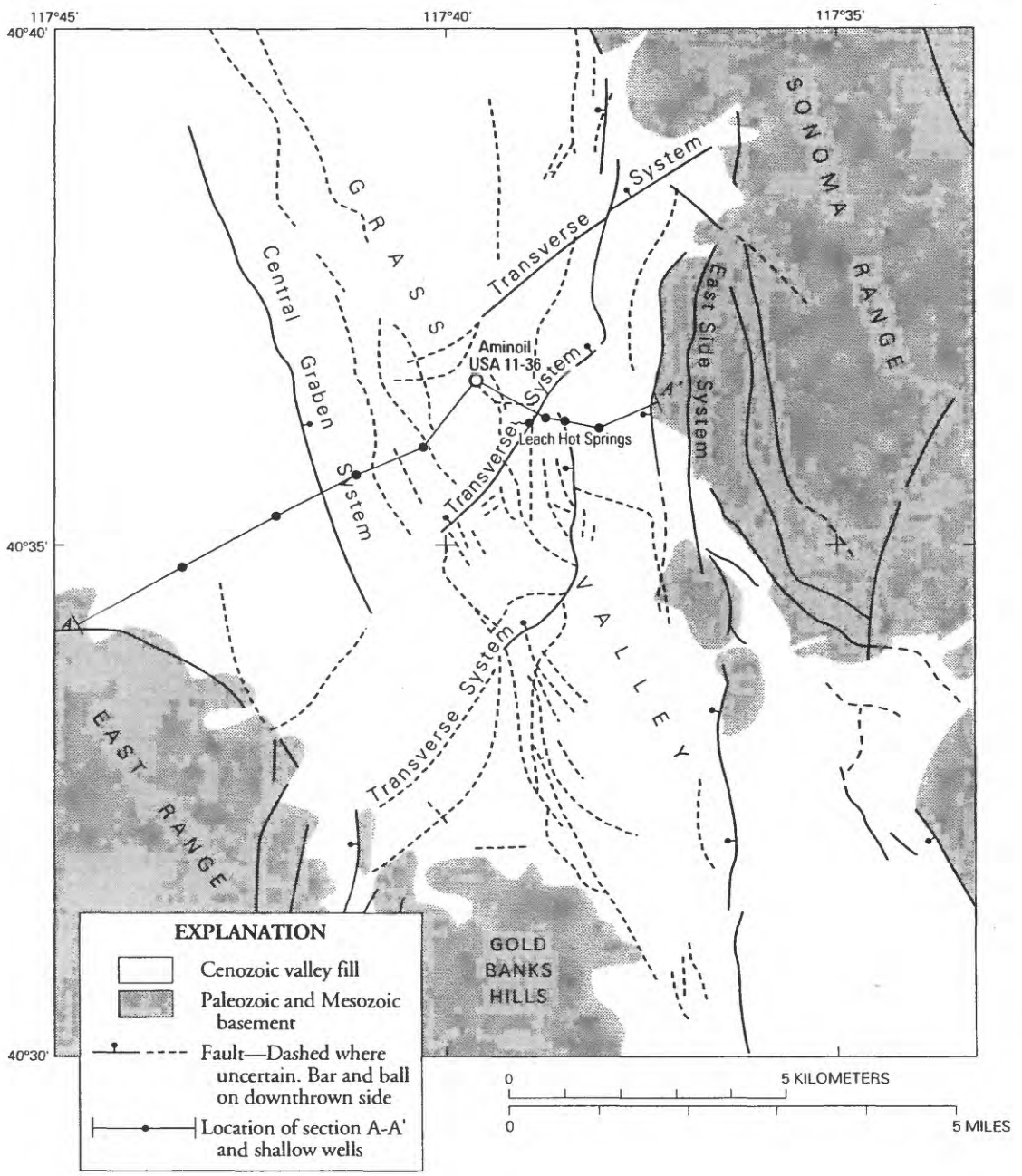

Figure 3. Sketch map of southern Grass Valley showing major Basin and Range faults.

fault. The southwestern part of the fault acts as a barrier to the northward movement of ground water (fig. 11).

The near-surface part of the LHS fault has a general northeasterly trend and therefore is part of the transverse system. However, gravity data, discussed later, suggests that the northeasterly trend characterizes only a relatively short segment of a west-dipping buried basement escarpment having a generally more northerly trend, as indicated by the direction of the closely spaced lines of equal Bouguer gravity anomaly (fig. 5). On the basis of both gravity and seismic reflection data, the fault zone appears to have a throw of more than 800 m, ½ km north of the hot springs (see figs. 4 and 6).

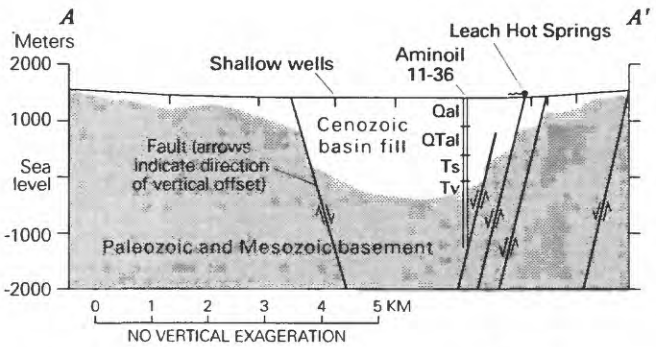

Figure 4. Section A-A' across southern Grass Valley.

The central-graben system may have resulted from localized crustal extension at depth (Noble, 1975). However, seismic-reflection data (UURI, 1981f) do not indicate significant offsets of reflecting horizons on this system. Instead, the seismic data indicate that the LHS fault zone separates the thick valley fill in the main part of the southern Grass Valley basin from relatively thin fill on the east side of the valley, and that an east-dipping fault of smaller displacement underlies the western part of the basin (Zoback and Anderson, 1983, p. 371). The dips of these faults are not well constrained by seismic and gravity data; an inferred dip of 74° N.W. shown in figure 4 for the LHS fault and other faults on the east side of the valley is based on the mean of dips ranging from vertical to 58° N.W. observed in a trench across the LHS fault 350 m northeast of the springs (Brogan and Birkhahn, 1981, fig. 50). An average dip of at least 60° is supported by an interpretation of Wilde and Koenig (UURI, 1981g, p. 13) that the Aminoil well did not intersect a major Cenozoic fault. (see fig. 4).

Brogan and Birkhahn (1981, p. 69-75) examined the surface morphology and geologic history of the LHS fault. On the basis of morphology indicated in three profiles normal to the fault trace, two of which were measured by Brogan and Birkhahn and the third by Wallace (1977), the fault appears to have undergone at least two, and possibly three, major periods of geologically recent movement near the hot springs. The maximum throw, measured immediately northeast of the hot springs, is about 10 m; about 1 km farther northeast, the throw decreases to less than 3 m (Brogan and Birkhahn, 1981, p. 72).

About 350 m northeast of the hot springs, a trench about 50 m long and 3-8 m deep, excavated approximately normal to the fault zone, revealed seven faults having a northeast strike and dips ranging from vertical to 58° N.W. (Brogan and Birkhahn, 1981, fig. 50). The fault farthest to the southeast, beneath the upper part of the fault scarp, is expressed as a buried steeply northwest-dipping contact between older and younger alluvium. The other six, younger, faults are clustered in a zone about 17 m wide near the northwest end of the trench, 25-42 m northwest of the first fault

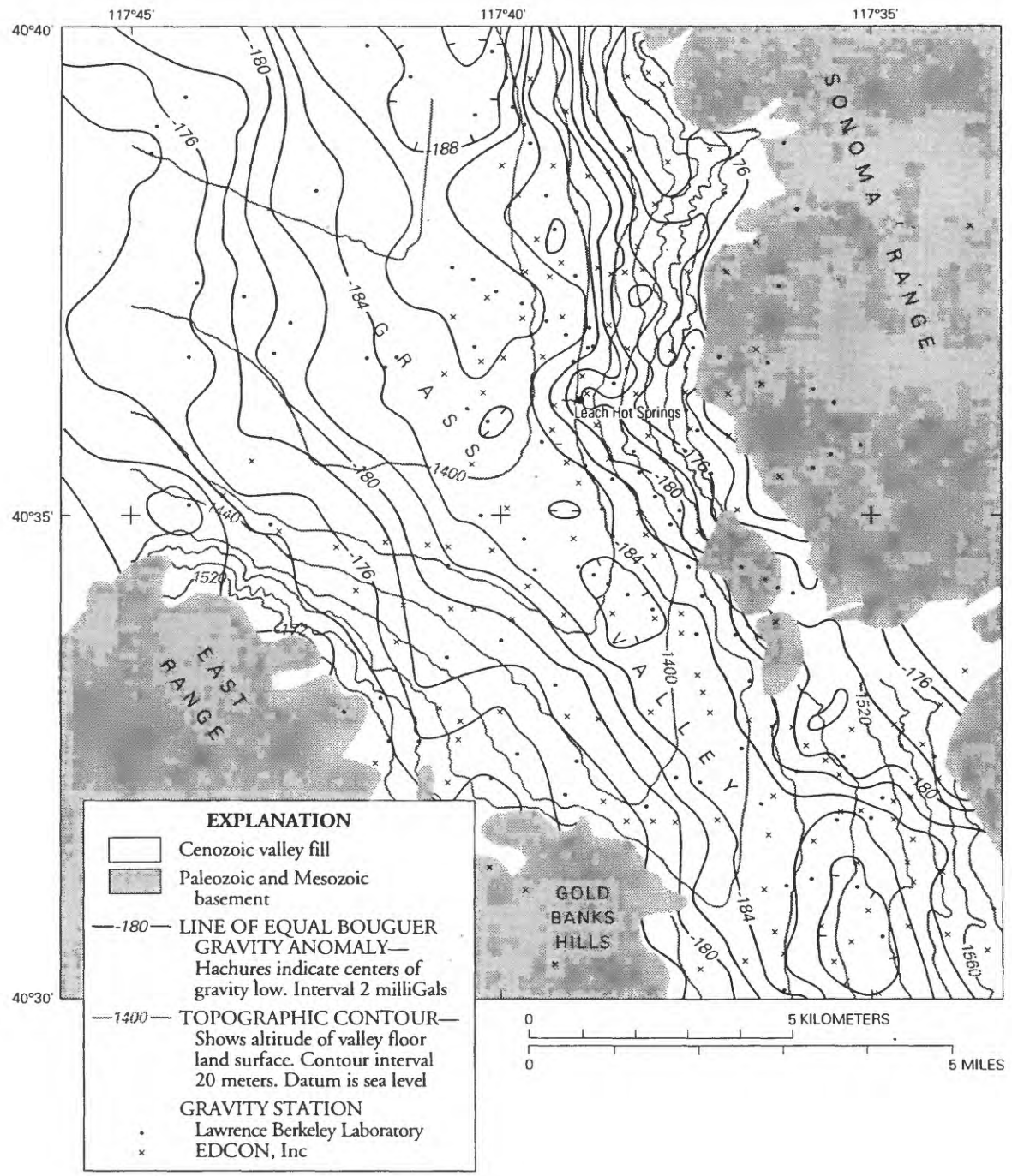

Figure 5. Complete Bouguer gravity anomaly map of southern Grass Valley.

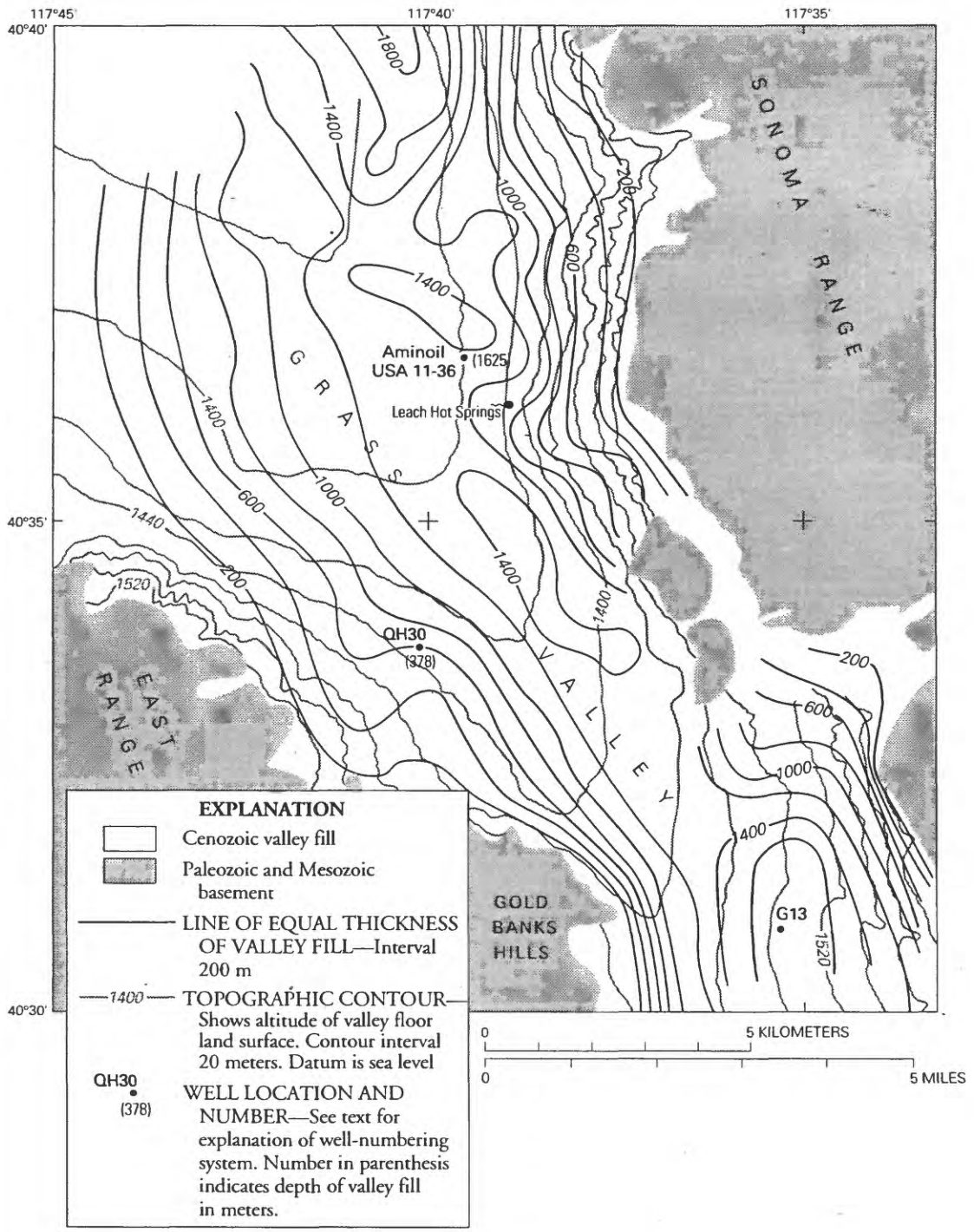

Figure 6. Thickness of fill in southern Grass Valley.

and 1-18 m northwest of the toe of the scarp. The entire fault zone is represented by a single line symbol on figures 2, 3, and 4 because of the difficulty of showing the individual fault traces at the scale of these illustrations.

In the Basin and Range province, faults associated with the discharge of thermal water have a smaller ratio of fault length to throw than faults not associated with hydrothermal discharge (Brogan and Birkhahn, 1981, p. 90-92). At LHS, the short length of the northeast-trending segment of the major basement-surface offset indicated by the gravity data described below may therefore be significant. The localization of discharge along relatively short active normal faults near sites of maximum throw appears to be characteristic of hydrothermal systems in the Basin and Range province. Also, the localization of discharge such as at Leach and other hot springs may be related to the intersection of major active Basin and Range faults.

Panther Canyon and vicinity (fig. 3), the site of a heat-flow anomaly separate from that associated with LHS, has many faults and fault intersections and is on a northeast-trending regional lineament (Beyer and others, 1976a). The fault associated with the magnitude 7.8 (Wallace, 1980) Pleasant Valley earthquake of 1915, which resulted in about 5 m of throw (Page, 1935), appears to terminate near Panther Canyon.

A major north-south fault apparently associated with the east-side fault system extends southward across SGV in the southeast part of the study area. Mud Spring lies along this fault, informally designated the Mud Springs fault, which is marked by a west-facing scarp in the alluvium and which is associated with a major offset in the water table, as discussed later.

Thickness of Valley Fill

Estimates of thickness of the Cenozoic valley fill in SGV are based on data from two test wells near the center of the valley, from other test wells that penetrated Paleozoic and Mesozoic basement near the margins of the valley, and from the interpretation of two existing sets of gravity data. No additional gravity data were collected for this study.

One of the data sets used was that of Goldstein and Paulsson (1977; 1978); the other set was collected by Exploration Data Consultants (EDCON), Inc. in 1978 (UURI, 1981b). Although generally similar, the two data sets differ in detail and in area of coverage.

The first set of gravity data, collected for Lawrence Berkeley Laboratory (Goldstein and Paulsson, 1977, 1978), consists of latitude, longitude, and complete Bouguer gravity anomaly values computed at a density of 2,670 kg/m^3. Measurements were made with a LaCoste-Romberg gravimeter at more than 350 stations in an area of about 200 km^2, mostly in the valley (Goldstein and Paulsson, 1978, p. 35). Most of the stations located on valley fill were spaced at approximately 0.5-km intervals along survey lines. In the vicinity of LHS, a 0.25-km interval was used for added detail. Station elevations were surveyed to an accuracy of 0.03 m, except for a few remote locations in the mountains, where elevation is known only to 3 m. Elevations of stations that were not surveyed were interpolated from the 7.5-minute series topographic maps of the area. Contour interval for most maps is 20 ft (6.1 m).

Gravity readings were observed at a base station established by the U.S. Air Force at Win-

nemucca once or twice daily to control drift. The accuracy of most Bouguer-gravity-anomaly values was estimated to be about 1.0 milliGal (mGal). The second data set, collected by EDCON, Inc. (UURI, 1981b), consists of data at 504 stations in SGV. Specifications of the gravity survey are not available but are believed to be similar to the Lawrence Berkeley Laboratory data.

The Bouguer gravity anomaly map (fig. 5) reflects, to a great extent, the subsurface structure of the valley. The Bouguer values range from a low of about -190 mGal in the deepest part of the valley to a high of at least -168 mGal in the mountain areas. The buried basement surface appears to form an asymmetrical trough with the axis located somewhat east of the center of the valley. The east side of the valley appears to be bounded by faults, as illustrated by the close spacing of the lines of equal Bouguer gravity anomaly. Linear contours and a steep gravity gradient suggest high-angle faulting separating dense basement from less dense valley fill or a possible boundary between basement rock types having greatly different density. The trough of the valley parallels these faults and trends generally north-northwest.

The basement outlier southeast of LHS (fig. 5) appears to have little or no effect on the Bouguer gravity anomaly. The apparent lack of effect could be due to two factors, either singly or in combination: (1) the outlier may be composed of material having a lower density than the rest of the basement complex; or (2) the outlier may be gravity slide block detached from the basement outcrop to the east and underlain by low-density valley fill, as suggested by EDCON (UURI, 1981b). Some support for the first interpretation is afforded by the fact that the outlier is composed of silicic metavolcanic rock, which almost certainly is less dense than average basement in the area. However, no data exist to rule out the second interpretation as at least a contributing factor. Deep test drilling within or near the margins of the outlier or, perhaps, a seismic-reflection survey might help to resolve this question.

The gravity data are used to estimate the thickness of the Cenozoic fill by first separating a regional field from the complete Bouguer gravity anomaly. This is accomplished by plotting the gravity stations that were located on the surrounding exposed basement and calculating a best-fit first-order trend surface to the Bouguer-gravity-anomaly values for these stations. The trend surface approximates the gravity field related only to the basement. This surface only approximates the regional gravity field and is used to isolate the effect of the valley fill. Undoubtedly, the actual regional field is more complex, owing to density variations within the basement block and errors caused by incorrect data reductions. Furthermore, data distribution is not ideal for a true regional surface calculation.

Values of the assumed regional gravity field are then subtracted from the observed Bouguer-gravity-anomaly values to obtain the values of the residual-gravity-anomaly field. In theory, the residual-gravity field indicates the effect of only the Cenozoic valley fill overlying the basement surface within the valley. The residual values are input to a model used to estimate the thickness of fill. The residual values in SGV range from zero mGal at the basement-fill boundary to a maximum of -21.0 mGal in the deepest part of the basin.

Thickness of Cenozoic fill is calculated by using an inversion model, employing the technique of Cordell and Henderson (1968). Input to

the model consisted of a gridded array of residual values and a density contrast between basement and fill. An array of thicknesses of prisms of fill that would account for the residual field, given a specific density contrast, is then calculated. An iterative process is used to obtain a best fit to the residual-gravity-anomaly values. The model does not, however, produce a unique solution, and the thicknesses obtained are rough estimates.

The density contrast chosen for the modeling process is 320 kg/m^3; this value enhances the fit of calculated basement-surface profiles to existing well data. Average density of the basement is assumed to be 2,670 kg/m^3 and the average density for the fill is assumed to be 2,350 kg/m^3. The assumed density for the fill is greater than the average of 2,060 kg/m^3 for the core samples obtained from test wells (see table 3). The larger assumed density is needed to more closely fit the thicknesses measured at test wells QH3D and Aminoil USA 11-36. Apparently most of the valley fill is significantly denser than the uppermost part sampled by the test wells. Another possible explanation is that the assumed regional anomaly incorporates the effect of a large density contrast between low-density basement rocks beneath the valley and more dense rocks surrounding the valley. This would yield a smaller residual anomaly and require a larger density contrast between valley fill and basement to resolve the discrepancy.

Available data and the modeling process used for this study do not permit a more refined estimate of thickness, using either a fill whose density contrast with basement varies with depth or a fill composed of two or more layers having different density contrasts. Available data also do not permit inferences as to density variations within the basement.

Modeled thicknesses range from 0 at the valley margin to more than 1,800 m in the deeper parts of the valley (fig. 6). The deepest part of the structural basin underlies the eastern part of the valley and is characterized by four structural lows separated by broad saddles. The northern low, at the north edge of the study area, appears to be the deepest, with an estimated fill thickness of more than 1,800 m. The next low to the south, with an estimated fill thickness of more than 1,400 m, is centered just north the Aminoil USA 11-36 well, where the model indicates a thickness of about 1,300 m, in comparison with a measured thickness of 1,625 m. The third low (1,400 m) is about 2 km east of a basement high at test well QH3D. Basement was penetrated at a depth of 378 m in QH3D, in comparison with a modeled depth of about 550 m. The southern low, southwest of Panther Canyon, has a modeled fill thickness of about 1,600 m (fig. 6).

A comparison of present estimates of fill thickness with previous estimates is presented in table 4. The thicknesses estimated by Goldstein and Paulsson (1977, 1978), using a two-layer inversion program of the gravity data and a basement-fill density contrast of 0.60 g/cm^3 (600 kg/m^3; incorrectly reported as 0.06 g/cm^3 (Goldstein, N.E., oral communication, 1980) are less than those estimated in the present report. However, Goldstein and Paulsson (1978) observed that electrical basement interpreted by Beyer (1977) was 200-300 m deeper along a line extending N.60°W. through LHS across the valley.

Welch and others (1981) modified the interpretation of Goldstein and Paulsson (1977, 1978) to obtain a better fit of fill thickness at wells

TABLE 4. Comparison of estimates of fill thickness (depth to basement) in southern Grass Valley.

[Thicknesses are in meters]

Site	Goldstein and Paulsson (1977) Gravity	Wilt and others (1980) Electrical	Welch and others (1981) Gravity	Edcon UURI (1981b) Gravity	Zoback and Anderson (1983) Gravity, seismic	This report Gravity
Northern low	1,520	---	1,200	>2,000	---	1,800
Aminoil USA 11-36	1,180[1]	---	940	>1,600	1,700	1,300[2]
Low 2 km E of QH3D	1,215	1,500	970	>2,000	1,000	1,400
QH3D	455	---	380	>300	---	550[3]
Low near G13	1,094	800	875	>2,400	500	>1,600
Assumed density contrast between basement and valley fill (kg/m^3)	600	---	750	400	500 (Qal) 350 (Ts) 250 (Fan deposits)	320

[1] Electrical data (Beyer, 1977) indicate thicknesses 200-300 m greater along a line extending N.60°W. through Leach Hot Springs and through a point near the site of the Aminoil well.
[2] Actual thickness or depth 1,625 m.
[3] Actual thickness or depth 378 m.

QH3D and G105 by using a density contrast of 0.75 g/cm^3 (750 kg/m^3). However, the values of fill thickness thus obtained were much too small, as shown by later data from the Aminoil well 1.2 km northwest of LHS.

Estimates by Exploration Data Consultants, Inc. (EDCON) (UURI, 1981b) are similar to those of the present report, although a different density contrast (400 vs. 320 kg/m^3) and different modeling methods were used.

The fill thickness at the site of the Aminoil well interpreted by Zoback and Anderson (1983) using both gravity and seismic-reflection data agrees closely with the actual thickness encountered in the well and with the thickness interpreted in this report from gravity data. Thicknesses interpreted by Zoback and Anderson (1983) at the low 2 km east of well QH3D and at the southern low near well G13 are substantially less than present interpretations. Electromagnetic data interpreted by Wilt and others (1980) seem to substantiate the smaller thickness at the southern low.

The difference in thickness estimates suggests possible variations in the density of both basement rocks and fill and makes interpretation particularly difficult in the southern part of the study area. It also shows how small differences in assumed basement density values can have a large effect on estimates of fill thickness. A more complete discussion of the effect of various uncertainties in assumed basement and fill densities on

estimated depth to basement in a similar setting north of Reno, Nevada, is given by Schaefer and Maurer (1981, p. 13). The configuration of the basement surface will remain especially uncertain in the southern part of the study area until deep test drilling and (or) seismic exploration is done.

HYDROLOGY

Climate

The northern Great Basin, of which Grass Valley is a part, has a middle-latitude desert climate, according to the classification of Köppen (1931). The arid to semiarid character of this climate is caused by the rain-shadow effect of the Sierra Nevada and the Cascade Range, which intercept the generally east-moving storms and drain them of much of their moisture.

Precipitation data are sparse; weather stations are widely scattered and mostly in the valleys. The nearest weather station is at Winnemucca Airport, about 45 km north of LHS. There, the long-term mean-annual precipitation is 213 mm, two-thirds of which occurs from December through May as rain or snow. (National Oceanic and Atmospheric Administration, Climatological Data, Annual summaries for Nevada). The higher altitudes in the Sonoma Range to the south may receive more than 500 mm/yr (Hardman, 1965). Potential evaporation from free water surfaces in the valleys, about 1,200 mm/yr (Kohler and others, 1959), is almost six times the annual precipitation. Diurnal temperature ranges are commonly 20°C, and mean monthly temperatures at Winnemucca Airport range from -2 to 22°C.

Surface Water

Most streams in SGV flow only during periods of rainfall or snowmelt, although a few spring-fed streams flow for short distances most of the year. Flows from the mountains, even during intense rainfall or warm rain on frozen ground, probably do not leave the valley as streamflow. Hansen (1963) reported that a large peak flow of 320,000 L/s from Clear Creek in the central Sonoma Range just north of the study area did not reach the Humboldt River north of Grass Valley. Instead, most of the floodwaters infiltrate the coarse-grained valley fill, especially near the apexes of alluvial fans built by larger streams, such as those in Sheep Ranch, Spaulding, and Pollard Canyons, and Clear Creek. Part of the infiltrated water evaporates or is transpired by native vegetation or crops; the remainder penetrates to the water table as ground-water recharge. A small part of the recharge moves downward to become deep, thermal water, but the locations and amounts can only be inferred from indirect evidence, as discussed below.

Ground Water

Ground-Water Recharge and Discharge

Ground water in SGV is derived chiefly or entirely from precipitation within the drainage basin. Little precipitation on the valley floor reaches the water table because the average annual potential evaporation of about 1,200 mm greatly exceeds the average annual precipitation of about 200 mm. Instead, all or almost all ground-water recharge is derived from precipitation in the

mountains within the drainage basin.

Recharge in SGV from precipitation in the mountains probably occurs in two principal ways: (1) by lateral subsurface flow into the basin fill from consolidated basement rocks that were recharged directly from precipitation in the mountains; and (2) by infiltration of runoff from the mountains into coarse-grained alluvial deposits near the mouths of canyons where the streams flow into the valley. The relative amounts of recharge that occur in these two ways are presently unknown. However, the total amount could be estimated by the method described below.

The percentage of the precipitation that becomes ground-water recharge was estimated using an empirical correlation of precipitation, altitude, and recharge developed by Maxey and Eakin (1949), as applied to the Grass Valley drainage basin by Cohen (1964) (see table 5).

The method of Maxey and Eakin (1949) was developed during studies of 13 basins in east-central Nevada and has been applied throughout Nevada in numerous reconnaissance ground-water studies. It continues to be used in water-budget estimates for individual ground-water basins. Maxey and Eakin (1949, p. 40-41) explained the development of their method as follows:

"The average annual amount of recharge to ground water in White River Valley can be estimated from the precipitation and from the results of recharge studies in comparable areas. This requires a determination or estimate of average annual precipitation for the drainage area, from which the recharge is calculated as a percentage. An estimate for the precipitation in the White River Valley was made from a precipitation map for the State of Nevada [Hardman, 1936] in which zones of average range of precipitation are designated. The zones are divided into the following ranges: less than 8 inches; 8 to 12 inches; 12 to 15 inches; 15 to 20 inches; and over 20 inches. The amount of water from the successive

TABLE 5. Estimate of ground-water recharge in the southern Grass Valley drainage basin on the basis of altitude (precipitation) zones.

[Based on an empirical method developed by Maxey and Eakin (1949), as adapted to Grass Valley by Cohen (1964)]

Altitude zone (m)	Area (km^2)	Precipitation (mm/yr)	Precipitation (hm^3/yr)	Recharge (% of precip.)	Recharge (mm/yr)	Recharge (hm^3/yr)
2,438-2,695	0.5	530	0.3	25	130	0.07
2,134-2,438	8.1	440	3.6	15	66	.54
1,829-2,134	79.8	340	27	7	24	1.9
1,524-1,829	258	250	65	3	7.5	1.9
1,369-1,524	230	150	34	0	0	0
Total or average	**576**	**230**	**130**	**3.4**	**7.7**	**4.4**

zones that reaches the ground-water reservoir is estimated as 0, 3, 7, 15, and 25 percent of the precipitation in the respective zones. The percentages are adapted for this area from preliminary recharge studies in east-central Nevada. These studies consisted of estimating the ground-water discharge by natural losses in east-central Nevada. The recharge for each valley was also estimated, using the rainfall-zone map as a basis. The recharge estimates were then balanced by trial-and-error with the discharge estimates. They also compare favorably with percentages determined in Las Vegas Valley by means of precipitation gages maintained at different altitudes in the Spring Mountains."

The relation between average annual precipitation and altitude was developed by Hardman (1936) and was used throughout Nevada by Maxey and Eakin (1949) and their successors. In general, each of the precipitation zones has an altitude range of 1,000 ft (305 m). However, the altitude of the 8-inch (200-mm) average annual precipitation line below which none of the precipitation contributes to recharge varies, depending on the location of the basin in question. On the basis of Hardman's (1936) map and precipitation records at Winnemucca AP, Cohen (1964, p. 19) selected an altitude of 5,000 ft (1,524 m) for Grass Valley. This is also the approximate altitude of the valley margin in southern Grass Valley.

Above 1,524 m, the amount of precipitation per unit area that furnishes recharge increases rapidly with increasing altitude, and a substantial proportion (15-25 percent) is estimated to provide ground-water recharge at altitudes above 2,134 m (7,000 ft). However, only 1.5 percent of the total drainage area and 14 percent of the total recharge are associated with these higher altitudes. Thus, most of the recharge probably is derived from precipitation in the mountains between altitudes of 1,524 and 2,134 m (5,000-7,000 ft). Within this altitude range, only 3-7 percent of the precipitation is estimated to contribute recharge. Small differences in these percentages cause large differences in the estimate of total volume; hence the estimate of 4.4 hm^3/yr in table 5 is crude at best. The actual recharge might lie within the range of one-half to twice this amount (2.2-8.8 hm^3/yr). An estimate of recharge during a colder and wetter period between 40,000 and 10,000 years before the present is made in a later section (table 9).

Not all ground-water recharge necessarily occurs directly within the altitude zones indicated. Instead, much of the precipitation leaves these zones as surface flow and later infiltrates coarse-grained alluvial deposits, especially near the mouths of canyons where the streams flow into the valley. The proportion of recharge in each environment is presently unknown.

Ground water discharges chiefly by subsurface flow across the valley portion of the northern boundary of the study area, but a small amount also discharges by evapotranspiration of hydrothermal upflow at LHS and evapotranspiration by phreatophytes within the valley (fig. 12). It is assumed that, for long periods, ground-water discharge equals ground-water recharge in the drainage basin that includes the study area.

The proportion of the total recharge that circulates deeply within the basement as thermal ground water was calculated by assuming a long-term net balance of recharge and discharge and by estimating hydrothermal discharge. Most

of the hydrothermal discharge occurs in the LHS area; an unknown but possibly significant amount occurs also as underflow northward from the study area.

The orifice designations at Leach Hot Springs are shown in figure 7, and the flow, which represents discharge consisting entirely or chiefly of thermal water from unknown depths, is shown in figure 8. The springs consist of two roughly linear arrays of orifices parallel to the fault scarp. About 80 percent of the discharge is from six of the western orifices. Intermittent measurements of discharge show distinct fluctuations, although no overall increasing or decreasing trend is indicated for the period of record, from November 1974 to July 1978 and November 1983 to October 1985 (fig. 8). The fluctuations in discharge are not obviously correlated with either precipitation or water temperature, although, unfortunately, temperature was not always measured concurrently with flow.

The average combined discharge from 29 orifices at LHS and spring S13 650 m to the southwest during the periods November 1974 to

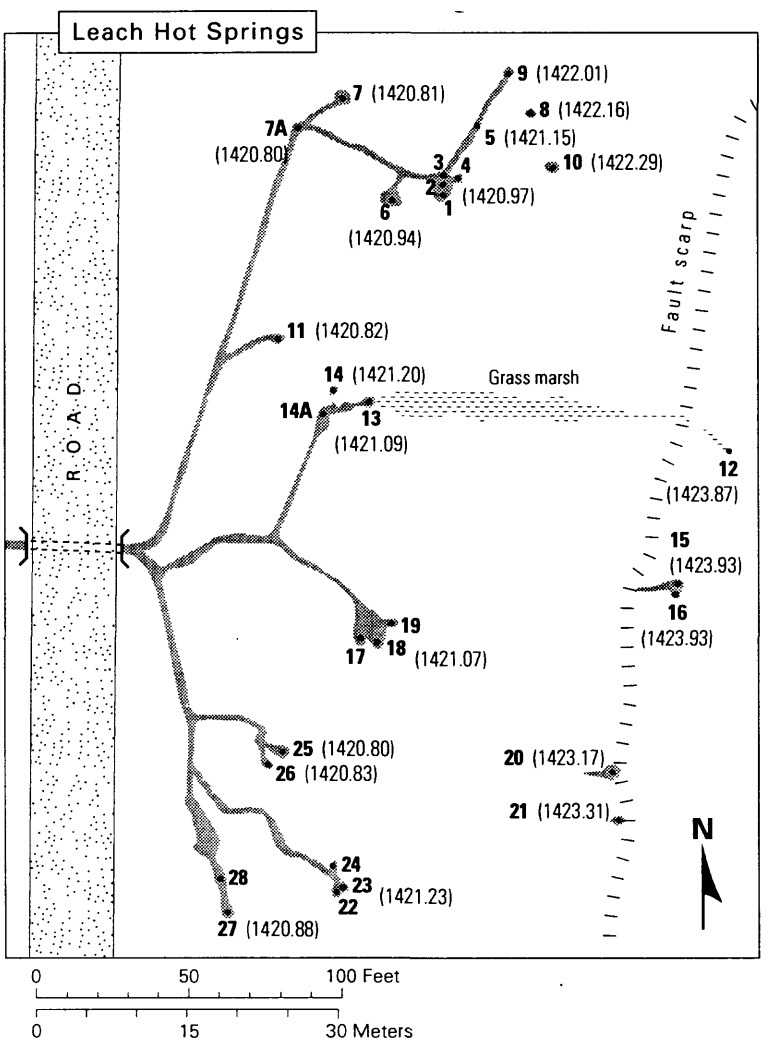

Figure 7. Location of orifices at Leach Hot Springs. Numbers indicate orifices from which significant discharge occurred during the period 1974-85, in order of original inventory; numbers in parentheses indicate altitudes of orifice pools, in meters above sea level.

July 1978 and November 1983 to October 1985 was 8.6 L/s (fig. 8). (Spring S13 contributed about 5 percent of the total.) Estimated evapotranspiration from the vegetated area surrounding the springs was 0.012 hm^3/yr (0.38 L/s) (Olmsted and others, 1975, p. 201). Evaporation from spring pools and discharge channels was estimated on the basis of a quasi-empirical mass-transfer equation of Harbeck (1962), using average monthly temperature, humidity, and wind velocity at the Winnemucca WBO AP weather station. Estimated annual evaporation is a function of water-surface temperature, as shown in figure 9. The evaporation rate from the hot-springs area was computed using data given in table 6. The total, 8,000 m^3/yr, is equivalent to a rate of 0.25 L/s.

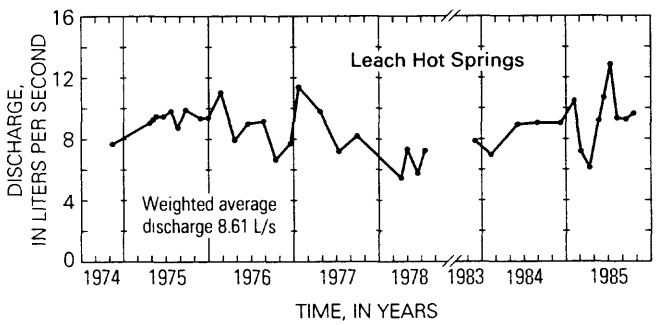

Figure 8. Discharge from orifices 1-29 at Leach Hot Springs, November 1974 to July 1978, and November 1983 to October 1985.

The evapotranspiration from vegetated areas and the evaporation from spring pools and discharge channels were added to the measured spring flow to obtain the total fluid discharge at LHS (table 7). The volume rates of discharge in table 7 were converted to mass rates, using a density of 0.974 kg/L at the weighted-average discharge temperature of 76.8°C. The total mean discharge at the surface for the period of record

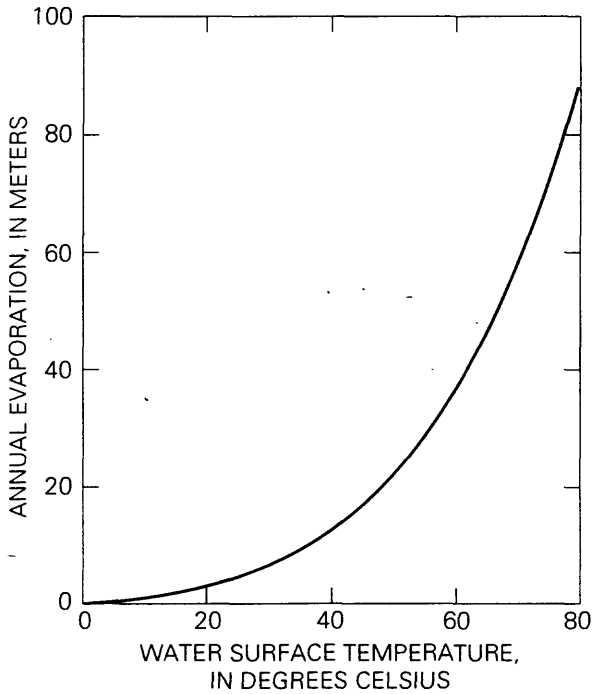

Figure 9. Estimated annual evaporation from hot-water surfaces as a function of temperature. Based on a quasi-empirical mass-transfer equation of Harbeck (1962), using weather data from the Winnemucca WBO AP weather station.

was estimated to be 9.2 L/s or 9.0 kg/s (table 7). The heat flux associated with this fluid discharge is used in a later section to estimate heat flow in the southern Grass Valley area.

The 9.2 L/s (0.29 hm^3/yr) discharge at LHS clearly is a small fraction (3-13 percent) of the estimated total ground-water recharge and discharge (2.2-8.8 hm^3/yr) from SGV. However, not all thermal water in SGV discharges at LHS. An unknown but probably significant amount of hydrothermal upflow that does not discharge at the land surface occurs in the southern and northwestern parts of the LHS thermal anomaly and also at several other thermal anomalies, especially that near Panther Canyon in the southeastern part of the area. All this discharge eventually leaves SGV as underflow across the northern boundary

TABLE 6. Estimated area, temperature, and evaporation rate for water surfaces at Leach Hot Springs.

	Water-surface		Evaporation rate	
	area (m^2)	temperature (°C)	(mm/yr)	(m^3/yr)
Runoff channels	184	60	36	6,600
Pools 1-29	16	78	81	1,300
Spring S13	10	37	10	100
TOTAL				**8,000**

of the study area. This additional amount of hydrothermal discharge is not known. However, because the combined heat flux from the thermal anomalies outside the LHS anomaly is less than that from the LHS anomaly, as discussed in a later section (p. 77-78; table 18), and because these other anomalies represent the only likely additional sources of significant hydrothermal discharge in SGV, such discharge probably does not exceed that at LHS. Thus, the thermal-water component of groundwater discharge from SGV probably is less than 25 percent of the total.

The location of recharge to the deep hydrothermal system is poorly known. Evidence discussed in the next section, "Hydrochemistry", indicates that present sources for shallow, nonthermal water cannot be the sources of the thermal water at LHS.

Ground-Water Movement in the Valley Fill

Information about ground water in the valley fill, both thermal and nonthermal, was obtained from test wells drilled during this study, from existing wells, and from test wells drilled for other studies. The test-drilling programs were described by Olmsted and others (1975), Sass and others (1976), Beyer and others (1976a), and Wilde and Koenig (UURI, 1981g). Data and explanations of the letter symbols for all the wells and springs are given in table A1 of the appendix; measured water levels are listed in table A2 of the appendix; and locations of the wells and springs are shown in figure 10.

Ground water moves through intergranular pores in the unconsolidated to semiconsolidated valley fill. The porosity of the upper 170 m of fill--the part penetrated by most test wells--ranges from about 20 to 70 percent (table 3). The porosity of the deeper fill is less because of compaction and lithification. Although laboratory or field data on permeability are lacking, poor size sorting suggests that it is low to moderate for most of the valley-fill deposits. The ratio of horizontal to vertical permeability probably is very large because of the abundance of poorly permeable layers in the horizontally stratified deposits.

The general directions of shallow groundwater movement in SGV may be inferred from the configuration of the water table--ground water moves approximately perpendicular to the contours in figure 11. Except near LHS and Mud

TABLE 7. Fluid discharge and convective heat flux at Leach Hot Springs.

Item	Volume flow rate (L/s)	Mass flow rate (kg/s)	Heat discharge (MW)
Springflow	8.6	8.4	2.3
Evapotranspiration from vegetated areas	.38	.37	.10
Evapotranspiration from spring pools and discharge channels	.25	.24	.07
TOTAL	**9.2**	**9.0**	**2.5**

Spring, the water-table contours in figure 11 are located only approximately, because wells and springs used for control are widely separated, and because measured water levels locally represent confined rather than unconfined (water-table) conditions. However, by using depths to water in conjunction with the configuration of the land surface and the distribution of phreatophytes (fig. 12), the configuration of the water table could be estimated in somewhat more detail than would have been possible by using only well and spring control, especially in the area near the center of the valley, southwest of LHS.

As shown in figure 12, depths to water in SGV range from zero at several springs (including LHS) to more than 70 m locally near the margin of the valley. Depths along the central axis of the valley range from less than 20 m near the north end of the study area and southeast of the LHS fault to about 45 m on the south.

Studies in northern and central Nevada indicate that the maximum depth from which phreatophyte roots can extract ground water may be about 20 m (P.A. Glancy, oral commun., 1981). In SGV, phreatophytes (mostly greasewood) are confined chiefly to areas near the center of the valley where depths to water are less than about 25 m (fig. 12). The presence of phreatophytes where the water table is deeper than 20 m in this area may be due in part to the infiltration of runoff. The best example is the growth of greasewood, rabbit brush, and salt grass that is supported by runoff from LHS northwest of the LHS fault (fig. 12). Infiltration of intermittent runoff also may help to support the stand of greasewood where depths to water probably exceed 20 m along the valley axis farther south. The greasewood in that area is characterized by the lack of vigor and wide spacing of individual plants.

Shallow ground water in SGV flows generally from the sides toward the center and then northward, approximately perpendicular to the water-table contours in figure 11. The wide spacing of the contours (small lateral hydraulic gradient) in the north-central part of the valley indicates either that the transmissivity of the shallow saturated deposits is high in that area or

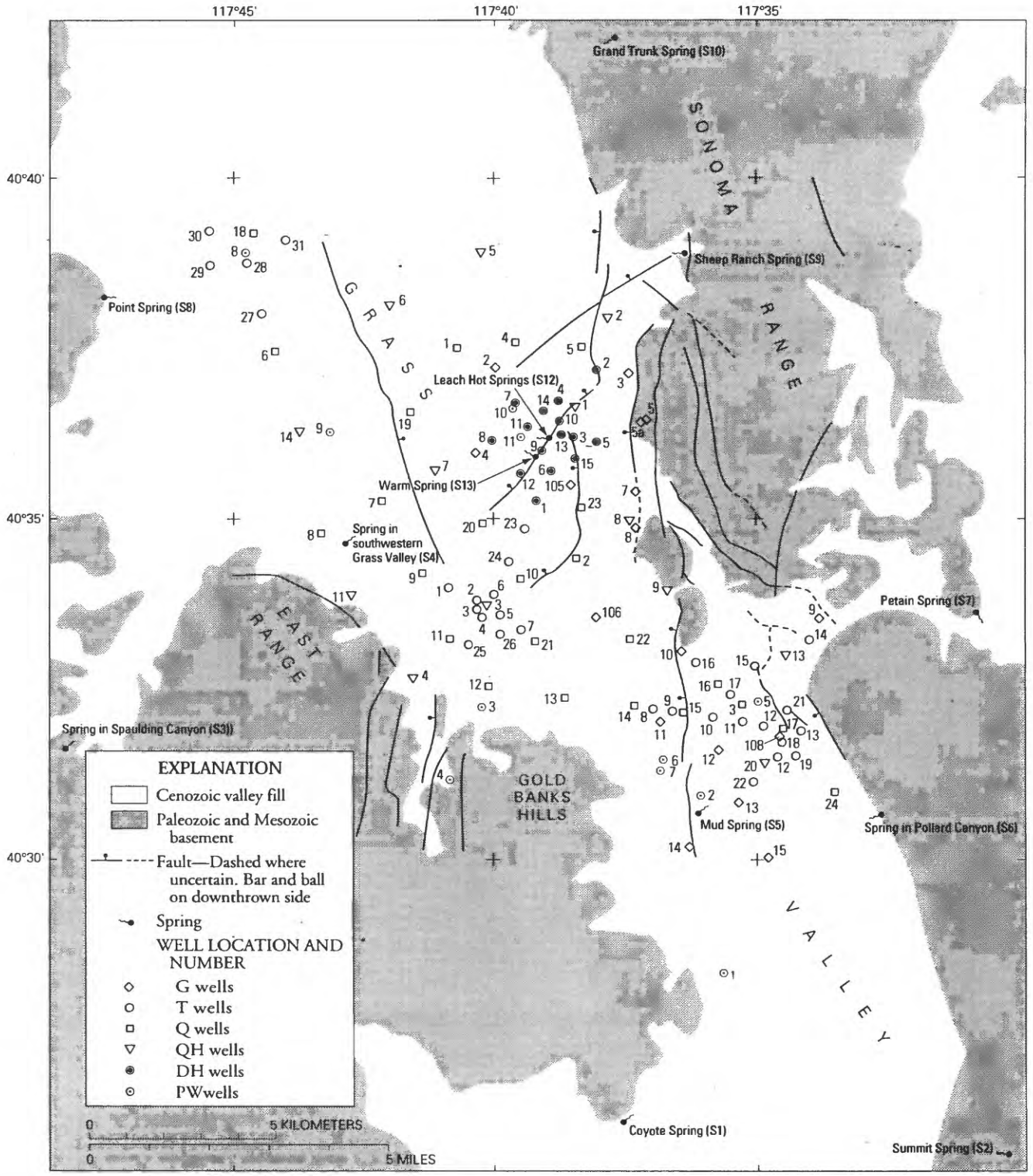

Figure 10. Map of southern Grass Valley showing locations of wells and springs.

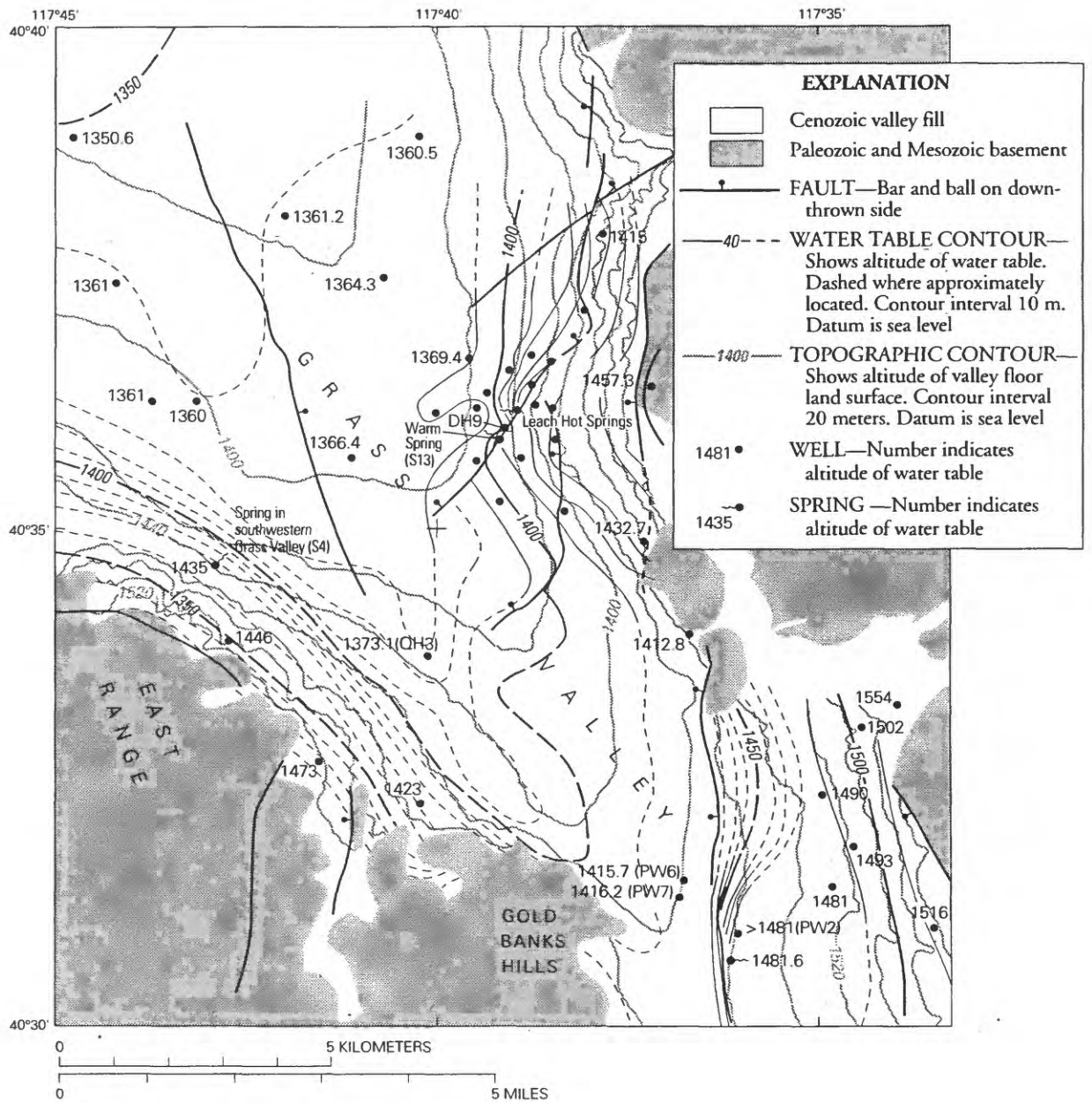

Figure 11. Configuration of water table in southern Grass Valley, June 1977.

that very little ground water is presently moving northward out of SGV. In much of the area near the north boundary of the study area, the water table in June 1977 appeared to be nearly flat, at an altitude of about 1,361 m above sea level. In contrast, the closely spaced water-table contours farther south, near the southwest margin of the valley (fig. 11), may indicate the effect of low-permeability valley fill, although, as discussed later, a ground-water barrier caused by an unmapped fault seems more likely.

Vertical components of flow may be signifi-

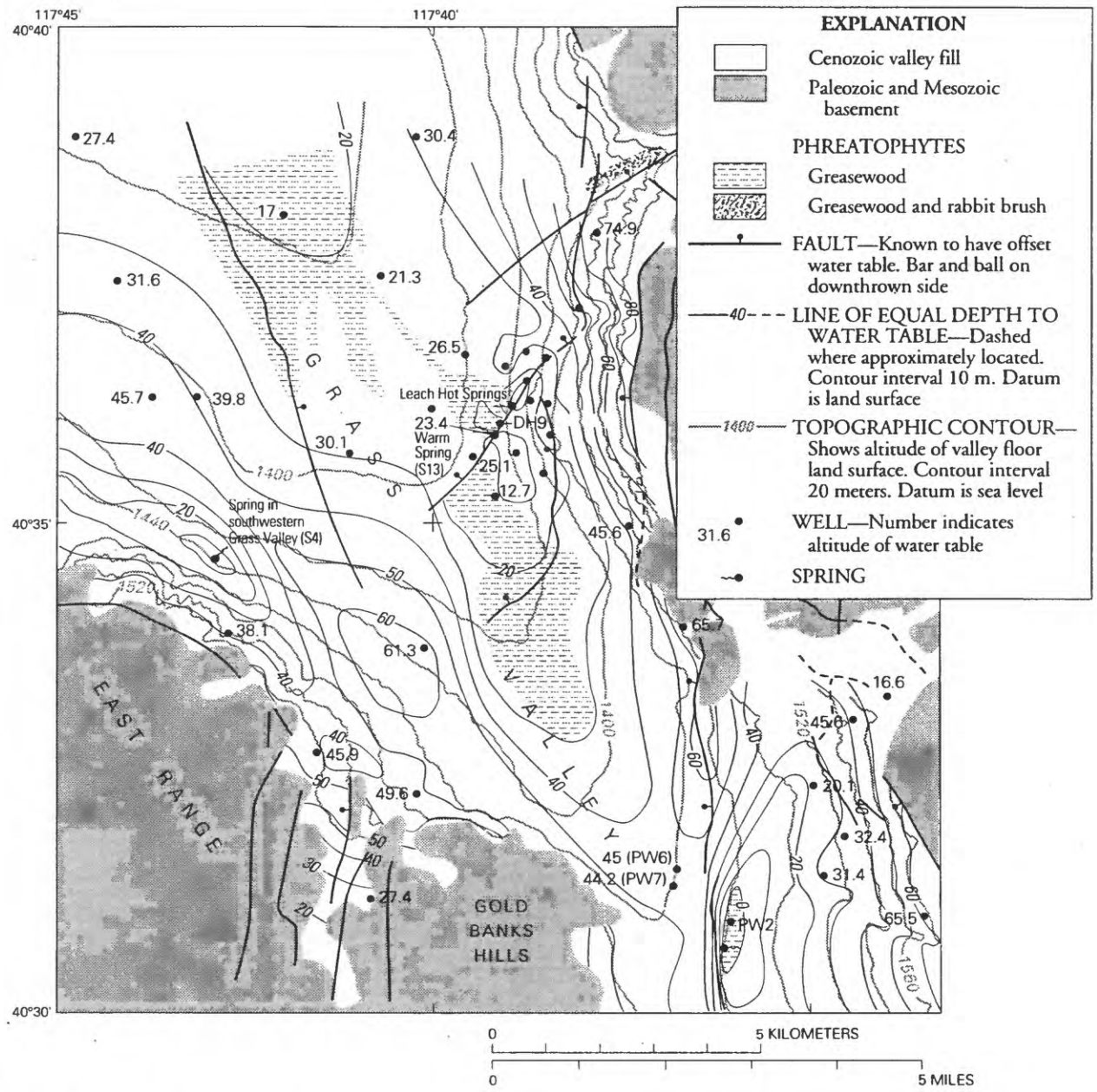

Figure 12. Depth to water table and distribution of phreatophytes in southern Grass Valley, June 1977.

cant locally. At well site QH1 along the LHS fault 1 km northeast of the hot springs, the deep well (QH1B), screened at a depth of 152.7 m, recorded a water-level altitude of 1,433.3 m -- about 13 m higher than the water-table altitude of 1,420.4 m in the shallow well (QH1C), which was screened at the water-table depth of 25.4 m. The water-table altitude was later confirmed by a neutron log made in QH1B. (See table A2.)

At well G105, 1.7 km south-southeast of LHS along another fault, the water level was 2.4 m above land surface in July 1980, after the well was gun-perforated at a depth of 139.3 m (table A2). The altitude of this water level--1,439.3 m

--is more than 15 m higher than a water-table altitude computed by assuming an upward hydraulic gradient of 0.1--the same as that observed at QH1. It is interesting to note that the water-level altitudes at QH1 and G105, as well as that at QH3D, 4.8 km south-southwest of LHS, all of which represent confined conditions, are higher than the altitude of LHS. The implications of this relationship are discussed in the section, "Ground water in the basement and consolidated volcanic rocks".

West and southwest of LHS, water levels interpreted from gamma-gamma and neutron logs are about the same as water levels measured in the most of the wells, indicating little or no potential for upward or downward flow. However, potentials for downward flow may exist at DH8 and DH12, and for upward flow at DH6 (see table A2).

Hydrologic Effects of Basin and Range Faults

In most desert basins like Grass Valley, depths to water are least near the center of the valley and greatest near the mountains, and the water table is a subdued replica of the land surface. Exceptions to this general situation are of interest because they reflect the complicating influences of other hydrologic factors, principally the effects of faults within the valley fill.

At LHS, rising thermal water has created an anomalously low lateral hydraulic gradient east of the springs and a high gradient west of the springs, but the water table does not appear to be sharply offset (fig. 11). The most plausible interpretation is that, in this area, the LHS fault acts as a conduit for rising thermal water. Southwest of the springs, however, the fault seems to serve as a groundwater barrier rather than as a conduit. Near spring S13 and well DH9, the fault is associated with an apparently abrupt water-table displacement of more than 30 m downward to the northwest (fig. 11). Still farther southwest, the distribution of greasewood, which ceases to grow northwest of the fault (fig. 12), reflects the abrupt change in water level across the fault. There, the water-table offset is about 15 m. It is interesting to note that, unlike the situation southwest of LHS, the water table does not appear to be offset along the LHS fault northeast and north of the springs (fig. 11).

The Mud Springs fault in the southeast part of the study area causes an even greater offset in the water table than the LHS fault. At Mud Springs (S2), the water table east of the fault is more than 60 m higher than it is to the west, near PWs 6 and 7 (figs. 11 and 12). The water table has a very gentle slope east of the fault, almost to the mouth of Panther Canyon. The shallow depth to water on the east side of the fault is indicated by a band of greasewood (fig. 12). In the absence of similar evidence of a shallow water table north of well PW2, it is assumed that the water-table offset decreases north of that well (fig. 11).

The large offset of the water table near the west side of the valley between well QH3, where the depth to the water table was 61.3 m in June 1977, and spring S4, where the water table intersects the land surface, may indicate the groundwater-barrier effect of an unmapped fault. The available data do not clearly define the trend of such a hypothetical fault. A likely possibility, however, is a fault 2-3 km west of, and parallel to, the north-northwest trending fault on the west side of the valley, as suggested by the depth-to-water pattern (fig. 12).

In summary, some Basin and Range faults in or near the margins of the valley obviously affect

the configuration of the water table and the related patterns of ground-water flow; other faults apparently do not. At LHS and probably near Panther Canyon, the faults seem to function as conduits for thermal water that rises from considerable depth within the basement beneath the valley fill. The nature of these conduits is poorly known. Sibbett (1983) attributed the localization of rising thermal fluid near the Beowawe Geysers 100 km east of LHS to a dilation breccia related to the intersection of two steeply dipping faults. A similar situation may obtain at LHS, where two major faults intersect just northeast of the springs. The rising thermal water also may be channeled along the fault contact of the valley fill northwest of the LHS fault and the basement rock to the southeast.

Elsewhere, especially within the valley fill, the faults appear to function as ground-water barriers rather than as conduits. The sharp offsets of the water table along the Mud Springs fault and the LHS fault southwest of the springs, and the possible offset along an unmapped fault on the southwest side of SGV all seem to indicate narrow zones of very low permeability associated with the faults. It may be significant that the springs associated with these faults are non-thermal. The nature of the low-permeability zones in SGV is unknown. Such barriers in similar fluvial deposits have been variously attributed to (1) impervious clayey gouge resulting from the pulverization of rocks and minerals along the fault plane, (2) offset of impermeable beds along the fault to block permeable beds on the other side of the fault, (3) rotation of elongated and flat clasts parallel to the fault surface so as to reduce permeability perpendicular to the fault, and (4) cementation of coarse-grained deposits caused by the deposition of minerals (commonly carbonates) by water rising along the fault (Davis and DeWiest, 1966, p. 396; Dutcher and Garrett, 1963, p. 43; Poland, Piper, and others, 1956, p. 119-126; Poland and others, 1959, p. 70-72).

Ground Water in the Basement and Consolidated Volcanic Rocks

The basement and consolidated volcanic rocks are well consolidated and have low primary porosity and permeability--porosity probably is less than 10 percent at most places. Vertical or steeply inclined fractures allow ground water to move upward or downward more readily than in the valley fill. Significant secondary porosity and permeability related to fractures and to solution openings in carbonate rocks are believed to control most ground-water storage and flow. Although it cannot be ruled out, large-scale interbasin movement of ground water through thick sequences of carbonate rocks, as in the southern Great Basin (Winograd and Friedman, 1972; Winograd and Pearson, 1976), is unlikely in the SGV region, owing to the thinness of the carbonate rocks and the structural complexity. Both factors interrupt the lateral continuity of potential carbonate-rock aquifers.

Information about deeply circulating thermal ground water is limited to geophysical data, hydrologic measurements and chemical and isotopic data from LHS and several nearby test wells and well site QH3, and geologic data from wells QH3D and Aminoil 11-36. Although some inferences may be drawn on the nature of deep thermal circulation by using numerical modeling, discussed later, the paucity of data permits only a sketchy analysis.

On the basis of the discovery of a heat-flow high apparently centered at well site QH3 (Sass and others, 1977, p. 54), a deep well (QH3D) was drilled at this location. The well penetrated Paleozoic and Mesozoic basement at a depth of 378 m to the bottom, at 415 m. The casing was perforated from 408.7 to 410.2 m, opposite a zone of high porosity and low clay content, as interpreted from borehole geophysical logs. Shortly after completion, the water level in well QH3D rose to within 5 m of the land surface, which indicated a strong upward hydraulic gradient when compared to a static water level of 62 m below the land surface in well QH3B, 154 m deep and screened in valley fill. The upward hydraulic gradient of 0.22 between depths of 154 and 408.7 m was not observed in the shallower part of the valley fill. Instead, a small downward gradient was observed between depths of 64 m (well QH3C) and 154 m (QH3B). As discussed later, the chemical and isotopic similarity of water at well QH3B to the thermal water at LHS suggests upward flow of thermal water from the basement into the lower part of the valley fill.

The only places other than well site QH3 where thermal water was sampled were the orifices of LHS and wells in the surrounding thermal anomaly. However, other water, not sampled, especially in deeper wells near Panther Canyon and in the deep Aminoil well, may be at least in part of thermal origin.

The exact hydrologic relation between LHS and the thermal water at well QH3D cannot be determined, owing to lack of data on groundwater-flow directions in the basement. The altitude of the confined water level at well QH3D (1,429.4 m) is higher than that of the orifices at LHS (1,420.8-1,423.9 m). Whether this indicates a potential for flow at depth from QH3D toward the springs is unknown. Such a determination would require a measurement of hydrostatic head at the same altitude in the spring conduit system as the altitude of the perforations in QH3D. Definitive conclusions as to the significance of the relations of temperatures and hydrostatic heads at well QH3D and LHS must await the acquisition of data from deep test wells.

As mentioned earlier (p. 42), confined water levels at wells QH1B, along the LHS fault 1 km northeast of the hot springs, and G105a, near a subsidiary fault 1.5 km south of the hot springs, are substantially higher than the springs. The water level in G105 on July 31, 1980 was, in fact, 2.4 m above the land surface (table 8). This supports the conclusion that thermal water rises along these faults at places other than LHS but does not reach the surface. At G105, the water may have enough head to reach the surface but, unlike LHS, does not have an active channelway to form a spring or springs.

Little is known about the depth and configuration of the Panther Canyon hydrothermal system, or, indeed, whether the system is separate from that discharging at LHS. The hydrothermal upflow, required to account for the heat-flow anomaly, seems to be related a fault or fault zone of large throw along the east margin of the basin. The west margin of the heat-flow anomaly lies approximately along the trace of the Mud Springs fault. Unlike the situation at LHS, the upflowing thermal fluid does not reach the land surface. Instead, it appears to spread laterally at depths poorly defined by subsurface data but generally greater than about 150 m, the depth of most of the deeper test wells in the area.

AQUEOUS GEOCHEMISTRY

The concentrations and proportions of dissolved inorganic constituents and the hydrogen- and oxygen-isotope composition of the waters in SGV are used to define the spatial occurrences of thermal and nonthermal water, indicate possible sources of ground-water recharge, and estimate the source temperature of the water discharging at LHS. Table A3 of the appendix lists chemical and isotopic analyses of 42 water samples from 31 sites in or adjacent to the study area. The sample sources are grouped in five categories: (1) Leach Hot Springs, representing surface discharge of thermal-water upflow from a deep source or sources; (2) thermal wells, chiefly near LHS, and probably representing leakage of thermal-water upflow into the shallow subsurface; (3) nonthermal springs; (4) nonthermal wells; and (5) Clear Creek, 14 km north of LHS.

Thermal-water samples (the first two categories) are defined as having a source within a thermal (heat-flow) anomaly; nonthermal-water samples (the last three categories) are from sources outside heat-flow anomalies. Although this classification is arbitrary, the thermal- and nonthermal-water samples thus defined form two distinct groups according to their chemical and isotopic composition, as discussed below.

No samples were collected of nonthermal water from wells deeper than 55 m or from wells within the Panther Canyon thermal anomaly in the southeast part of the study area. Therefore, the characteristics of presumed nonthermal ground water within the valley fill below a depth of 55 m and of the thermal ground water in the southeast part of the valley are unknown.

Dissolved Constituents

On the basis of the similarity between the hydrogen-isotope composition of local meteoric water and thermal water (see White and others, 1973), most, perhaps all, thermal (as well as nonthermal) ground water in SGV is believed to be of meteoric origin. Samples that would indicate the chemical and isotopic composition of precipitation in the area were not obtained. However, unpublished U.S. Geological Survey data from seven localities in central Nevada indicate that the precipitation contains only small concentrations (4-25 mg/L) of dissolved inorganic constituents (for convenience, hereinafter called "dissolved solids").

The sample that chemically most closely resembles precipitation in the SGV area is that from Summit Spring in the Mt. Tobin Range, 23 km southeast of LHS (figs. 1 and 10). The spring lies at an altitude of 2,570 m on the north slope of the ridge that forms the summit of the range at Mt. Tobin, 5.8 km farther south, at an altitude of 2,979 m. The catchment area for the spring is small, flow paths for ground water issuing at the spring are short, and residence time for the water is short. The concentration of dissolved solids in the spring water, only 40 mg/L, is much less than that in any of the ground water sampled in SGV and is less than the 215 mg/L in the only sample of surface runoff, in Clear Creek (table 9).

As precipitation infiltrates the ground-water reservoir, the concentration of dissolved solids is increased, primarily by rock-water chemical reactions. The processes that control the type and concentration of dissolved solids in the water depend on numerous factors, including chemical composition of the rock, nature of the pore space,

residence time of the water, temperature, and evaporation. Longer ground-water flow paths and residence times generally produce higher concentrations of dissolved solids, so that the deeply circulating thermal ground water is likely to have a higher dissolved-solids concentration than shallow nonthermal water. In some cases, these factors may be offset by other factors such as evaporation of shallow ground water or solution of evaporite minerals like halite and gypsum.

Grass Valley, unlike many other basins in northern and central Nevada, is characterized by a generally deep water table and by the absence of extensive evaporite deposits. In addition, most of the basement rocks in the drainage basin probably are relatively insoluble. For these reasons, most ground waters, both thermal and nonthermal, have fairly low concentrations of dissolved solids. As shown in table 8, concentration of dissolved solids in all the water samples ranges from 210 to 910 mg/L. Except for four samples from nonthermal springs, in which concentrations range from 600 to 910 mg/L, dissolved-solids concentrations are lower in the nonthermal waters

TABLE 8. Ranges in concentration of dissolved constituents in thermal and nonthermal waters in southern Grass Valley.

[All values are in milligrams per liter]

Constituent	Leach Hot Springs[1]	Thermal wells[2]	Nonthermal springs[3]	Nonthermal wells
Dissolved solids	550-590	500-620	340-910	210-370
Calcium (Ca)	8.5-11	8.0-15	65-150	18-68
Magnesium (Mg)	0.1-1.2	0.3-2.3	9.1-61	6.2-19
Sodium (Na)	160-180	170-270	29-130	38-53
Potassium (K)	11-16	7.6-14	1.8-6.5	2.3-4.5
Bicarbonate (HCO_3)	324-390	360-470	140-480	137-208
Chloride (Cl)	24-32	23-29	36-180	36-81
Sulfate (SO_4)	48-57	19-52	38-190	15-53
Fluoride (F)	2.7-9.0	1.3-8.8	<0.1-1.4	0.1-0.8
Boron (B)	1.2-1.3	0.44-1.8	0.08-0.63	0.11-0.30
Lithium (Li)	0.78-1.7	0.24-0.91	0.008-0.22	0.008-0.05
Silica (SiO_2)	95-145	7.5-97	7.4-58	4.6-25

[1] Orifice 15 not included.

[2] Wells QH3B and DH13A not included.

[3] Summit Spring not included.

(210-430 mg/L) than in most of the thermal waters (500-620 mg/L), which tends to support the generalization that longer flow paths and residence times and higher temperatures tend to increase dissolved-solids concentrations in the thermal waters.

The four nonthermal spring samples having relatively high concentrations of dissolved solids all appear to be affected to some degree by evaporation, solution of evaporite minerals, or admixture with thermal water. Point Spring (S8), with 910 mg/L dissolved solids, has the highest concentration of calcium (150 mg/L) and sulfate (350 mg/L) and third highest concentration of chloride (110 mg/L) of all the sampled waters. Calcium (99 mg/L) and sulfate (150 mg/L) are fairly high in the sample from the spring in Spaulding Canyon (S3), as well. The high calcium and sulfate suggest the presence of gypsum in the source rocks for these waters. The high sodium (110 mg/L) and chloride (180 mg/L) in the sample from the spring in southwestern Grass Valley (S4) indicates possible concentration by evaporation or solution of evaporite deposits. The high sodium (130 mg/L) and bicarbonate (480 mg/L), together with the water temperature of 22 °C, suggest the presence of a thermal-water component in the sample from Coyote Spring (S1).

Water from the other nonthermal springs and from the nonthermal wells is not characterized by a dominant cation or anion (see fig. 13). Calcium and magnesium are more abundant and sodium and potassium less abundant than in the thermal waters, probably owing to cation exchange at elevated temperatures in the thermal waters.

Among the major anions, considerable overlap exists in the concentrations of bicarbonate and sulfate between the thermal and nonthermal waters (see table 8). However, measured chloride concentrations in the nonthermal water (36-180 mg/L) all are greater than in the thermal water (23-32 mg/L). The only nonthermal water having a chloride concentration less than 23 mg/L is represented by samples of surface water from Clear Creek (S11), issuing from the Sonoma Range northeast of the study area (14 mg/L), and water from Summit Spring (S2) at an altitude of 2,570 m, north of Mt. Tobin, southeast of Grass Valley (4.0 mg/L). As discussed later, these samples may represent types of water that could percolate downward to recharge the nonthermal and (or) thermal ground-water systems in the SGV area.

Dissolved-solids concentrations in the water from most of the thermal wells (500-620 mg/L) are similar to those in the hot springs (550-590 mg/L, excluding the anomalous sample from orifice 15, an acid-sulfate water diluted by steam condensate, which has a dissolved-solids concentration of 500 mg/L). However, the concentrations are 270 mg/L and 760 mg/L at wells QH3B and DH13A, respectively (table A3 of the appendix). Hydraulic-head data (see p. 3-4), indicate ground-water downflow at QH3B, which, together with the low dissolved-solids concentration of 270 mg/L and the relatively low concentrations of sodium and potassium--57 and 3.5 mg/L, respectively, suggests that the water in QH3B contains a significant fraction of nonthermal water. However, the stable-isotope composition, discussed later, is like that of other water of undoubted thermal origin.

Well DH13A, 260 m east of orifice 15, probably is not far east of the LHS fault zone. The dissolved-solids concentration of the water in the well may be increased because of steam loss represented by the apparent steam condensate in the

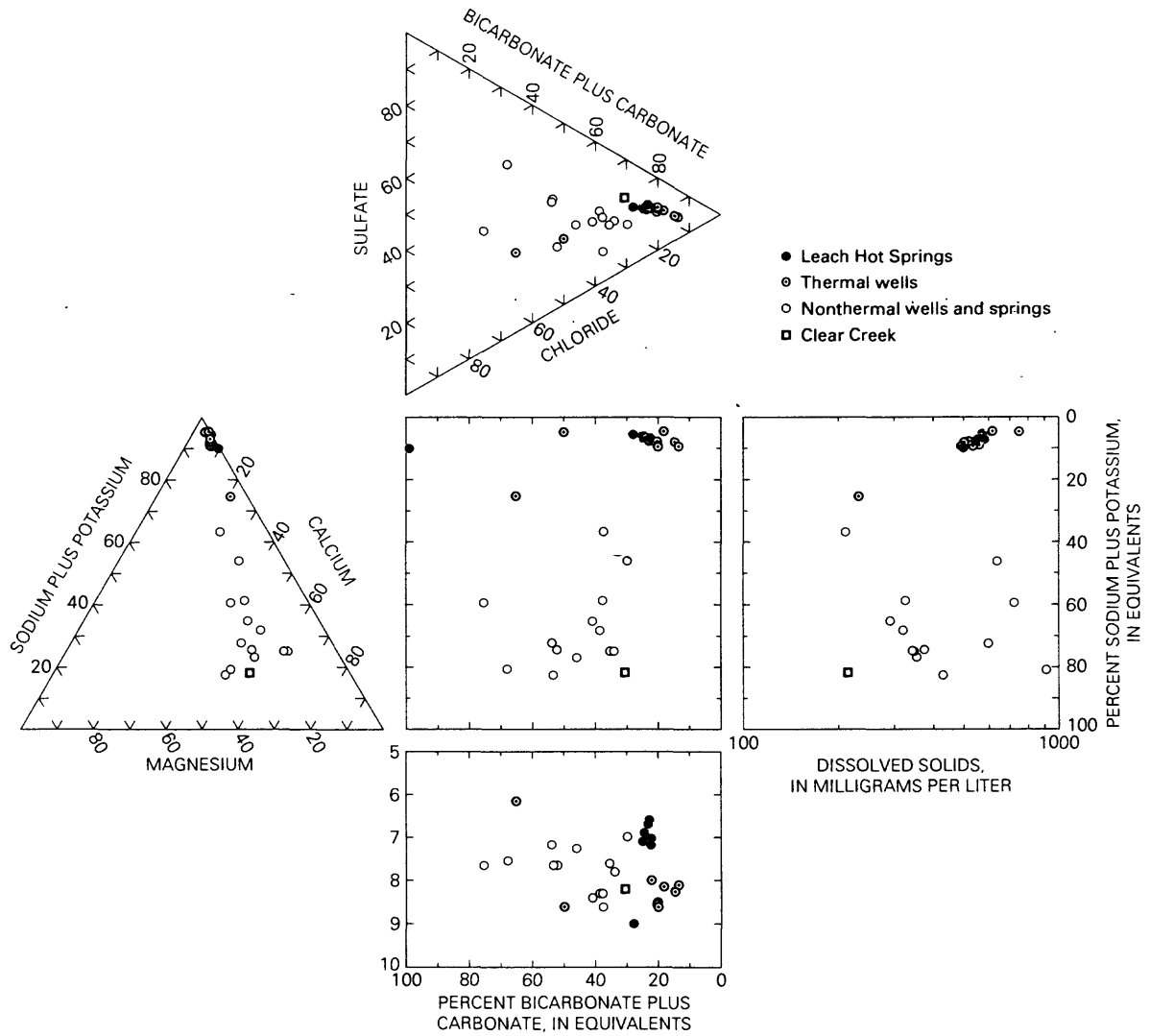

Figure 13. General chemical character of thermal and nonthermal water in southern Grass Valley area. For details on the construction of this type of diagram, see Zaprozec (1972, p. 38).

water at orifice 15. The inference that the two waters are fractionated from a single source fluid is supported by the fact that the dissolved-solids concentration in the water from DH13A (760 mg/L) is higher than the average of 565 mg/L for the hot-springs orifices other than 15, whereas the concentration in orifice 15 (500 mg/L) is lower than that for the other orifices. The low bicarbonate content of both waters also supports a genetic relationship. Relative concentrations of individual constituents in the two waters qualitatively support a steam-loss relationship, although the chloride concentration in the DH13A water, 140 mg/L, compared to an average of 26 mg/L for the spring orifices other than 15, is several times too large to be attributable to concentration by steam loss alone. Warm water in well DH13A also has greater concentrations of sodium and sulfate than the water at LHS. These higher concentrations may result from dissolution of sodium salts

formed by shallow boiling water.

Sulfate concentrations in the thermal water are within the lower range of those in the nonthermal water. The low concentrations in the thermal water may be due to removal of sulfate from solution by the precipitation of sulfur-bearing minerals or the production of hydrogen sulfide.

The constituents fluoride, boron, and lithium, which are present in minor amounts in most ground waters, have proved useful at other places as indicators of the presence of thermal water. This has proved to be the case in SGV, where, with one minor exception discussed below, concentrations of all three constituents are higher in thermal than in nonthermal water samples.

Fluoride concentrations in thermal water are at or near saturation with respect to the mineral fluorite (CaF_2) at the measured spring orifice and down-hole temperatures (fig. 14). Thermal water in the northern Basin and Range province generally is saturated with respect to fluorite (Nordstrom and Jenne, 1977). The high fluoride concentrations result from low calcium concentrations in the thermal water. Most nonthermal water has lower fluoride concentrations than thermal water and is undersaturated with respect to fluorite. The one minor exception to the lower fluoride concentrations in the nonthermal water is the sample from Coyote Spring (F = 1.4 mg/L, compared to 1.3 mg/L in one of two samples from thermal well DH13A); as discussed above, Coyote Spring probably includes a thermal-water component.

Concentrations of lithium and boron also are higher in the thermal water than in the nonthermal

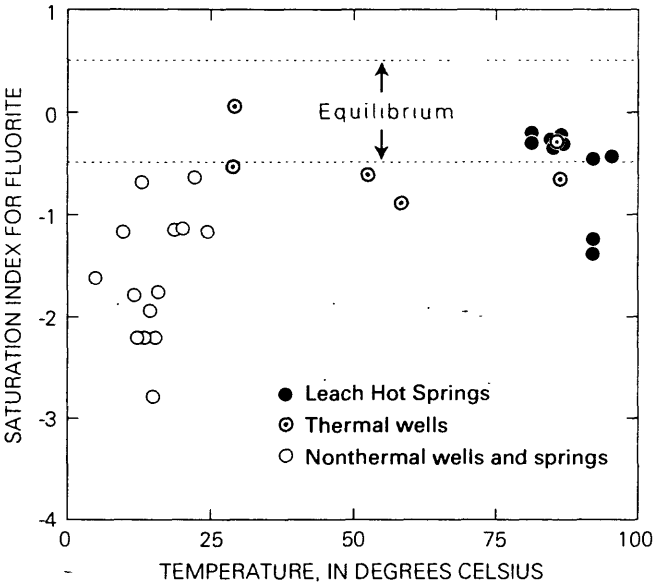

Figure 14. Saturation index for fluorite (CaF_2) versus source temperature.

water (fig. 15). Empirical chemical geothermometers based on the relation between lithium and either magnesium (Fouillac and Michard, 1981) or sodium (Kharaka and others, 1985) have been developed. If a general temperature-dependent relationship exists between lithium and other cations, then lithium concentrations may be controlled by an equilibrium reaction within a deep thermal aquifer, although specific reactions have not been identified.

Because of increasing solubility of silica with increasing temperature, silica concentrations in thermal water, especially that at LHS, are higher than those in nonthermal water (see table 8). The somewhat lower concentrations in the well samples may indicate precipitation of silica during upflow or subsequent lateral subsurface flow, or, especially in the sample from DH13A,

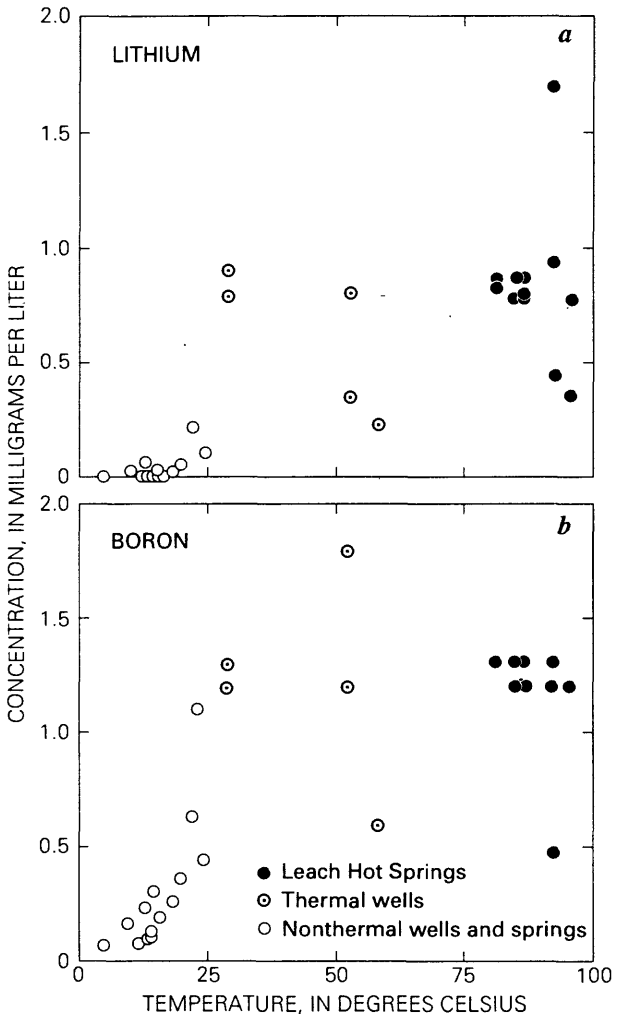

Figure 15. Dissolved lithium and boron versus source temperature.

dilution by nonthermal water.

In summary, thermal water may be distinguished from nonthermal water in SGV by its higher concentrations of sodium, potassium, fluoride, boron, and lithium, and its lower concentrations of calcium, magnesium, and chloride. Silica has higher concentrations in all the LHS water than in the nonthermal water, but concentrations in several thermal well waters are lower than in some of the nonthermal water.

Stable Isotopes of Hydrogen and Oxygen

Analyses of the stable isotopes of hydrogen and oxygen are useful in distinguishing thermal from nonthermal ground water, evaluating processes that result in isotopic change from precipitation to ground water, determining the sources of thermal and nonthermal ground waters in SGV, and establishing the age of the thermal water.

Hydrogen- and oxygen-isotope data for water generally consist of analyses of the ratio of deuterium (hydrogen-2) to hydrogen-1 ($^2H/^1H$) and of oxygen-18 to oxygen-16 ($^{18}O/^{16}O$). These ratios are related to comparable ratios for a standard called "Vienna Standard Mean Ocean Water" (V-SMOW) (Gat, 1980, p. 21-24). The differences from the standard are expressed as delta deuterium (δD) and delta oxygen-18 ($\delta^{18}O$), the units being expressed as permil (‰). Most delta values are negative, that is, concentrations of the two heavier isotopes relative to hydrogen-1 and oxygen-16 are less than those of the standard. Because of the convention adopted for calculating delta values relative to V-SMOW, larger negative delta deuterium and delta oxygen values are isotopically lighter than less negative values (Gat, 1980, p. 20-21). Hydrogen- and oxygen-isotope data generally are shown on an x-y plot in which the delta deuterium values are plotted on the y axis and the delta oxygen-18 values on the x axis, as shown in figure 16.

Isotopic Composition of Precipitation

Line 1 in fig. 16 is a commonly used regression line for modern precipitation worldwide and is generally referred to as the "meteoric-water line" (Craig, 1961). Although the isotopic composition of precipitation at a site commonly varies

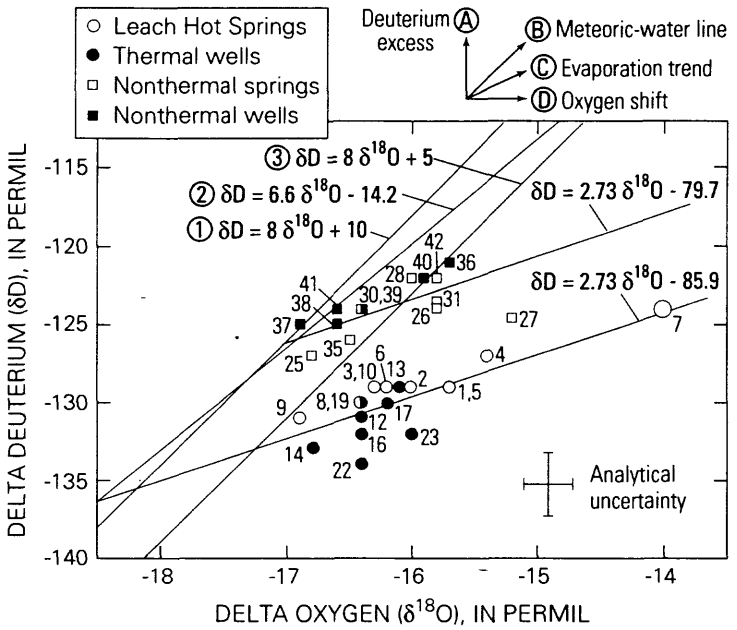

SAMPLE NO.	SAMPLE SITE	SAMPLE NO.	SAMPLE SITE
1	Leach H.S. orifice 1	21	Well DH10
2	do	22	Well DH13A
3	do	23	do
4	Leach H.S. orifice 12	25	Summit Spring
5	Leach H.S. orifice 13	26	Spring in Spaulding Cyn
6	do	27	Spring in SW Grass Valley
7	Leach H.S. orifice 15	28	Mud Spring
8	Leach H.S. orifice 22	29	Spring in Pollard Cyn
9	do	30	Petain Spring
10	do	31	do
12	Well DH6	35	Grand Trunk Spring
13	Well QH3B	36	Goldbanks Windmill
14	Well QH3D	37	Well DH1
16	Well G105	38	Well QH7B
17	Well DH4	39	Well QH13B
19	Well DH14A	40	Well near Mud Spring
20	Well DH10	41	Well DH8
		42	Clear Creek

Figure 16. Hydrogen and oxygen composition of thermal and nonthermal waters in the southern Grass Valley area.

widely from storm to storm, depending on factors such as time of year and storm source (Ingraham and Taylor, 1991, p. 85-86), average compositions for periods of a year or more tend to lie along the meteoric-water line.

Craig's (1961) meteoric-water line is based on about 400 samples worldwide, of which about 40 percent were from North America. The slope of the regression is the approximate ratio of the combining weights of oxygen to hydrogen in the water molecule:

$$\delta D = 8\ \delta^{18}O \qquad (4)$$

The position of an average isotopic composition

along the regression line is determined largely by the weighted-average temperature of precipitation at the site: isotopically heavier (less negative) values of δD and $\delta^{18}O$ are associated with higher temperature.

The data of Craig (1961) also show that the precipitation is heavier in deuterium than indicated by the simple relation of equation 4. The meteoric-water line is displaced upward by 10‰ δD from a plot of equation 4. This upward displacement (arrow A in fig. 16) is commonly called the "deuterium excess parameter" (d) (Dansgaard, 1964). The equation of Craig's meteoric-water line, therefore, is:

$$\delta D = 8\ \delta^{18}O + 10 \qquad (5)$$

Distinction of Thermal from Nonthermal Ground Water

Deuterium and oxygen-18 data for thermal ground water in SGV consist of analyses of 10 samples from 5 orifices at Leach Hot Springs and 10 samples from 8 wells; for nonthermal ground water, the data consist of analyses of 8 samples from 7 springs, 6 samples from 6 wells, and 1 sample of surface water from Clear Creek (fig. 16). Multiple samples from a site are plotted separately rather than averaged because most of the samples were collected at times differing by several years. We believe the differences indicated are in part real and not simply analytical uncertainty, which is reported to be $\pm$0.2‰ $\delta^{18}O$ and $\pm$1.5‰ δD (Pritt and Jones, 1989).

The thermal and nonthermal waters in SGV form two distinct sets isotopically. Although the $\delta^{18}O$ values of the two sets are similar (the average $\delta^{18}O$ values are -16.1 and -16.2‰ for the thermal and nonthermal waters, respectively), the thermal water, except for the water at LHS orifices 12 and 15, is lighter in deuterium than all the nonthermal water.

Because the data are compatible with the hypothesis that the slopes of a linear regression for the thermal and nonthermal waters are equal ($p = .31$), the average difference between the values of delta deuterium for the thermal and nonthermal water samples is estimated by fitting an equal-slopes model to the data for both groups. Multiple samples from a single site were averaged to obtain a more conservative estimate of the standard error of the difference, with the result that the relations for the thermal (1) and nonthermal (2) samples are, respectively,

$$\delta D = 2.73\ \delta^{18}O - 79.7 \qquad (6)$$

and

$$\delta D = 2.73\ \delta^{18}O - 85.9 \qquad (7)$$

The thermal waters therefore are on average 6.2 ± 0.52‰ lighter (more negative) in δD than the nonthermal waters. A 95 percent confidence interval for the difference is -5.2 to -7.3‰ δD. This result is in substantial agreement with that of Flynn and Buchanan (1993, fig. 6), who found that, in the region that includes SGV, thermal waters are 4-8‰ lighter in δD than nonthermal waters.

Isotopic Changes from Precipitation to Ground Water

Shallow ground water that has not undergone significant change due to evaporation or chemical interaction with soil or rock has about the same δD and $\delta^{18}O$ as the precipitation from

which it was recharged. Nevertheless, the ground water in many Basin and Range settings is heavier in $\delta^{18}O$ than local meteoric water. If the meteoric-water line of Craig (1961) (line 1 in fig. 16) represents the source of recharge of both thermal and nonthermal water in SGV, then all the samples except that from well DH1 (#37) are heavier in $\delta^{18}O$ than the precipitation. The enrichment in $\delta^{18}O$ in the ground water may be the result of oxygen shift (line D in fig. 16), evaporation (line C in fig. 16), or a combination of both processes.

Oxygen shift, which results from ^{18}O exchange between water and rock, is greater in a high-temperature environment, owing to the enhancement of many water-rock chemical reactions at elevated temperature. Thermal water therefore commonly displays greater oxygen shift than nonthermal water. This might account for the greater displacement of the thermal water samples than the nonthermal samples from the meteoric-water line.

Evaporation differs from oxygen-shift in that it involves a change to heavier isotopic composition for δD as well as $\delta^{18}O$. In this respect, the effects of evaporation resemble those of the precipitation trend (meteoric-water line 1 in fig. 16), although the slope of the δD vs. $\delta^{18}O$ line is smaller for the evaporation trend (compare line B with line C in fig. 16).

In figure 16, the slope of 2.73 for the line δD vs. $\delta^{18}O$ (equations 6 and 7 discussed above) may indicate an evaporation trend. Evaporated waters are reported to typically have a slope of 3 (Sheppard, 1986, p. 178). An evaporation-trend slope of 3.5 has been reported for the Carson Desert area 150 km southwest of SGV (Welch and others, 1984, p. 75), a value of 4.5 has been reported for the western Black Rock Desert 160 km west of SGV and the Bradys Hot Springs area 160 km southwest of SGV (Welch and Preissler, 1986; 1990), and a value of 5 has been reported for surface waters in East Africa (Craig, 1961).

Because of analytical uncertainty, the slope of the regression line for the SGV samples is not well defined, and it may not represent an evaporation trend entirely. The SGV samples may be affected by both evaporation and oxygen shift.

Sources of Thermal and Nonthermal Ground Waters

The isotopic composition of the precipitation from which the thermal and nonthermal waters were derived is estimated by projecting the equal-slopes curve fits described previously (equations 6 and 7) to the meteoric-water line. Using the line of Craig (1961) (line 1 in fig. 16), the resultant δD values for thermal and nonthermal water sources are, respectively, -135.6 and -126.2‰. Thus the difference is 9.4‰--about 50 percent larger than the 6.2‰ difference between the average thermal and nonthermal samples.

The meteoric water line of Craig (1961) may not be appropriate for the SGV area or for the surrounding Great Basin region. A least-squares linear curve fit for 127 samples of shallow ground waters in northern Nevada having dissolved chloride concentrations of 25 mg/L or less gave

$$\delta D = 6.6\ \delta^{18}O - 14.2 \qquad \textbf{(8)}$$

(line 2 in fig. 16). The low-chloride samples were selected from a larger set of analyses as most

nearly representing precipitation because they are presumed to be least affected by evaporation or oxygen shift. As shown in figure 16, the difference between lines 1 and 2 is small for the range of isotopic composition of the SGV samples. Using line 2, the δD difference between thermal and nonthermal water sources is 10.6‰.

The meteoric water line representing the source of the nonthermal water may differ from that representing the source of the thermal water. Using stable-isotopic data from several areas, Gat (1971, p. 987-989) noted that past precipitation had a lower deuterium d value than present-day precipitation, and that old water has a lower deuterium content than recent ground water. A d value of 5‰, which has been observed to yield a good fit for worldwide old-water data (Criss and Taylor, 1986, p. 388), may be more appropriate than the 10‰ of Craig (1961) for the source of thermal water in SGV. Using a meteoric water line of

$$\delta D = 8\ \delta^{18}O + 5 \qquad (9)$$

(line 3 in fig. 16), the source of the thermal water in SGV has a δD of-133.0‰, which is 6.8‰ lighter in deuterium than the inferred source of the nonthermal water.

In summary, thermal ground-water samples in SGV average about 5-7‰ lighter in δD than nonthermal water samples, but the difference in δD values for the inferred meteoric sources of these waters is greater--about 7-10‰. Dansgaard (1964, p. 442-444) found that, for data from Greenland, changes in temperature of 1 °C corresponded to changes of 0.69‰ in $\delta^{18}O$ and 5.6‰ in δD. From temperature and $\delta^{18}O$ records for Antarctica and Europe, Rozanski and others (1992, p. 984) reported a somewhat smaller coefficient of 0.56-0.63‰ per °C for $\delta^{18}O$, which is equivalent to 4.5-5.0‰ per °C for δD. The precipitation that recharged thermal ground water in SGV therefore averaged 1 to 2 °C colder than precipitation that recharged shallow, nonthermal ground water.

Age of Thermal Water

Two principal explanations have been suggested for the lower deuterium content and therefore lower source temperature of thermal water compared to nonthermal water (Welch and others, 1981, p. 85-92; Flynn and Buchanan, 1993, p. 63-64): (1) modern recharge (<10,000 years before the present--B.P.) at higher altitude than recharge for nonthermal water; and (2) "paleo-recharge" (>10,000 years B.P.), not necessarily at higher altitude than recharge for modern nonthermal water, but at a time when deuterium was depleted relative to modern-day values. In evaluating these two explanations, evidence bearing on the age of the thermal water obviously is of vital importance. The age of the thermal water may be inferred from (1) radiocarbon (^{14}C) dating, (2) stable-isotopic evidence, and (3) estimation of the time required for the water to circulate through the hydrothermal flow system.

Reliable ^{14}C ages have not been determined for thermal water in SGV. However, apparent ^{14}C ages of some thermal waters elsewhere in Nevada range from 11,000 to 28,200 years B.P. (Ingraham and Taylor, 1991, p. 78). The ^{14}C age of thermal water in the Upsal Hogback hydrothermal system in the Carson Desert 150 km southwest of SGV is reported to be about 25,000-35,000 years B.P. (Olmsted and others, 1984, p. 146). If the

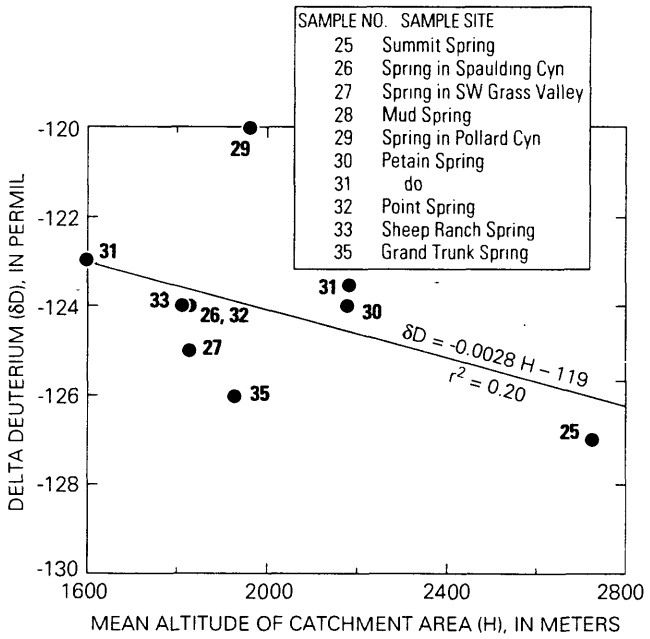

Figure 17. Relation of deuterium composition to altitude for nonthermal springs.

hydrothermal system in SGV resembles those elsewhere in Nevada, the radiocarbon evidence therefore suggests a late Pleistocene (>10,000 years B.P.) age for the deeply circulating thermal water.

Stable-isotopic evidence discussed earlier indicates a colder source for the thermal than for the nonthermal ground water in SGV. Such a source could be precipitation at a higher average altitude than the precipitation recharging the nonthermal ground water. The low chloride concentrations of the waters from Clear Creek and Summit Spring suggest the possibility that the thermal water represents deep percolation of nonthermal water in the mountains, perhaps derived from precipitation at high altitudes. On the basis of precipitation sampling in Dixie Valley, 100 km south-southwest of southern Grass Valley, Jacobson and others (1983) estimated a decrease of about 4.2‰ in δD per 305 m increase in altitude. If such a decrease occurs in the SGV area, present-day precipitation at high altitudes in the mountains could be sufficiently depleted in deuterium to be a source of thermal water.

Figure 17 is a plot of delta deuterium values versus mean altitude of catchment area for 11 samples from 9 nonthermal springs in the SGV area. The mean altitude of the catchment area for each spring is estimated as the arithmetic mean of the altitude of the spring and that of the highest point in the surface drainage area above the spring. Such a measure, although very approximate, is believed to more closely reflect average precipitation supplying the spring water than the altitude of the spring itself. As shown in figure 17, delta deuterium appears to decrease with altitude, although the correlation is weak ($r^2 = 0.20$)[3]. The least-squares regression is

$$\delta D = 0.0028H - 119 \qquad \textbf{(10)}$$

where H is mean altitude of the catchment area above the spring, in meters. This corresponds to a decrease in δD of only 0.8‰ per 305 m, instead of the 4.2‰ per 305 m reported by Jacobson and others (1983) for Dixie Valley.

Summit Spring, because of its high altitude, is of critical importance in defining the δD vs. altitude relation of equation 10. The small catchment area for this spring suggests the possibility that the isotopic composition of the ground water

[3] If the somewhat questionable delta deuterium value for the spring in Pollard Canyon (sample 29, for which no corresponding oxygen-18 value was obtained) is omitted, the least-squares linear regression becomes δD = 0.0026 H - 119 and r^2 increases to 0.43.

feeding the spring fluctuates more in response to fluctuations in the composition of the precipitation than it does at most locations. Therefore, the single analysis of the spring water probably does not represent a long-term average composition. If the long-term average δD composition were lighter, then δD would show a greater decrease with increasing altitude, and the possibility would remain that present-day precipitation at high altitudes in the SGV area could be the source of the thermal water.

To summarize, although the stable-isotopic data do not rule out the possibility of modern (<10,000 years B.P.) recharge for the thermal water, radiocarbon age data and estimates of ground-water circulation time, discussed later, support a greater age. The lighter deuterium composition of the thermal water compared to local nonthermal water could be due to recharge of the thermal water during a period of colder precipitation. Stable-isotopic data from core-drilling in the Greenland ice cap (Dansgaard and others, 1969, p. 379) and in the Antarctica ice cap (Epstein and Gow, 1970) showed significant shifts in hydrogen- and oxygen-isotopic composition between about 11,000 and 8,000 years B.P. This time is correlated with the last major retreat of continental glaciers. An age of 10,000 years B.P. is generally regarded as the end of the last major glacial epoch (Wisconsin). Since 10,000 yrs B.P., fluctuations in climate indicated by stable-isotopic composition have occurred, but these are generally minor in comparison with the change at the end of the Wisconsin.

The timing of the Pleistocene-Holocene transition corresponds to a warming trend coupled with increasing aridity in the northern Basin and Range region beginning about 9,000 years ago, as evidenced by changes in water levels of Pleistocene Lake Lahontan (Benson, 1978) and Searles Lake in southeastern California (Phillips and others, 1994). Reconstruction of late Pleistocene climate in the Great Basin using material in pack-rat middens indicates colder and wetter conditions from about 40,000 to 10,000 years B.P. (Wells, 1983; Spaulding, 1985). Using stable-isotopic and radiocarbon data from a macrofossil assemblage from a midden at an elevation of 1,800 m in southern Nevada, Spaulding (1985, table 10) determined the following pattern for the interval 45,000 to 10,000 years B.P., where dTs is difference in summer temperature from the present, in °C, dTw is difference in winter temperature, dTavg is difference in average annual temperature, and dP is difference in average annual precipitation from the present, in percent.

Years B.P.	dTs	dTw	dTavg	dP
45,000	-2 to -3	---	-1 to -3	0
38,7000	---	---	-1 to -2	+10 to +20
37,8000	---	---	-5	+20
30,000	---	---	-3 to -6	+10 to +25
18,000	>-6	-7 to -8	0	+30 to +40
10,000	-1 to -2	+1 to +2	---	+1 to +20

Spaulding's (1985) inferred differences in average annual temperature range up to 7°C colder at 18,000 years B.P., whereas the difference in temperature of thermal-water recharge in SGV is estimated to be only 1-2°C. If, as seems likely, the thermal water in SGV was recharged at some time during the interval 45,000 to 10,000 years B.P., then perhaps it is either older than 38,000 years or younger than 18,000 years B.P.

Colder and wetter average conditions did not

characterize all areas. In the mid-continent region of the United States, paleoclimatic conditions deduced from ancient-wood cellulose indicate a climatic shift at about 9,500 years B.P., although deuterium was *less* depleted during the interval 22,000- 9,500 years B.P., indicating *warmer* precipitation (Yapp and Epstein, 1977, p. 339). Within the Great Basin, warmer recharge is also suggested in some areas along the margins of Lakes Lahontan and Bonneville, where chloride concentrations in thermal fluids are high (Flynn and Buchanan, 1993, p. 66).

Whatever the temperature differences may have been, the evidence seems clear that the climate in the Great Basin before 10,000 years ago was wetter than the present. The implications for the amount of ground-water recharge that occurred in SGV are significant. Table 9 is based on the same assumptions as those in table 7, the difference being that the average annual precipitation is assumed to have been 25 percent greater than the present--the approximate average increase estimated for the period 40,000 to 10,000 years B.P. by Spaulding (1985, table 10). The proportions of precipitation that constitute recharge are assumed to have the same relations to the average annual precipitation as those postulated by Maxey and Eakin (1951) (see table 7). A 25 percent increase in precipitation results in a more than 140 percent increase in recharge, from an estimated 4.4 hm^3/yr present rate (table 5) to 10.8 hm^3/yr rate (table 9) for paleorecharge. This estimated increase may, in fact, be conservative. If temperatures also were lower >10,000 years B.P., the ratio of recharge to precipitation for a given precipitation rate would have been higher than present because of decreased evapotranspiration. Present discharge rate of thermal

TABLE 9. Estimate of ground-water recharge in the southern Grass Valley drainage basin during the period 40,000-10,000 years before the present.

[Based on an empirical method developed by Maxey and Eakin (1949), as adapted to Grass Valley by Cohen (1964); modified on the basis of an assumed precipitation 25 percent greater than the present--see Spaulding (1985, p. 50). See table 5 for an estimate of present ground-water recharge in the southern Grass Valley drainage basin]

Altitude zone (m)	Area (km^2)	Precipitation (mm/yr)	Precipitation (hm^3/yr)	Recharge (% of precip.)	Recharge (mm/yr)	Recharge (hm^3/yr)
2,438-2,695	0.5	660	0.33	36	240	0.12
2,134-2,438	8.1	550	4.5	26	140	1.13
1,829-2,134	79.8	420	34	14	59	4.7
1,524-1,829	258	310	80	5.5	17	4.4
1,369-1,524	230	190	44	1.0	1.9	.44
Total or average	**576**	**280**	**163**	**6.6**	**19**	**10.8**

water at LHS therefore reflects a higher past recharge rate, so that the long-term trend in discharge probably is now decreasing.

The third type of evidence indicating a late Pleistocene age of the thermal water in SGV is based on estimates of travel time required for the thermal water to be recharged, presumably at some place in the mountains, to move downward and probably laterally at a depth sufficient to attain a high temperature, and then to move upward in a fault zone to discharge at LHS or into shallow aquifers in the valley fill. This concept is developed in a later section, "Models of Basin and Range hydrothermal systems." Suffice it to say here that calculations based on reasonable as sumptions of system configuration and flow rates indicate ages of greater than 10,000 years for the water in other, presumably similar, hydrothermal systems in the region. In the northern Dixie Valley hydrothermal system 100 km south-southwest of LHS, Karst and others (1988), using a three-dimensional mixing-cell flow model, calculated ages ranging from 13,600 to 19,500 years B.P. for the water in the lower tier of cells representing the thermal flow system. Olmsted and others (1984, p. 134-137) estimated time of travel of hydrothermal fluid through the Soda Lakes system in the western Carson Desert 150 km southwest of LHS to be in the range of 3,400-34,000 years B.P. on the basis of assumed piston or displacement flow. The apparent radiocarbon age of 25,000-35,000 years B.P. cited earlier for the thermal water in the Upsal Hogback system immediately to the northeast suggests an age closer to 34,000 than to 3,400 years B.P. for the thermal water in the Soda Lakes system.

To summarize, the thermal water discharging at LHS probably is at least 10,000 years old and may be 40,000 years old or more. It was recharged at places not well known but probably in the Sonoma and Tobin Ranges and possibly in the East Range at a time when precipitation was perhaps 25 percent higher and average temperature 1-2 °C lower than at present. The long-term trend in discharge rate at LHS probably is decreasing.

Chemical Geothermometry

Temperatures of hydrothermal reservoirs or aquifers not penetrated by drilling can be estimated using chemical geothermometers. Chemical geothermometers are mathematical equations that relate the chemical or stable isotope composition of a water sample to the source temperature of the water. These geothermometers are based on the principle that the chemical or isotopic compoosition of water acquired in a deep, hot environment tends to be preserved as the water rises, cools, and is sampled at a spring or shallow well.

Three principal types of geothermometers are commonly used: (1) silica geothermometers, which are based on the temperature-dependent solubility of silica minerals such as quartz; (2) cation geothermometers, which are based on empirically derived relations of temperature to the proportions of two or more dissolved cations; and (3) isotope geothermometers, which are based on the temperature-dependent fractionation of stable isotopes between water and one of the dissolved constituents.

The geothermometer temperature estimates are affected by one or more of the following factors: (1) partial reequilibration with aquifer materials after the water left a hotter source; (2) mixing, generally of hotter water with cooler water

TABLE 10. Chemical geothermometry for thermal water at Leach Hot Springs.

[Chemical geothermometer temperatures calculated using formulas given in table 11. The chemical quartz and sodium-potassium-calcium temperatures are based on formulas given in Fournier (1981, p. 114). The sodium-potassium and the potassium-magnesium temperatures are based on the method of Giggenbach (1988). The sulfate-oxygen-isotope data for orifice 13 and description of the method are from Nehring and Mariner (1979). The data for orifices 1 and 22 were determined by Cathy Janik, U.S. Geological Survey, Menlo Park, CA.]

			Temperature, in degrees Celsius								
Sample number	Sample site	Date of sample (yr mo da)	Sample at collection point	Quartz conductive	Quartz adiabatic	Sodium-potassium	Potassium-magnesium	Sodium-potassium-calcium Uncorrected	Sodium-potassium-calcium Mg-corrected	Sulfate-oxygen-isotope conductive	Sulfate-oxygen-isotope adiabatic
1	Orifice 1	77 06 ...	85	145	139	206	102	169	144	-----	-----
2	Do	78 09 14	86	140	135	208	100	170	136	151	143
3	Do	83 12 28	86.5	150	143	204	99	166	137	-----	-----
4	Orifice 12	79 03 20	92	145	139	223	143	182	182	-----	-----
5	Orifice 13	72 06 17	92	155	147	216	111	176	162	170	159
6	Do	83 12 28	95.5	159	151	210	106	172	153	-----	-----
7	Orifice 15	78 12 13	92	173	162	261	123	195	194	-----	-----
8	Orifice 22	77 06 ...	81	137	133	206	99	168	135	-----	-----
9	Do	78 09 14	81	134	130	200	94	163	126	163	154
10	Do	83 12 29	84.5	145	139	210	99	171	136	-----	-----

having a different source; (3) nonattainment of equilibrium with appropriate mineral phases; (4) factors other than temperature affecting equilibrium with mineral phases; or (5) analytical variations. In order to minimize the effects of some of these factors, especially the first two, water samples from the thermal wells are omitted; only the waters sampled at LHS are considered here.

The source temperature of thermal water sampled at LHS is estimated using all three types of geothermometers described above (see table 10). The equations used in the calculations are given in table 11. The quartz-silica (conductive and convective) and the sodium-potassium-calcium geothermometers use the equations given by Fournier (1981, table 4.1). The sodium-potassium and the potassium-magnesium geothermometers use the equations given by Giggenbach (1988). The sulfate-oxygen-isotope ($^{18}O[SO_4\text{-}H_2O]$) geothermometer uses the experimental data of Lloyd (1968), with refinements by McKenzie and Truesdell (1977).

For the quartz-silica geothermometers, the conductive temperatures are best applied to the non-boiling orifices (1 and 22), whereas the appropriate source temperatures are believed to be

TABLE 11. Equations used for geothermometer temperature estimates given in table 10 for thermal water at Leach Hot Springs.

[Chemical symbols represent concentrations of those constituents, in milligrams per kilogram (liter)]

Quartz, conductive, no steam loss (Fournier, 1981, table 4.1):

$$T_{°C} = \frac{1309}{5.19 - \log SiO_2} - 273.15$$

Quartz, adiabatic, maximum steam loss (Fournier, 1981, table 4.1):

$$T_{°C} = \frac{1522}{5.75 - \log SiO_2} - 273.15$$

Sodium-potassium (Giggenbach, 1988):

$$T_{°C} = \frac{1390}{1.75 - \log (K/Na)} - 273.15$$

Potassium-magnesium (Giggenbach, 1988):

$$T_{°C} = \frac{4410}{14 - \log (K^2/Na)} - 273.15$$

Sodium-potassium-calcium (Fournier, 1981, table 4.1):

$$T_{°C} = \frac{1647}{\log (Na/K) + \beta [\log (\sqrt{Ca}/Na) + 2.06] + 2.47} - 273.15$$

$$\beta = 1/3 \text{ for } \sqrt{Ca}/Ca < 1 \text{ also } T_{NaKCa}(\beta = 4/3) > 100°C$$

$$\beta = 4/3 \text{ for } \sqrt{Ca}/Na > 1 \text{ also } T_{NaKCa}(\beta = 4/3) < 100°C$$

R for magnesium correction to sodium-potassium-calcium geothermometer:

$$R = \frac{Mg}{Mg + Ca + K} \times 100$$

Magnesium correction to sodium-potassium-calcium geothermometer for R<5:

$$-T_{mg} = -1.03 + 59.971 \log R + 145.05 (\log R)^2 - 36711 (\log R^2)/T - 1.67 \times 10^7 (\log R/T^2)$$

Magnesium correction to sodium-potassium-calcium geothermometer for R = 5-50:

$$-T_{mg} = 10.66 - 4.74515 R + 325.87 (\log R)^2 - 1.032 \times 10^5 (\log R)^2/T - 1.968 \times 10^7 (\log R)^2/T^2 + 1.605 \times 10^7 (\log R)^3/T^2$$

TABLE 11. Equations used for geothermometer temperature estimates given in table 10 for thermal water at Leach Hot Springs -- **continued.**

Sulfate-oxygen-isotope (Nehring and Mariner, 1979):

$$T_{°C} = \sqrt{\frac{2.88 \times 10^6}{1000 \ln \alpha + 4.1}} - 273.15$$

$$\alpha = \frac{1000 + \delta^{18}O_{(HSO_4)}}{1000 + \delta^{18}O_{(H_2O)}}$$

---

closer to the adiabatic values for orifices 12 and 13, which are at or near boiling temperature (table 10). Orifice 15, also boiling, presents a special case. As discussed previously, its water's mildly acid-sulfate composition and comparatively low concentration of dissolved solids indicate the presence of steam condensate. This probably precludes application of the quartz-silica (and other) geothermometers; accordingly, temperatures estimated for this orifice are not considered in the following discussion. All the other quartz temperatures at LHS are believed to be minimum rather than most likely values because of mixing with nonthermal water and (or) precipitation of silica (sinter). Excluding orifice 15, estimates of the source temperature based on the quartz-silica geothermometer range from 134 to 151 °C and average 143 °C.

Cation geothermometers are useful where mixing is suspected, because they are less affected by dilution than the silica geothermometers. However, one of the requirements for the successful application of the cation geothermometers is the attainment of water-rock equilibrium in the geothermal reservoir.

A triangular diagram was proposed by Giggenbach (1988, p. 2758) for evaluating the degree of water-rock equilibrium attained by geothermal waters. The diagram indicates the proportions of magnesium, sodium, and potassium, normalized so that the square-root of the magnesium concentration, in milligrams per liter, is at one apex, the sodium concentration, divided by 1,000, at the second, and the potassium concentration, divided by 100, at the third apex (see fig. 18).

As shown in figure 18, the waters from LHS are substantially less equilibrated than the waters from several other hydrothermal systems in northern and central Nevada. At Beowawe, Desert Peak, and Soda Lakes (DH14), where potassium-magnesium temperatures equal or approach sodium-potassium temperatures, indicating that full or nearly full equilibrium is attained, the geothermometer temperatures have been confirmed by drilling.

In contrast, at LHS, the samples from orifices 13 and 22 represent immature waters and that from orifice 12 represents a partly equilibrated or mixed water according to the criteria of Giggenbach (1988). For such waters, the sodium-

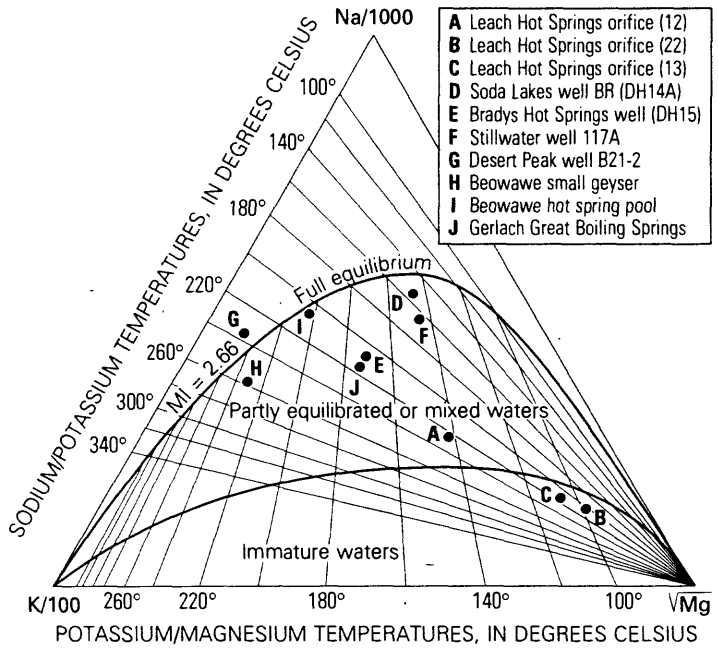

Figure 18. Triangular diagram for evaluating sodium-potassium and potassium-magnesium geothermometer temperatures of selected geothermal waters in northern Nevada. This diagram and the geothermometer temperatures are those of Giggenbach (1988). The chemical symbols at the corners of the diagram represent concentrations of those constituents, in milligrams per liter; each corner represents 100 percent of that component. Partly equilibrated or mixed waters are defined as having a maturity index (MI) between 2.00 and 2.66; immature waters have a MI less than 2.00.

potassium geothermometer is especially difficult to apply, and the potassium-magnesium geothermometer probably indicates only the temperature of the most recent reequilibration of the thermal water rather than the temperature of a deep source. Although the high temperatures of 200-223 °C indicated by the sodium-potassium geothermometer (table 10) cannot be ruled out, such temperatures are believed to be less likely than the lower temperatures indicated by some of the other geothermometers.

The sodium-potassium-calcium geothermometer was developed by Fournier and Truesdell (1973) for calcium-rich waters that indicate anomalously high temperatures by the sodium-potassium method (Fournier, 1981, p. 119). The temperatures indicated by the sodium-potassium-calcium geothermometer are too high if the thermal water is diluted by mixture with more than 70-80 percent of less saline nonthermal water, or if calcium is lost by precipitation resulting from boiling (Fournier, 1981, p. 119-120). However, neither of these factors appears to be significant at LHS.

The sodium-potassium-calcium method also gives anomalously high results for waters high in magnesium. A correction for magnesium was devised by Fournier and Potter (1979) to deal with this difficulty. However, such a correction is inappropriate if, as may be the case at LHS, a significant part of the magnesium content of the water results from chemical reactions after the thermal fluid leaves the reservoir (see Fournier, 1981, p. 120-121).

At LHS, the uncorrected sodium-potassium-calcium geothermometer indicates temperatures ranging from 163 to 182°C (table 10). The magnesium-corrected temperatures generally are somewhat lower, 126-162°C, and the average, 146°C, is only 3°C higher than the average for the quartz-silica geothermometer. This close agreement may be fortuitous: the quartz method probably yields somewhat low values as a result of mixing with nonthermal water and (or) the precipitation of silica during upflow, and part of the magnesium in the spring water may have been added after the thermal water left the deep source, as discussed above. As a result, both the quartz-silica and the magnesium-corrected sodium-potassium-calcium temperature estimates may be too low. The uncorrected sodium-potassium-calcium geothermometer temperature estimates may therefore be more valid than the magnesium-corrected estimates.

The third type of geothermometer--the sulfate-oxygen-isotope method--indicates temperatures ranging from 151 to 163°C for three samples from orifices 1, 13, and 22 (the conductive values are most appropriate for 1 and 22, whereas the adiabatic is more appropriate for orifice 13). These temperatures are somewhat higher than those indicated by the quartz-silica and magnesium-corrected sodium-potassium-calcium methods but are the same to somewhat lower than those indicated by the uncorrected sodium-potassium-calcium method.

Considering all the evidence discussed above, the geothermometers indicate thermal-aquifer temperatures of 150-180°C or possibly higher for the LHS system. The higher temperatures indicated by some of the cation geothermometers may be more reliable than the quartz geothermometer estimates because the cation geothermometers are less affected by mixing with nonthermal water.

SUBSURFACE TEMPERATURE AND HEAT FLOW

Temperature Distribution in Valley Fill

Temperature-depth profiles were measured in more than 100 test wells during the years 1976-80. The location of these wells, which constitute most of the wells drilled during the present study, is shown in figure 19. Most wells were less than 170 m deep, whereas the fill attains maximum thicknesses of 1,000-1,800 m in the east-central part of the valley (fig. 6). Therefore, temperature distribution with depth throughout much of SGV is well defined for only the uppermost fill.

Temperature gradients in unsaturated fill are greater than in underlying saturated fill. However, unsaturated deposits constitute only a small fraction of the total thickness of fill at most places and are not discussed below.

Variations in temperature gradient within the upper part of the saturated fill that appear to be due chiefly to variations in thermal conductivity were observed at many well sites, such as DH3, DH4, DH6, and DH13 (fig. 20). Significant hydrologic effects on temperature gradient were observed at several other sites, such as G14 (fig. 20), QH3, and G105, (fig. 21). Poorly documented effects of lateral flow of thermal water from the Leach Hot Springs area may exist near the Aminoil well and DH7, as discussed later.

As in most of the wells that penetrate only

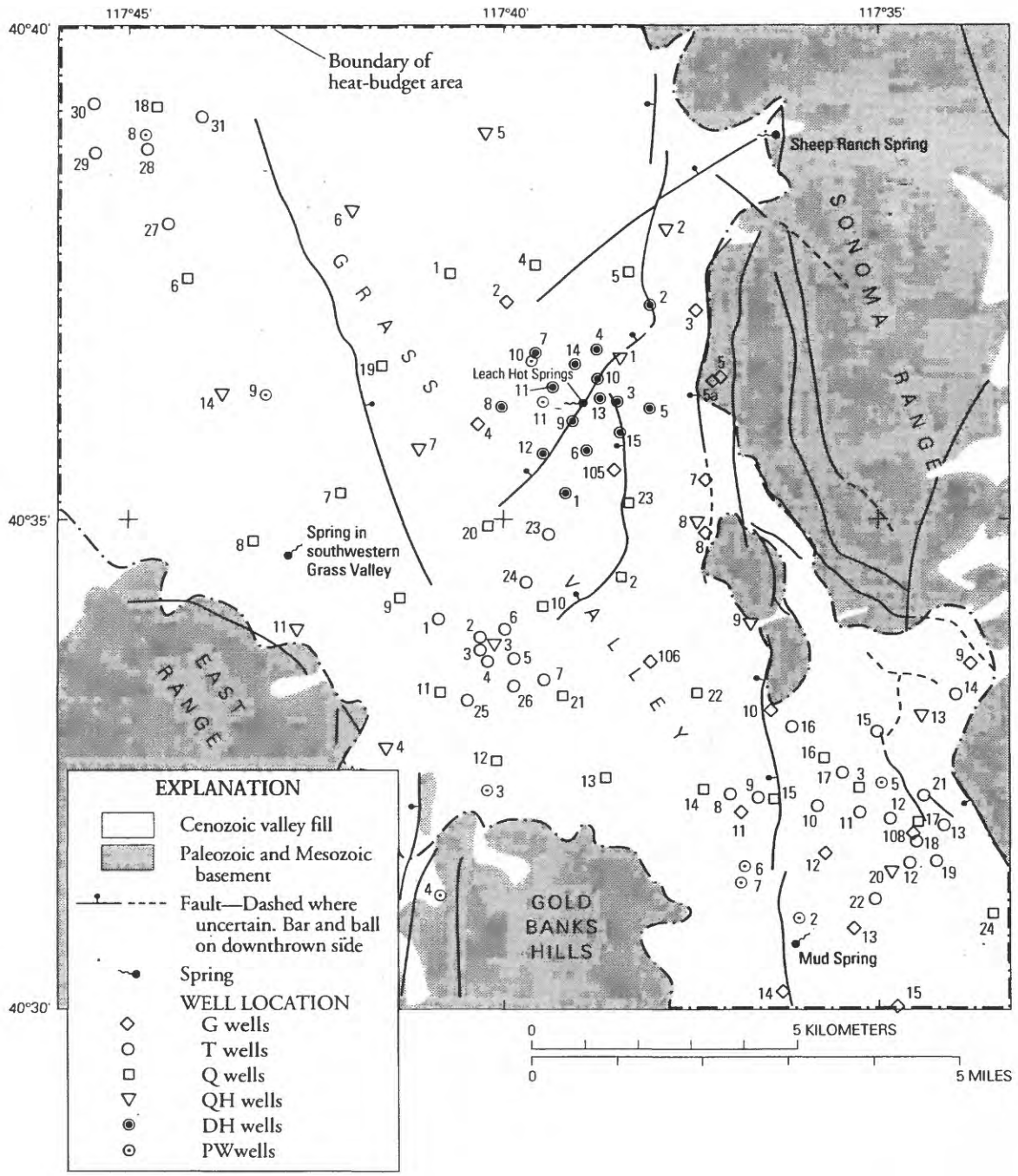

Figure 19. Heat-budget area and location of text wells used for temperature measurement. Dashed-and-dotted line indicates margin of heat-budget area.

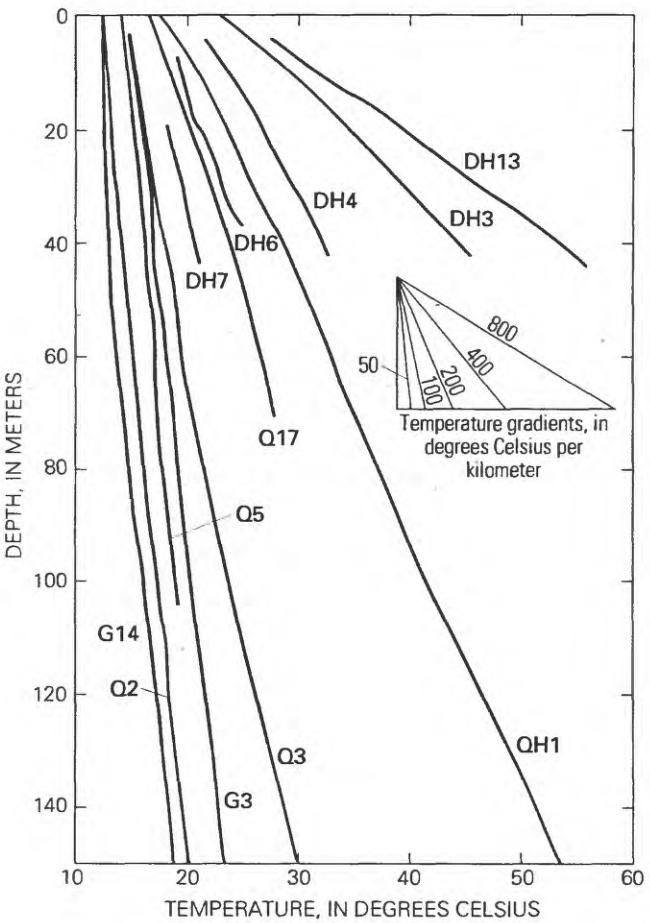

Figure 20. Temperature-depth profiles in selected wells. Data for wells are given in tables A1 and A4; locations are shown in figure 19.

the uppermost fill, temperature gradients in six of the nine wells that either bottom in basement or penetrate more than one half of the fill (QH4A, QH2A, G10, G3, G108, and QH1A) exhibit minor changes apparently related to changes in thermal conductivity (fig. 21). Vertical heat transfer by conduction probably predominates at these well sites. Temperature gradients in the fill at many places may decrease with depth because of a presumed downward increase in thermal conductivity. The Tertiary and Quaternary alluvium and, especially, the Tertiary sedimentary rocks in the lower part of the fill, probably have higher density and lower porosity and therefore higher thermal conductivity than the overlying Quaternary alluvium (p. 15).

Evidence for a decrease in gradient with depth is provided by data from the Aminoil well (fig. 22), although some of the data are difficult to interpret. All the data discussed below are from Wilde and Koenig (UURI, 1981g); some of their interpretations have been modified by the present writers.

Before completion of the drilling, 20-inch (508-mm) surface casing was cemented to a depth of 97.5 m and 13-3/8-inch (340-mm) casing was cemented to a depth of 823 m; drilling then continued as open hole to a final depth of 2,611 m. After completion in June 1980, three temperature logs were made in the well. These logs were finished 7, 51-1/2, and 89 hours after mud circulation ceased (UURI, 1981g). The first log consisted of twelve 10-minute stops from 1,524 m to the bottom at 2,611 m, the second log involved temperature readings at the same depths as the first, and the final log consisted of a continuous traverse from 152 m to the bottom, which by then had filled in to a depth of 2,600 m.

Temperatures below a depth of 1,524 m increased only a minor amount between the 51-1/2 and 89-hour runs. Therefore, the 89-hour log probably represents near-equilibrium conditions below 1,524 m (fig. 22). Below 1,524 m, equilibrium temperatures were estimated from the three temperature logs using a method of extrapolation to infinite time described by Parasnis (1971). The equilibrium temperatures shown in figure 22 ranged from 0.1 to 1.6°C higher than the 89-hour temperatures.

The temperature-gradient data are puzzling. In the fill above 1,402 m (Tertiary sedimentary

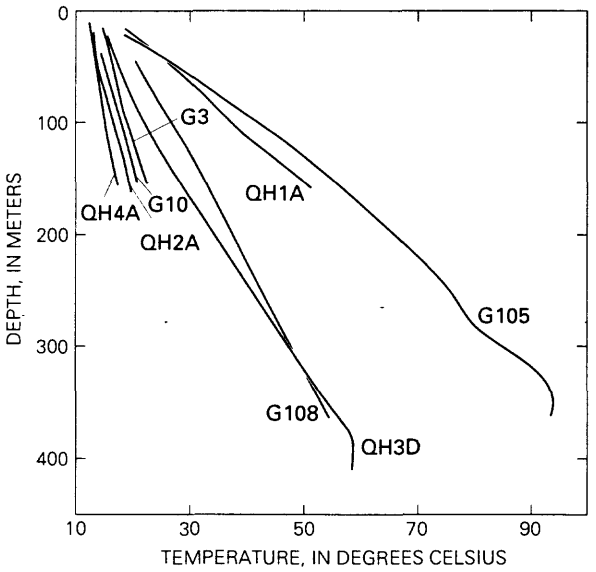

Figure 21. Temperature-depth profiles in wells penetrating all or a substantial thickness of valley fill.

rocks, Tertiary and Quaternary alluvium, and Quaternary alluvium), an increase in thermal conductivity associated with the inferred increase in density of the fill with depth could account for at least part of the apparent decrease with depth of temperature gradient from 46 °C/km for the interval 152-372 m to 19 °C/km for the interval 933-1,402 m. Also, the marked change in gradient at 933 m corresponds reasonably well with the inferred contact of Tertiary sedimentary rocks and Tertiary and Quaternary alluvium at 991 m.

However, temperatures in the well for the upper part of the fill seem too high and temperature gradients for all the fill too low. Upward extrapolation of the 152-372 m temperature gradient gives a surface temperature of 45 °C--much higher than the 11.5 °C indicated by data from shallow test wells. Moreover, temperature-depth data from well DH7, 0.2 km north of the Aminoil well, also suggest that the measured temperatures in the valley fill, especially the upper part, in the Aminoil well are much too high. The temperatures measured in DH7 were less than 20 °C, but the gradient from 29-49 m in that well was 112 °C, which is much greater than the 46 °C/km measured for the 152-372 m interval in the Aminoil well (see fig. 22).

Possible explanations for the high temperatures and low gradients in the upper part of the Aminoil well include: (1) upward flow of water in the well above a depth of 1,402 m; (2) lateral flow of thermal water in the formation(s) below the 49-m depth of DH7 and above 152 m in the Aminoil well, which would decrease the temperature gradient below the aquifer carrying the warm water and increase the gradient above the aquifer; and (3) upward ground-water flow across the bedding of the valley fill, which would result in a downward decrease in temperature gradient.

The first explanation--upward flow of water in the well--could account for the temperatures observed below the cased depth of 823 m but is implausible for the cased section above that depth. In order for upward flow to occur within the casing, breaks in the casing where the flow could exit to the formation would have to exist somewhere above a depth of 152 m. No evidence for such breaks was reported (UURI, 1981g). However, water could flow upward in the annulus between the casing and the walls of the drill hole. Although the casing was cemented, breaks or places where the cement did not completely fill the annulus could allow upward flow of warm water.

The second explanation--lateral flow of warm water in an aquifer between depths of 49 and 152 m--cannot be ruled out. There are serious difficulties with this mechanism, however. The minimum temperature gradient above such an

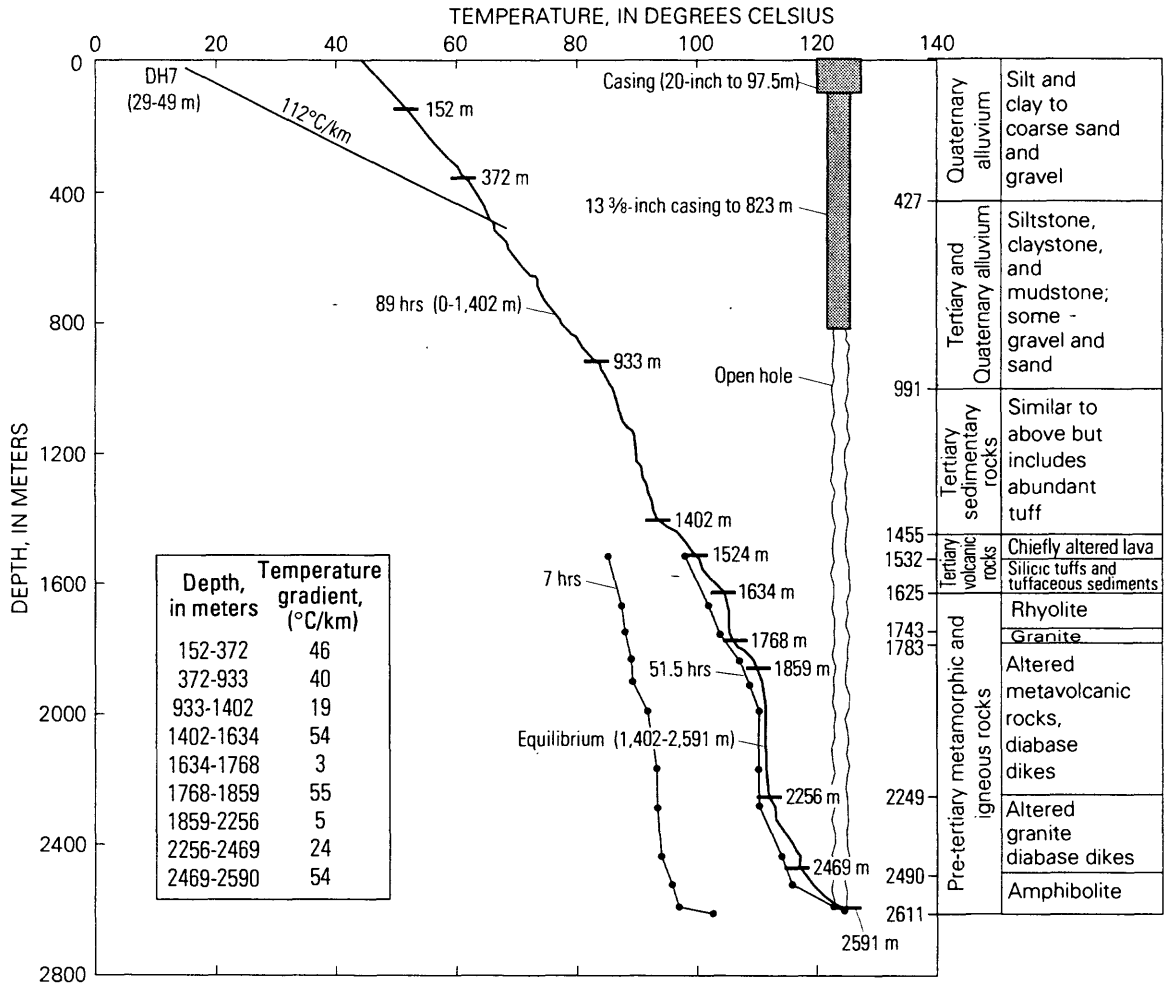

Figure 22. Temperature-depth profiles and generalized log of Aminoil USA 11-36 well.

aquifer would exceed 260°C/km, which is more than double the 112°C/km measured for the 29-49 m interval in well DH7. The high conductive heat flow that would be associated with such a gradient does not fit the heat-flow pattern established by several other shallow test wells northwest of Leach Hot Springs (See fig. 27).

The third explanation--upward flow of warm water across the bedding in the alluvium--is less plausible. The flow rate required to cause such a marked curvature in the temperature-depth profile, as discussed below, would be exceedingly unlikely in deposits having low vertical permeability.

In summary, a convincing interpretation of the temperature-depth profile opposite the valley fill in the Aminoil well is not possible with information at hand. In any case, it is doubtful that the measured temperatures, at least in the upper part of the fill, represent formation temperatures outside the well. However, below a depth of 1,524 m, the calculated equilibrium temperatures are believed to indicate formation temperatures outside the well.

Temperature gradients in the fill do not everywhere decrease with depth, as they may do

near the Aminoil well, and also in well G105, 1.7 km south-southeast of Leach Hot Springs. Several wells record a nearly uniform gradient to depths exceeding 150 m, and, in wells QH3D and G106 in the south-central part of the valley, the gradient increases gradually with depth. The downward increase in gradient at QH3D and G106 may indicate downward ground-water flow, across the bedding in the valley fill. Supporting evidence consists of the downward hydraulic gradient observed in the fill between depths of 64 and 154 m at QH3 (p. 37).

Vertical ground-water flow rates can be estimated by the curvature of the temperature-depth profiles, using the methods of Bredehoeft and Papadopulos (1965), Sorey (1971), or Lachenbruch and Sass (1977). These methods either assume constant thermal and hydraulic conductivities with depth (and also constant vertical hydraulic gradient) or, in the more general case, that thermal conductivity is not constant, but that the changes in heat flow with depth are known. In the latter case, where vertical ground-water flow occurs, heat flow changes with depth according to the relation given by Lachenbruch and Sass (1977, p. 642, equation 10):

$$q1/q2 = e^{z/s} \qquad \textbf{(11)}$$

where q1 is heat flow at a shallower depth (z_1), q2 is heat flow at a greater depth (z_2), z is $z_2 - z_1$, and s is a characteristic vertical distance having the sign of v, the vertical ground-water flow. The term s is calculated from the expression

$$s = k/\Delta' c' v \qquad \textbf{(12)}$$

(Lachenbruch and Sass, 1977, p. 642 equation 11a) where k is thermal conductivity, Δ' is density of the moving fluid (water), c' is heat capacity of the moving fluid, and v is vertical ground-water flow rate.

Because both Δ' and c', for practical purposes, are equal to unit in cgs units, equation 12 simplifies to

$$s = k/v \qquad \textbf{(13)}$$

or, in S.I. units used in this report,

$$s(m) = 7{,}574\ k(W/m.K)/v(mm/yr) \qquad \textbf{(14)}$$

Rearranging terms in equation 11 to solve for q1, the heat flow at the shallower depth, the expression becomes

$$q1 = q2e^{z/s} \qquad \textbf{(15)}$$

and, incorporating equation 15 with the units used in equation 14,

$$q1 = q2e^{zv/7{,}574k} \qquad \textbf{(16)}$$

Rearranging terms in equation 16 to solve for v, the expression becomes

$$v = \frac{7{,}574k \ln q1/q2}{z} \qquad \textbf{(17)}$$

where q1 is heat flow (mW/m^2) at shallower depth, q2 is heat flow (mW/m^2) at greater depth, k is harmonic-mean thermal conductivity (W/m.K) for depth interval s, z is depth interval (m) between shallower and greater depths, and v is vertical Darcian flow rate of ground water (mm/yr).

Three wells that have fairly uniform changes in temperature gradient and estimated heat flow with depth are QH3D, G105, and G106 (table 12). Heat flows for different depth intervals are based on measured temperature gradients and estimated thermal conductivities, and the vertical ground-water flow rates (Darcian velocities) are computed using equation 17 above.

As mentioned above, downward ground-water movement at QH3D is also indicated by a downward component of the hydraulic gradient. The computed vertical Darcian velocities of -30 and -34 mm/yr for the intervals encompassed by the upper and lower pairs of depth intervals, respectively (table 12), are reasonable, and their close agreement suggests a uniform downward velocity throughout most of the valley fill, which is 378 m thick at this location. It should be noted, however, that the elevation of the water level in the pre-Tertiary basement is higher than that in wells QH3B and QH3C, which are screened at depths of about 153 and 64 m, respectively, in the middle and upper parts of the valley fill. This indicates a potential for upward flow from the basement into the lower part of the fill--the opposite direction from the downward flow in most of the fill. The basal part of the fill therefore appears to be a hydraulic sink at this location.

Downward ground-water movement is indicated also at well G106, 2.8 km east of QH3D (fig.10). Computed vertical Darcian velocities at G106 range from -32 to -46 mm/yr, similar to those at QH3D (table 12). However, as discussed in the next section, site QH3 is near the center of a near-surface heat-flow high, whereas site G106 is at a heat-flow low. Actually, the near-surface heat flow at both sites is substantially less than it would be without the convective component associated with the downward ground-water flow (see equation 16 above). The low near-surface heat flow and associated low temperature gradient at G106 (and also at nearby shallow wells) were the basis for the low temperatures estimated by Welch and others (1981, figs. 17 and 18) at the base of the fill in the south-central part of the valley.

The temperature-depth data for well G105T (table 14) illustrate the opposite case from wells QH3D and G106: the temperature gradient and conductive heat flow decrease with depth, indicating probable upward ground-water flow. The computed vertical Darcian velocity is not nearly constant with depth as it is at QH3D and G106 but, instead, appears to increase with depth. A possible explanation for the increase is that the upward ground-water flow encounters an aquifer somewhere between depths of 50 and 100 m, where much of the flow is diverted laterally.

Unlike the procedure of Welch and others (1981, p. 103-112), in which measured temperature gradients were extrapolated linearly in the lower part of the fill at most well sites, changes in gradient with depth are used in the extrapolation at well sites within about 1 km of the nine wells for which such information is available.

Temperatures at the basement-fill boundary are estimated from the extrapolated temperature gradients in wells and the depth to basement computed from gravity and seismic data (see table 13 and fig. 23). The data are too sparse to define lines of equal temperature at the basement-fill boundary (fig. 23), as was attempted by Welch and others (1981, p. 114). However, the temperatures in the center of the valley between the temperature highs at Leach Hot Springs and Panther Canyon estimated by Welch and others (1981, fig. 17) clearly are too low: the probable temperature at the site of well G106 within the low-temperature area is at least 84°C (table 13 and fig. 23), not 50°C as estimated by Welch and others (1981, p. 112). The 84°C may be a minimum estimate; if the downward ground-water flow indicated above a depth of 450 m at this site continues below that depth, the temperature at the

TABLE 12. Change in heat flow with depth and computed vertical ground-water flow rate (Darcian velocity) in wells QH3D, G105, and G106.

Depth (m)	Temperature gradient (°C/km)	Estimated thermal conductivity (W/m.K)	Heat flow (mW/m^2)	Computed vertical Darcian velocity (mm/yr)
QH3D				
64-125	109	1.8	200	
				-30
125-244	122	2.0	240	
				-34
244-366	140	2.2	310	
G105				
20-50	290	1.4	410	
				+12
100-150	264	1.4	370	
				+42
236-270	141	1.6	230	
G106				
50-150	25	1.55	39	
				-32
150-250	32	1.60	51	
				-46
250-350	45	1.65	74	
				-37
350-450	58	1.70	99	

TABLE 13. Temperature gradient in test wells and estimated temperature at base of valley fill.
[The symbol m in the last two columns indicates measured values]

Test well	Reference depth (m)	Temperature at reference depth (°C)	Depth range (m)	Measured temperature gradient (°C/km)	Extrapolated temperature gradient (°C/km)	Estimated depth to base of valley fill (m)	Estimated temperature at base of valley fill (°C)
QH 1A	155	50,2	90-155	224	224	200	60
2A	130	19.0	25-130	52	52	200	23
3D	------	------	------	------	------	378m	58m
4A	------	------	------	------	------	155m	17m
8A	49	16.5	41-49	69	69	150	23
9A	75	16.8	67-75	40	40	150	20
11A	55	14.3	40-55	52	52	100	17
13A	52	9.6	46-52	116	116	300	38
14A	73	14.6	46-73	30	30	350	23
Q 5	107	18.1	54-107	29	29	450	28
6	55	15.4	39-55	32	32	400	26
7	73	15.0	35-73	25	25	300	20
8	66	17.4	44-66	59	59	100	19
9	57	13.8	49-57	30	30	400	24
11	78	15.2	46-78	48	48	300	26
12	62	15.3	51-62	45	45	100	17
13	82	15.1	38-82	39	39	250	22
21	61	14.4	49-61	48	48	400	31
23	124	27.1	57-124	144	144	900	140
24	151	19.4	87-151	45	45	300	26
G 2	151	24.0	99-151	39	39	1,700	84
3	------	------	----------	------	------	50m	16m
4	150	20.6	120-150	36	36	1,600	73
7	80	17.5	60-80	43	43	100	18
8	------	------	----------	------	------	50m	17m
9	------	------	----------	------	------	40m	16m
10	------	------	----------	------	------	30m	17m
105	------	------	----------	------	------	600m	94m
106	400	26.8	325-400	52	52	1,500	84
108	362	54.0	260-362	102	102	700	88
Aminoil USA	------	------	----------	------	------	1,625m	105m

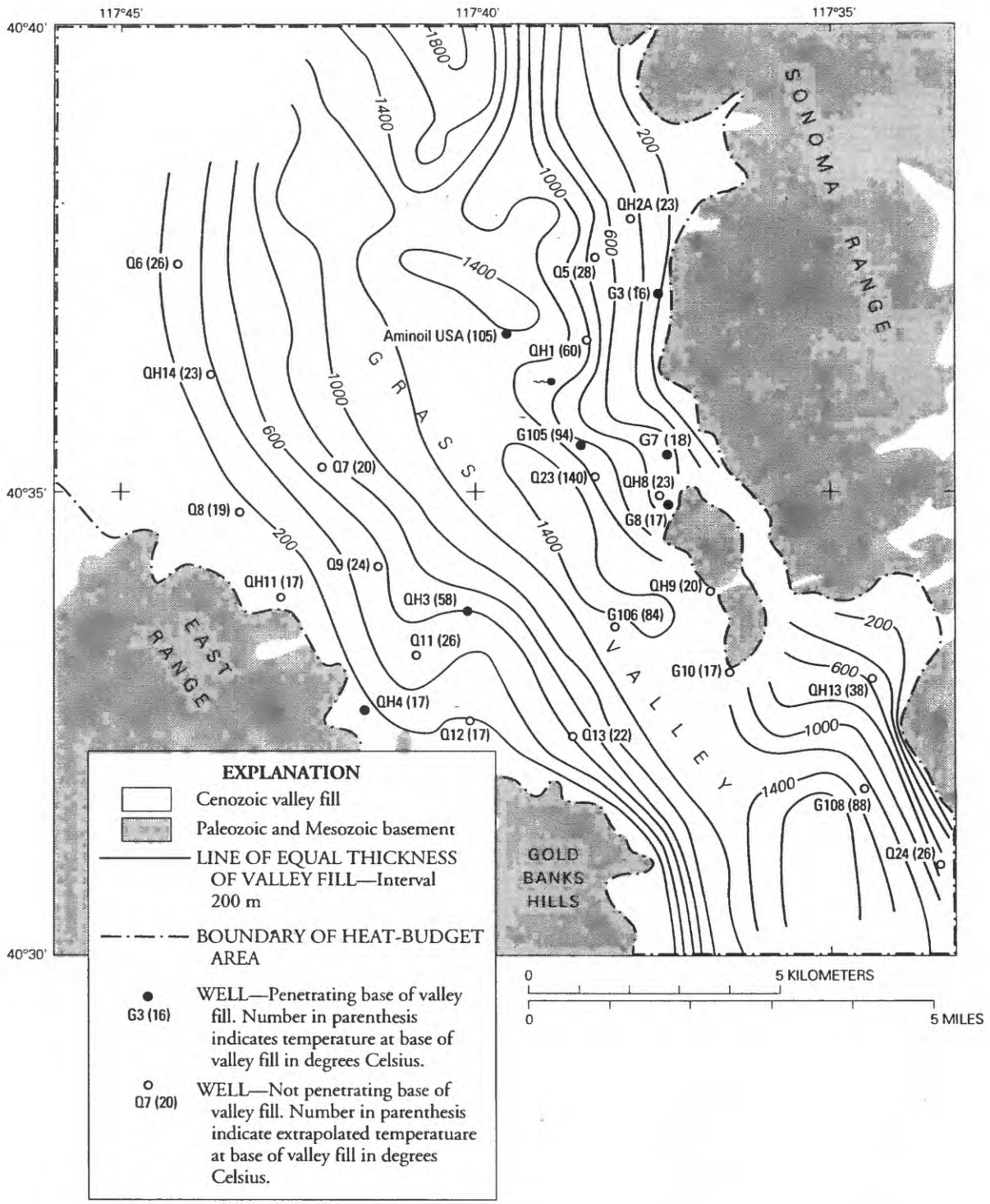

Figure 23. Estimated temperature at base of valley fill in southern Grass Valley.

TABLE 14. Values of thermal conductivity assigned to categories of material classified in interpreted logs of test wells.

Category of material	Thermal conductivity (W/m.K)
Saturated Quaternary alluvium or Tertiary and Quaternary alluvium:	
Gravel; coarse or clean gravel; gravel and sand; sandy gravel; conglomerate; cemented gravel	1.9
Sand and scattered gravel; clay and gravel; coarse sand; sand; coarse sand with clay and silt	1.7
Sand and silt; silty sand; clayey sand and silt; clay and silt with scattered gravel; fine sand	1.5
Sandy clay; silty clay; clayey silt; clay and silt	1.3
Clay or ash (high porosity)	1.0
Saturated Tertiary sedimentary rocks:	
Sandstone; pebbly sandstone; conglomerate	2.1
Siltstone; dense mudstone; soft sandstone; dense claystone	1.9
Soft claystone; tuff; soft siltstone	1.7

base of fill would be substantially greater, perhaps as much as 100°C.

Temperature Distribution in Basement

Little is known about the distribution of temperature with depth in the Paleozoic and Mesozoic basement. Scanty evidence suggests that vertical flow, associated at least in part with convection, is more important in the basement than in the fill. Decreases in temperature with depth were observed in two of the deeper wells (QH3D and G105) (fig. 21), and nearly zero gradients occurred in the deepest well, Aminoil USA 11-36, at depths of 1,634-1,758 m and 1,859-2,256 m, within the basement (fig. 22).

Well QH3D penetrates pre-Cenozoic metagraywacke underlying Tertiary sedimentary rocks from a depth of 378 m to the bottom of the well at 457 m. The temperature gradient changes rather abruptly from 130°C/km in the lower part of the valley fill (Tertiary sedimentary rocks) to a slightly negative gradient in the metagraywacke (fig. 21).

Test well G105, about 1.7 km south-southeast of Leach Hot Springs, penetrates rhyolite of probable Tertiary age from a depth of 323 m to the bottom of the hole, at 360 m. The temperature gradient in the overlying fill (chiefly Tertiary and Quaternary alluvium) averages about 250-270°C/km but decreases to zero, then becomes slightly negative in the rhyolite (fig. 21). Although the rhyolite and other Tertiary volcanic rocks are grouped stratigraphically with the Cenozoic valley fill, the hydrologic characteristics of these consolidated volcanic rocks probably are

more like those of the Paleozoic and Mesozoic basement than of the Tertiary sedimentary rocks.

Thus, limited evidence suggests that vertical convective heat transport is much more significant within the Paleozoic and Mesozoic basement and Tertiary volcanic rocks than in the Tertiary sedimentary rocks, Tertiary and Quaternary alluvium, and Quaternary alluvium. Vertical ground-water flow, presumably through fractures, appears to be less inhibited in the consolidated rocks than in the overlying sedimentary deposits, in which almost all ground-water flow is through intergranular pores rather than through fractures. However, the exact causes of the gradient reversals within the metagraywacke in well QH3D and the rhyolite in well G105, and of the nearly zero gradient in the Aminoil USA 11-36 well at depths of 1,634-1,758 m and 1,859-2,256 m, within the Paleozoic and Mesozoic basement, cannot be determined from present information.

Heat Flow

The principal objective of the heat-flow studies was to estimate regional heat flow, using a heat budget for most of the valley area instead of the more common method of measuring conductive heat flow at a few deep wells. Using a similar method, Sass and others (1977, p. 55-60) and Welch and others (1981, p. 121-148) concluded that heat flow in the SGV region is about 140-160 mW/m^2 and that SGV clearly is within the Battle Mountain heat-flow high. In the present study, the basic data used by Sass and others (1977) and Welch and others (1981) were reevaluated, and data obtained since 1981 were incorporated into a new estimate of regional heat flow.

Heat Budget

A heat budget was estimated for a 211-km^2 area that includes most of SGV. The area is bounded on the east by the somewhat generalized margin of the Paleozoic and Mesozoic basement outcrop, on the south by the 40°30' N. latitude parallel, on the southwest by the margin of the basement outcrop, on the northwest by the 117° 45' 55" W. longitude meridian, and on the north by the 40°40' N. latitude parallel (fig. 19). The extent is greater than that of the 125.5-km^2 budget area of Welch and others (1981, p. 100) but is roughly the same as that used by Sass and others (1977, p. 55) to estimate a heat budget.

Modes of Heat Flux

Geothermal heat flux in SGV includes four modes: radiation, convection, advection, and conduction. Radiation, which occurs from warm ground and hot-water surfaces, is believed to be small. It was not estimated separately because that from warm ground was included in estimates of conductive heat flux and that from hot-water surfaces was included in estimates of convective heat flux. The other three modes were estimated by the procedures described below.

Convection

Convective heat flux, considered here as the heat discharged at the land surface by springflow and evapotranspiration of thermal water, occurs only at LHS. It includes the heat transported by (1) springflow, (2) steam and heated air, (3) evaporation from spring pools and discharge channels, (4) radiation from pool surfaces and discharge

channels, and (5) evapotranspiration from the vegetated area surrounding the springs. Item 1 accounts for most of the flux. Items 2 and 4 are believed to be small and were not estimated. Items 3 and 5 contribute significant amounts to the total flux and were included in the estimate, as summarized in table 7 in the section, "Deep Ground Water." The heat flux associated with the water discharge in table 7 was estimated as follows. The weighted-average temperature of the discharge is 76.8°C. Average annual air temperature is 9.3°C (National Weather Service, Annual Summaries for Nevada: Data for Winnemucca AP weather station). The net enthalpy of the discharge is equal to the enthalpy of water at 76.8°C minus the enthalpy of water at 9.3°C, or (321-39) J/g = 282 J/g. Total convective heat flux at the land surface is therefore 9.0 kg/s x 282 kJ/kg = 2.5 MJ/s = 2.5 MW.

Advection

Advective heat flux is defined herein as heat transported by lateral ground-water flow. A complete heat balance for the study area should account for the net advective flux--the heat advected out of the area minus the heat advected into the area. However, this quantity is exceedingly difficult to estimate, owing to the absence of reliable data to define the quantities and temperatures of both ground-water inflow and outflow. Because the advective component cannot be estimated reliably with data at hand, it is not included in the estimates of total heat flux.

Conduction

Assuming that the advective flux is small (less than or equal to convective flux), conduction in near-surface valley-fill deposits and locally in consolidated rocks is the dominant mode of geothermal heat flux in SGV. The method used to estimate conductive heat flow at each well site is similar to that described by Welch and others (1981, p. 122-127) but differs substantially from the methods described by Sass and others (1977, p. 39-53) and Olmsted and others (1975, p. 62-69). As a measure of the precision of the estimates or of the magnitude of hydrologic and other perturbations, heat flow was estimated for three depth ranges: (1) a "shallow" range, generally above the water table, at depths of 14-18 m below land surface in most of the T wells and 14-20 m in most of the DH, QH, and Q wells; (2) an "intermediate" range, just below the water table, usually at depths of about 30-80 m below land surface; and (3) a "deep" range, at depths of about 80-150 m below land surface. The shallow range was used to estimate the conductive heat flow as close to the land surface as possible but below the approximate depth of measurable seasonal temperature change (about 10-14 m).

Least-squares temperature gradients calculated from point-temperature measurements in the wells were used for all three depth ranges. Most of the temperature data were from Sass and others (1977, table C-1). Several measurements were made by Olmsted in DH wells near LHS and by Sass in G wells drilled by GeothermEx Company in 1979. Temperature-depth data for the T wells were supplied by J.H. Sass (written commun., 1979).

Thermal conductivities measured by needle probe on cores or cuttings (Sass and others, 1977, table C-1) were used for the intermediate and deep ranges in the QH and Q wells. However,

unlike the procedure of Sass and others (1977), only the data for samples from the saturated zone were used. For the DH wells, harmonic-mean thermal conductivity was calculated for the depth range in which the temperature gradient was measured. Thermal conductivities assigned to several categories of materials described in the interpreted logs of the DH wells (table 14) are approximately those used by Welch and others (1981, p. 124). The conductivities assigned to the two coarsest categories (1.9 and 1.7 W/m.K) bracket the harmonic mean value obtained from the core samples (1.75 W/m.K; see table 3). Likewise, the conductivities assigned to the two finer categories of alluvial fill (1.5 and 1.3 W/m.K) bracket the harmonic mean value obtained from the core samples (1.33 W/m.K; see table 3). The value assigned to clay or ash is the harmonic mean value for five samples of tuff (table 3). Values for the three categories of saturated Tertiary sedimentary rocks in table 14 are based on those for individual core samples believed to represent Tertiary rocks; they are probably less certain than the conductivities assigned to saturated Quaternary alluvium or Tertiary and Quaternary alluvium.

The following method was used to estimate thermal conductivity for the unsaturated deposits of the shallow depth range. For 27 test wells in which temperature gradients were measured both above and below the water table, the ratio of the temperature gradient below the water table to the gradient in the depth range 14-20 m (or approximately that depth range in some of the wells) was determined. The mean ratio is 0.7, which is equivalent to the average ratio of the thermal conductivity of the unsaturated materials from 14 to 20 m to that of the materials in the saturated zone below the water table. Accordingly, thermal conductivities for 14-20 m were obtained by multiplying the measured or estimated thermal conductivities of the saturated materials in all the test wells penetrating the saturated zone by 0.7. For the T wells, all of which penetrate unsaturated materials, the average thermal conductivity for 14-20 m was obtained by interpolation or extrapolation of thermal conductivities for 14-20 m in the adjacent Q or QH wells.

For all three depth ranges, conductive heat flow at the sites of the DH, QH, and Q wells was calculated as the product of the thermal conductivity and the temperature gradient. At the T-well sites, only the heat flow for the shallow depth range was calculated. At the G-well sites, only the heat flows for the intermediate and deep ranges were calculated.

Sass and others (1977, p. 45-46) used a different method to estimate heat flow at the T-well sites. Instead of using the temperature gradients and estimated thermal conductivities, their estimates were based on a correlation of temperature at a depth of 15 m with heat flow at other well sites, where both kinds of data were available. The average of their estimated heat flows for the T wells is almost the same as that in this report, although heat flows at individual well sites differ by as much as 50 percent. Sass and others (1977, p. 47) considered the uncertainty in their estimates to be on the order of 20-40 mW/m^2.

The heat-flow data are given in table A4 of the appendix and shown in figures 24-26. In table A4, heat-flow estimates for the shallow, intermediate, and deep ranges are designated q1, q2, and q3, respectively. In general, q1 estimates are the most abundant but the most uncertain and also the most subject to hydrologic and other perturbations.

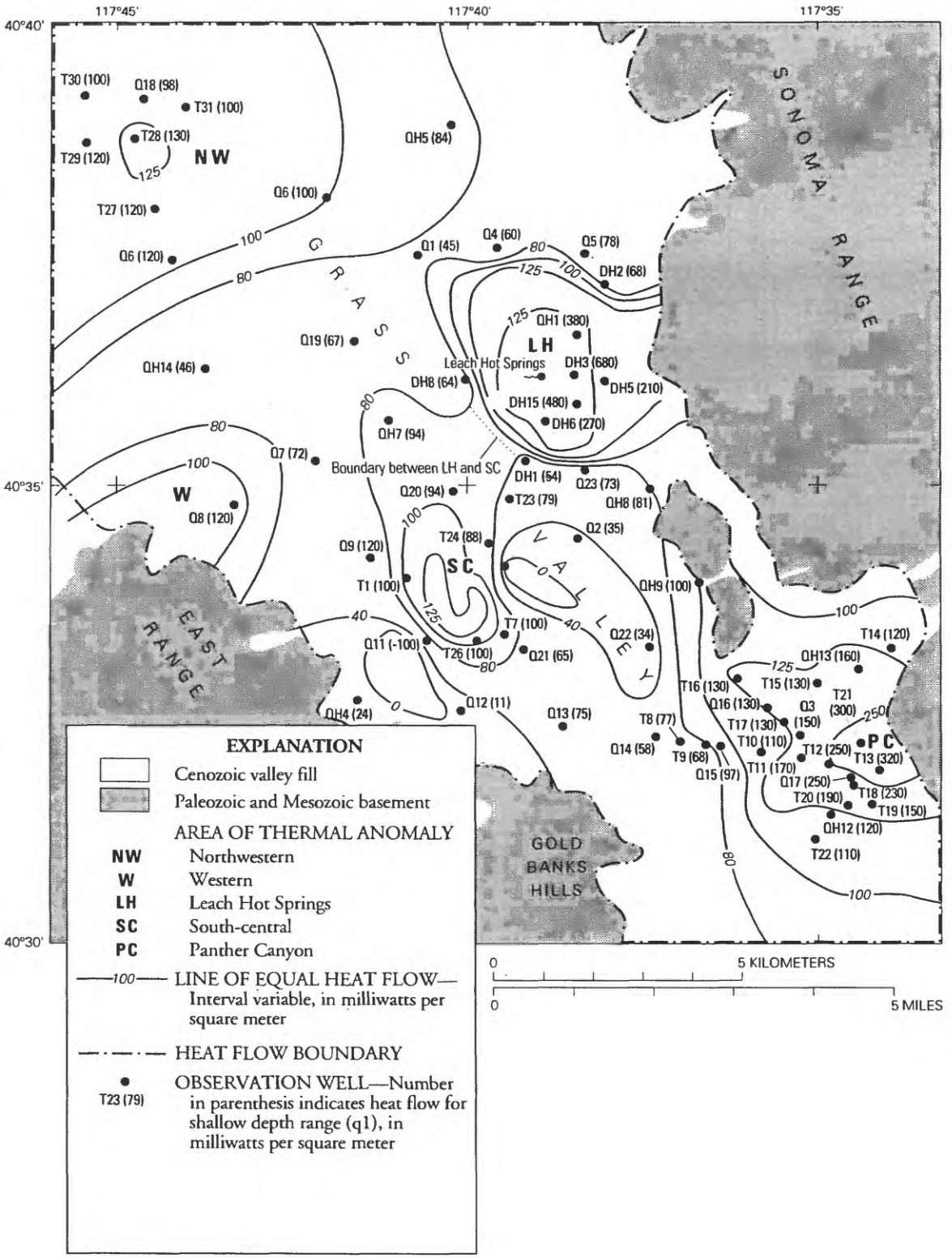

Figure 24. Conductive heat flow for shallow depth range (q1) in southern Grass Valley.

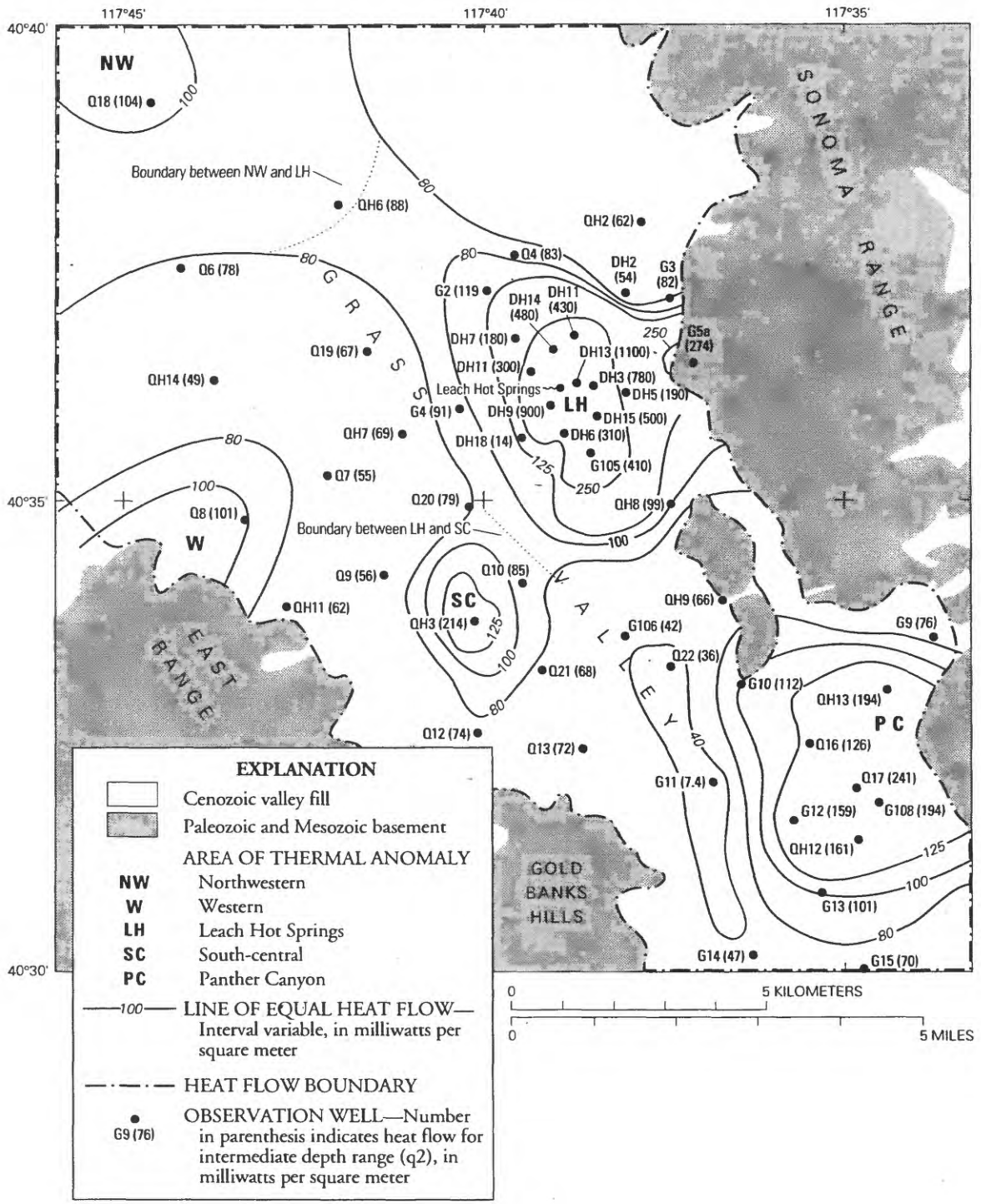

Figure 25. Conductive heat flow for intermediate depth range (q2) in southern Grass Valley.

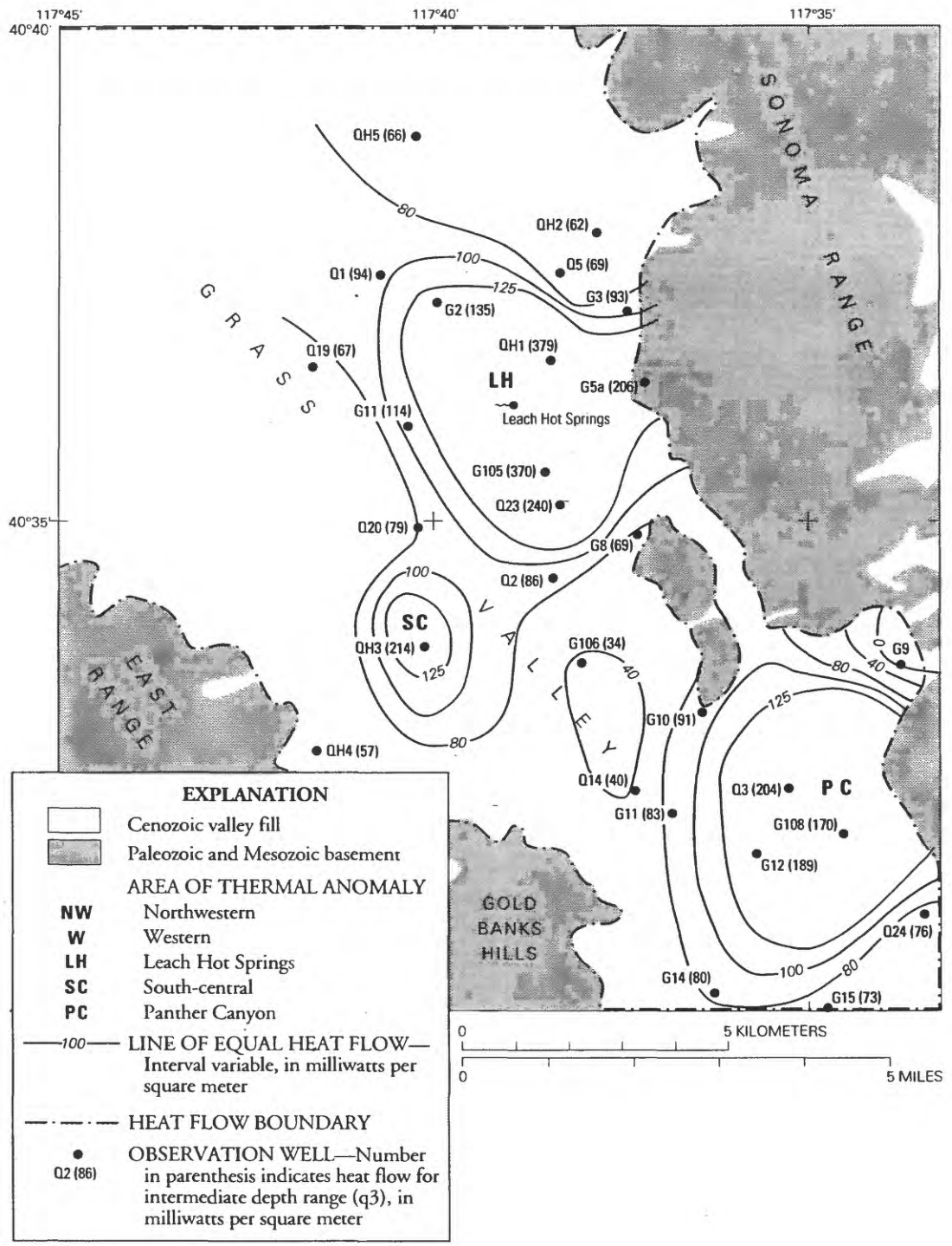

Figure 26. Conductive heat flow for deep depth range (q3) in southern Grass Valley.

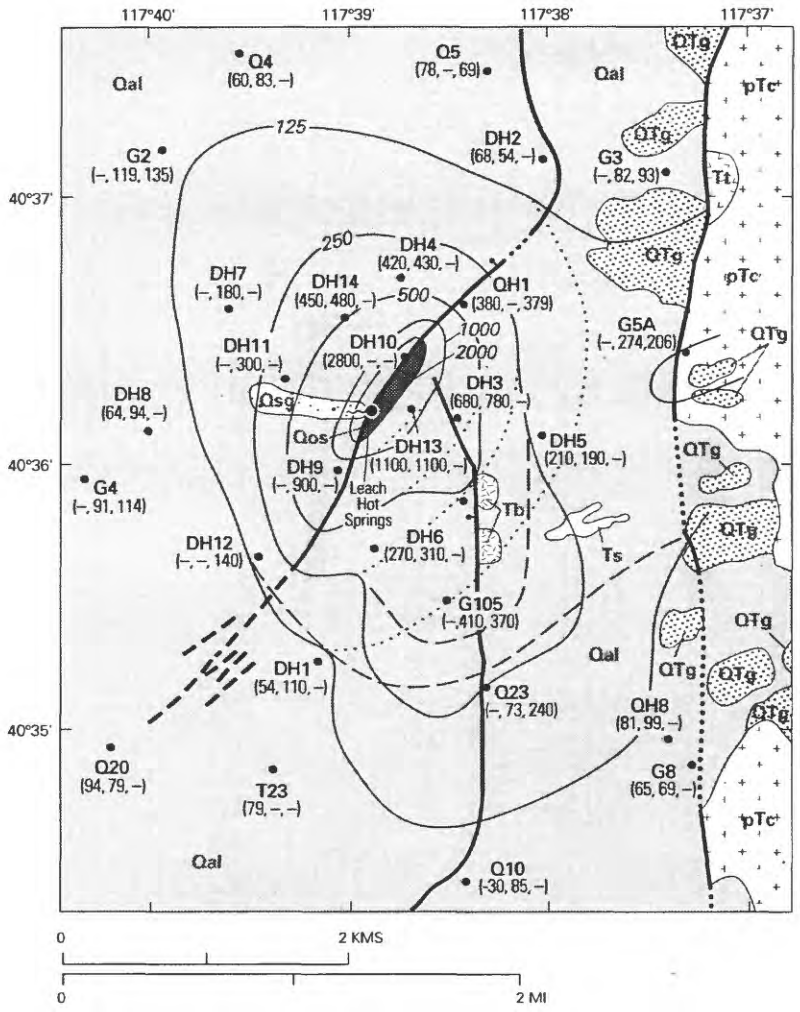

EXPLANATION

FAULT—Dashed where uncertain; dotted where concealed. Bar and ball on downthrown side

LINE OF EQUAL HEAT FLOW—Interval variable, in milliwatts per square meter. Solid for shallow and intermediate depth ranges (q1 sand q2); dashed for shallow depth range (q1) in southern part of area; dotted for interpreted locations in southern part of the area attributable to convective flow that discharges at the land surface at Leach Hot Springs, as explained in text.

Q5 (34, 78, 69)

TEST WELL PROVIDING CONTROL POINT AND NUMBER—Numbers in parenthesis indicate heat flow in milliwatts per square meter. The first number indicates heat flow for shallow depth range (q1); second number indicates heat flow for intermediate depth range (q2); third number indicates heat flow for deep depth range (q3). (see table 5.4)

CORRELATION OF MAP UNITS

Qal	Qsg	Pleistocene to Holocene	QUATERNARY
	Qos	Pleistocene	
	QTg	Pliocene and/or Pleistocene	TERTIARY and/or QUATERNARY
	Ts		TERTIARY
	Tt		
	Tb		
	pTc		PENNSYLVANIAN to TRIASSIC

DESCRIPTION OF MAP UNITS

Qal – ALLUVIUM – Unconsolidated fluvial deposits ranging from clay to gravel. Sorting poor to moderate; caliche fragments and coatings locally abundant. Forms thin pediment cover on flanks of Sonoma Range but thickens valleyward.

Qsg – SINTER GRAVEL – Pebbles, granules, and sand-size fragments of white to light-gray opaline sinter downgradient from Leach Hot Springs. Shown as sinter (Qs) in figure 2 and included in Quaternary alluvium in table 1.

Qos – OLD SINTER – Dense, gray to red chalcedonic sinter, in places associated with partly silicified and kaolinized alluvium; exposed on upthrown side of Leach Hot Springs fault. Shown as sinter (Qs) in figure 2 and included in Quaternary alluvium in table 1.

QTg – OLD GRAVEL DEPOSITS – Unconsolidated to semiconsolidated deposits of local provenance ranging from boulders to silt and clay; obscurely bedded. Tilted eastward, with dips as much as 20°. Exposures deeply dissected. Included in Quaternary-Tertiary alluvium (QTa) in figure 2 and table 1.

Ts – SEDIMENTARY ROCKS – Semiconsolidated deposits ranging from ash and tuff to mudstone, sandstone, and siltstone; characteristically pale gray, yellow, or green. Slightly to moderately deformed, with generally eastward dips within area of map.

Tt – TUFF – Greenish-gray to pink welded tuff of rhyolitic or rhyodacitic composition. Included in Tertiary volcanic rocks (Tv) in figure 2 and table 1.

Tb – BASALT – Dense, dark-gray to brownish-gray holocrystalline rock composed of plagioclase laths, pyroxene, altered olivine, and opaque minerals. Included in Tertiary volcanic rocks (Tv) in figure 2 and table 1 .

pTc – CONSOLIDATED ROCKS, UNDIVIDED – Unmetamorphosed to slightly metamorphosed chert, argillite, and greenstone. Included in Paleozoic and Mesozoic basement in figure 2 and table 1.

Figure 27. Areal geology and near-surface conductive heat flow in the Leach Hot Springs thermal area.

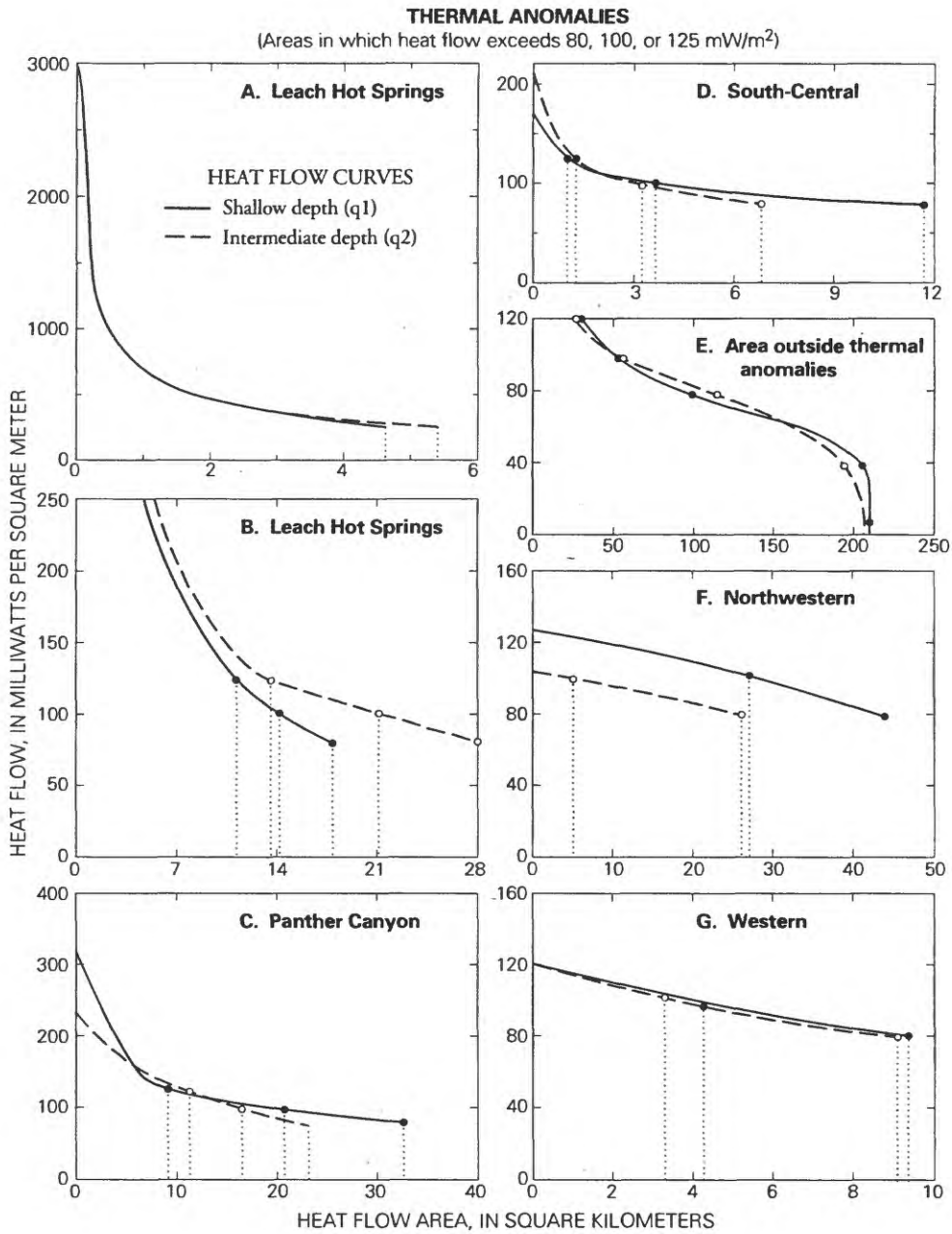

Figure 28. Plots of heat flow versus area for: A. And B. Leach Hot Springs thermal anomaly; C. Panther Canyon thermal anomaly; D. South-central thermal anomaly; E. Area outside thermal anomalies; F. Northwestern thermal anomaly; G. Western thermal anomaly. The X axes indicate areas in square kilometers. The Y axes indicate heat flows in milliwatts per square meter. The heat-flow--area curves were integrated graphically to derive conductive heat flux, as explained in the text. The thermal anomalies are defined as the areas in which the heat flow exceeds 80, 100, or 125 milliwatts per square meter. The solid lines indicate heat flow for the shallow depth range (q1). The dashed lines indicate heat flow for the intermediate depth range (q2).

In contrast, the q3 estimates probably are the most reliable but have the disadvantage of being widely scattered. Accordingly, lines of equal heat flow for the deep range are not shown for the entire heat-budget area in figure 26.

Heat flow for the LHS area is shown in figure 27 in greater detail than possible in figures 24-26. Also shown in figure 27 is the portion of the thermal anomaly interpreted to result from upflow of thermal fluid at the conduit or conduit system along the fault at the hot springs.

All the heat flows listed in table A4 and shown in figures 24-27 are uncorrected. In general, corrections required to estimate conductive heat flow at greater depths include those for thermal refraction in dissimilar rocks, topographic relief, vertical ground-water flow, drilling disturbance, climatic change, uplift, erosion, sedimentation, and regions of anomalous surface temperature such as rivers and lakes (Sass and others, 1971, p. 6382). In SGV, the significant corrections are probably those for thermal refraction and sedimentation. Corrections for both thermal refraction and sedimentation are positive; that is, the observed heat flows in the valley are likely less than the regional average. The implications of this fact are discussed later.

Conductive heat flux for the budget area and for the LHS and Panther Canyon thermal anomalies was calculated by graphic integration (using a polar planimeter) of the heat-flow-area curves shown in figure 28. The results are given in table 15.

The pattern of areal variation in conductive heat flow indicates the effects of vertical and lateral transport of heat by moving ground water, both thermal and nonthermal. The lowest heat flows, less than 40 mW/m^2 in both the shallow and intermediate depth ranges (figs. 24 and 25), are in the south-central part of the valley, south of LHS and west of Panther Canyon. Elsewhere, outside the LHS and Panther Canyon thermal anomalies, heat flows are generally 40-130 mW/m^2.

For present purposes, thermal anomalies are defined as areas in which the heat flow exceeds 80, 100, or 125 mW/m^2. The low value of 80 mW/m^2 is less than the minimum of 2.5 heat-flow units (~100 mW/m^2) used by Sass and others (1971, fig. 4) to define the outer limits of the Battle Mountain High, but the other two values represent the low and mid range for the Battle Mountain High. The relatively low heat-flow values used to define the limits of the thermal anomalies were selected on the assumption that average near-surface conductive heat flow in the valley would be less than the regional average because of net advection of heat from the valley area by ground-water flow and thermal refraction, as discussed by Blackwell (1983, p. 85-87). The thermal anomalies include: (1) the northwestern anomaly at the northwest corner of the study area; (2) the western anomaly at the west-central margin of the study area; (3) the LHS anomaly; (4) the south-central anomaly 5 km south-southwest of LHS; and (5) the Panther Canyon anomaly in the southeast part of the study area.

As defined by the 80-mW/m^2 line, the northwestern anomaly is of considerable extent, but the maximum heat flow for the shallow depth range, at well T28, is only 130 mW/m^2 (fig. 24). Because of the absence of deep subsurface data in this area, the cause of this anomaly is unknown.

Like the northwestern anomaly, the western anomaly does not have a large maximum heat flow (probably <125 mW/m^2), and the cause of

TABLE 15. Conductive and convective heat flux from southern Grass Valley study area.

Heat-flux values are in megawatts (MW)
(1) Shallow depth range conductive (q1)
(2) Intermediate depth range conductive (q2)
A Anomalous heat flow = >80 mW/m^2
B Anomalous heat flow = >100 mW/m^2
C Anomalous heat flow = >125 mW/m^2

Average heat flow for study area (1) = 22.7 MW ÷ 211 km^2 = 108 mW/m^2
(2) = 21.8 MW ÷ 211 km^2 = 103 mW/m^2

Item		Heat flux		
		A	B	C
Northwestern anomaly (all conductive)	(1)	4.5	3.0	0.12
	(2)	2.4	0.54	0
Western anomaly (all conductive)	(1)	0.92	0.46	0
	(2)	0.87	0.35	0
Leach Hot Springs anomaly: Convective		2.5	2.5	2.5
Conductive	(1)	4.6	4.2	3.9
	(2)	5.9	5.3	4.2
Total	**(1)**	**7.1**	**6.7**	**6.4**
	(2)	**8.4**	**7.8**	**6.7**
South-central anomaly (all conductive)	(1)	1.17	0.45	0.15
	(2)	.75	0.52	0.19
Panther Canyon anomaly (all conductive)	(1)	4.2	3.1	1.8
	(2)	3.2	2.6	2.0
Total for heat-flow anomalies	**(1)**	**17.9**	**13.7**	**8.5**
	(2)	**15.6**	**11.8**	**8.9**
Area outside anomalies (all conductive	(1)	4.8	9.0	14.2
	(2)	6.2	10.0	12.9
Total for study area	**(1)**	**22.7**	**22.7**	**22.7**
	(2)	**21.8**	**21.8**	**21.8**

the anomaly is unknown. If regional heat flow is 125 mW/m^2 or more, neither the western nor the northwestern anomaly should actually be considered thermal anomalies at all. This interpretation is supported by the absence of a marked inflection in the heat flow vs. area plots for both areas in figure 28.

The LHS anomaly is the most intense thermal anomaly within the study area. The maximum conductive heat flow at the hot springs probably exceeds 3,000 mW/m^2 (fig. 27). The anomaly consists of three parts: (1) the principal part surrounding the hot springs, elongated toward the northeast and attributed to convective hydrothermal upflow along the LHS fault; (2) a part along the fault that extends southward from well DH3, about 0.8 km east of the springs; and (3) a smaller, perhaps slightly separated part apparently centered at well G5a, largely east of the budget area. The heat flux from the last part is not included in the data shown in table 15.

The south-central anomaly is small, and its maximum heat flow, at well QH3D, is only 100 mW/m^2 for the shallow depth range and 210 mW/m^2 for the intermediate depth range. The anomaly clearly is related to hydrothermal convection within the pre-Cenozoic basement at a buried basement high.

The Panther Canyon heat-flow anomaly is extensive, but the maximum heat flow is only about one-tenth as great as that at LHS, probably because thermal water does not rise to the land surface as it does at LHS. The pattern of the anomaly suggests rising thermal water along the Basin and Range fault at the western edge of the basement exposures east of the valley but also suggests high temperatures in the basement and lower part of the valley fill at depth, farther west.

Total Heat flux and Average Heat Flow

Total heat flux from the study area is estimated as the sum of the convective and conductive heat components discussed above. The convective heat flux (all at LHS) is estimated at 2.5 MW. The total heat flux is 22.7 MW using the conductive estimate for the shallow depth range, and 21.8 MW using the conductive estimate for the intermediate depth range; the corresponding average heat flows are 108 and 103 mW/m^2 (table 15). As discussed earlier, the advective component could not be estimated reliably and is not included in the total. The estimates of total heat flux and average heat flow therefore are regarded as minimum rather than most likely values.

An important question is whether the average heat flow calculated for the study area is a valid estimate of the heat flow at the base of the hydrothermal system (or systems) in SGV--the heat flow unaffected by vertical or lateral heat transport by ground-water flow or by the various other perturbations described earlier. (It is assumed that the thermal mechanism driving the convection system(s) is high regional heat flow rather than localized shallow crustal heat sources.) The boundaries of the hydrothermal system(s) in southern Grass Valley are unknown, but, for present purposes, we assume that the system(s) are co-extensive with the surface drainage basin. The budget area used in this study obviously is a biased sample of the geology and topography of the drainage basin of SGV--it includes most of the valley area but none of the tributary mountainous area (see fig. 19). Furthermore, the 211-km^2 budget area is only 37 percent of the 576-km^2 drainage basin above the northern boundary of the study area.

Because, according to generally accepted interpretations of Basin and Range geohydrology, the mountains are likely to include more areas of ground-water recharge than of discharge (Maxey and Eakin, 1949; Mifflin, 1968), the average conductive heat flow there may be less than the average for the entire drainage basin. Under this condition, the heat-flow estimate for the budget area could be too high to represent the heat flow at the base of the hydrothermal system(s) in SGV.

However, data from widely scattered heat-flow holes in the mountains near Grass Valley (Sass and others, 1971; 1977) indicate heat flows as high or higher than those estimated for SGV in this study or by Sass and others (1977). Lack of correction of these values for thermal refraction, however, tends to yield heat flows at sites in the mountains unaffected by recharge greater than those measured in the valleys (Blackwell, 1983, p. 85-87). The average heat flow calculated for the budget area, which is largely in the valley, therefore may be lower rather than higher than the average for the entire SGV basin, more than half of which is mountainous. Correction for sedimentation and inclusion of the unknown advective component also would increase the average heat flow in the study area.

Additional support for an average heat flow greater than that indicated by the budget-area calculations is afforded by temperature data from the Aminoil well (fig. 22). Near-linear temperature gradients of 54°C/km measured from 2,469-2,591 m in the amphibolite near the bottom of the well and 55°C/km from 1,768-1,859 m in granite and altered metavolcanic rocks suggest a conductive thermal regime for those intervals. Although thermal-conductivity data for these rocks are lacking, grain thermal conductivities of valley-fill deposits (excluding tuff and tuffaceous sediments), which presumably represent basement rocks in the SGV area, average 2.72 ± 0.54 W/m.K (table 3). Assuming that this average applies to the amphibolite, granite, and altered metavolcanic rocks in the Aminoil well, the conductive heat flow for the two intervals described above is 150 ± 30 mW/m^2.

In summary, because of all the uncertainties, the average heat flow in SGV cannot be estimated within narrow limits. The 103-108 mW/m^2 estimated for the budget area (all within the valley) almost certainly is too low. A more likely value is in the 120-180 mW/m^2 range. Heat flows in this range were determined at several sites in the region that includes SGV, as shown in figure 1. A heat flow of 150 mW/m^2 is used in modeling calculations discussed in the next section.

MODELS OF BASIN AND RANGE HYDROTHERMAL SYSTEMS

Results of geohydrologic investigations indicate that conditions are favorable for the existence of a high-temperature (≥150°C) hydrothermal system in southern Grass Valley. Such conditions include boiling-point hot springs for which chemical geothermometer temperature estimates exceed 150°C, a measured maximum temperature of 125°C in a well 2,600 m deep, an estimated average heat flow for the region of 120-180 mW/m^2, and an extensional tectonic setting with normal faults of relatively large vertical offset. Thermal-water circulation in shallow alluvial and bedrock aquifers appears to be responsible for localized areas of abnormally high (>125-250 mW/m^2) surficial heat flow. Without additional deep drilling, however, the details of flow within the hydrother-

mal system, including the existence of a reservoir[4] with a size and permeability sufficient for commercial exploitation, cannot be determined.

On the basis of available information, simplified conceptual models of Basin and Range hydrothermal systems, such as the system in southern Grass Valley, can be developed. Numerical simulations of limiting-case models can be used to delineate relations between heat flow and fluid flow in these systems, as influenced by factors such as the depth and extent of fluid circulation, the rate of fluid flow, and the age of the circulation system. Thermal-refraction effects related to different thermal conductivities in basin fill and surrounding bedrock can also be simulated with these models.

Fault-Plane Model

Various authors have suggested that the circulation systems associated with Basin and Range hot springs are mostly confined to the fault zones from which the springs discharge (Hose and Taylor, 1974; Beyer and others, 1976a; Bodvarsson, 1979). This could be termed the fault-plane model (fig. 29). Only the fault zone is assumed to be permeable, and circulation in the fault zone would result from some combination of density differences between upflowing hot water and downflowing cold water and elevation differences between recharge and discharge areas. High-temperature reservoirs within the fault zone would be relatively small and have limited resource development potential. The fault zone separates basement from valley fill, and heat is conducted into the base of this model at a rate equal to the regional heat flow within the fault zone and the adjacent bedrock.

Free, or natural convection in the fault plane can take several forms, depending on the permeability distribution and elevation differences along the trace of the fault. For some systems the elevation of the recharge area may be lower than that of the discharge area, so that fluid density differences alone must drive the circulation system. In the absence of permeability and elevation differences, one or more convection cells could form, depending on the depth/length ratio of the permeable section of the fault. Conditions under which natural convection can occur in steeply dipping faults have been investigated by Lowell (1979), Murphy (1979), and Lopez and Smith (1995). Analytical solutions indicate that the critical Rayleigh number (minimum value for natural convection to develop) is relatively large for faults that are narrow and deep because of the inhibiting effects of conductive heat loss away from the fault

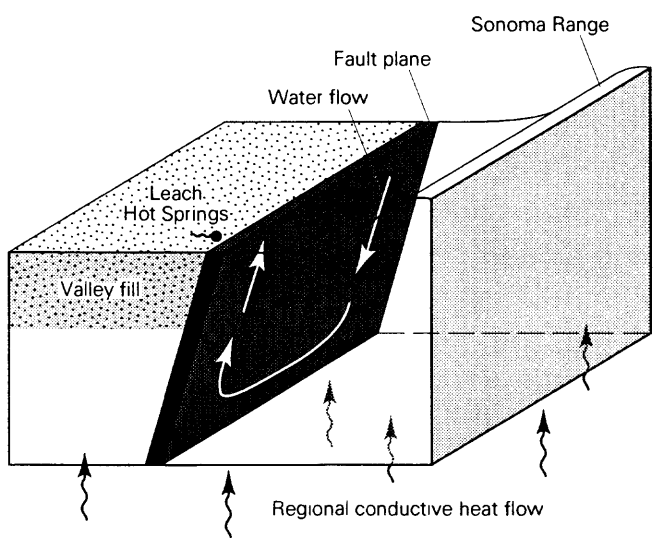

Figure 29. Fault-plane conceptual model of a Basin and Range hydrothermal system.

[4] As used in this discussion, the term "reservoir" is synonymous with "thermal aquifer" used elsewhere in the report.

plane. Higher vertical than horizontal permeability, as is common in extensional fault zones, also tends to increase the critical Rayleigh number. Thus, the permeability and (or) the regional heat flow must be relatively large for natural convection to occur in fault zones. Numerical results discussed by Lopez and Smith (1995) and Lopez and others (1994) place limits on fault-zone permeability values needed for natural convection to develop in a three-dimensional model that also includes topographically driven fluid inflow from an adjacent mountain block.

In most field situations, fluid circulation within a fault zone is also influenced by topography and permeability differences, resulting in a component of forced convection, or advection. The numerical simulations discussed below apply to a two-dimensional vertical cross-section model in which fluid flow at a specified rate is restricted by the permeability distribution to a single recharge (downflow) zone and an adjacent discharge (upflow) zone. General issues to be considered with this model include (1) the relationships between the rate of fluid flow, the depth of circulation, and the maximum temperature attained at depth, and (2) the amount of heat lost conductively from the upflow part of the circulation system and the resultant drop in fluid temperature between the reservoir and the surface.

Computational Model

The two-dimensional computational model (fig. 30) can be applied to either the downflow or upflow region within a fault plane. For the downflow region, the fault plane acts as a heat sink by capturing part of the regional heat flow over some distance on either side of the fault. Under transient conditions, heat initially stored in rocks adjacent to the fault is conducted to the downflowing fluid so that fluid temperature at any given depth exceeds that at steady state.

The applicability of results obtained with the two-dimensional analysis to the fault-plane model depends on whether most of the heat input to fluid circulating within the fault plane occurs within the downflow region. This would seem to be the case unless there were an extensive region of lateral flow, for example in a permeable formation penetrated by the fault zone. Comparison of results obtained with the two-dimensional model analysis with those obtained by Pottorff (1988) using a three-dimensional Discrete State Compartment (DSM) model supports the validity of the analysis presented here.

Other relevant parameters in this model are the depth of fluid circulation (D), thermal conductivities of basement and valley fill, and the rate of fluid flow per unit fault length over which downflow or upflow occurs (Q_w). For the downflow region, mass inflow rate at the top of the fault plane is specified at a temperature of 10°C, and

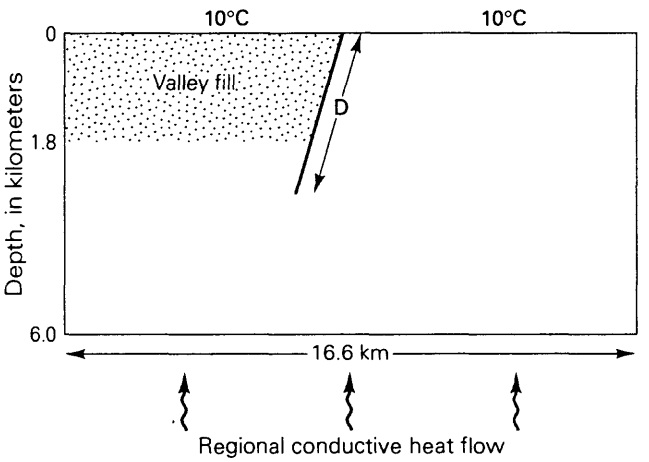

Figure 30. Fault-plane model for numerical analysis of the downflow part of a Basin and Range hydrothermal system.

mass is removed from the fault at depth D at the same rate but at an unspecified temperature which varies during the course of each simulation. For the upflow region, mass inflow rate at the bottom of the fault plane is specified at a temperature of 180°C. The total thickness of the model was 6 km. The total width was 16.6 km; width of the fault plane was 50 m.

Values used in these simulations for the thermal conductivity of the valley fill (K_1) and basement (K_2), heat flow into the base of the model (q), and the depth of fill are listed below.

K_1 = 1.7 W/m.K
K_2 = 3.4 W/m.K
q = 150 mW/m^2
depth of fill = 1.8 km

These conductivity values are within the ranges of corresponding values determined for deposits sampled in southern Grass Valley, although the ratio of K_2 to K_1 used in the model is higher than for the mean conductivity values computed in the section, "Physical properties of rock materials". This difference affects the magnitude of thermal-refraction effects on heat flow near a high-angle Basin and Range fault, as discussed below. Heat flow specified at the base of the model probably represents an upper limit to the actual crustal heat flow in the southern Grass Valley area.

The dip of the fault shown in figure 30 is 60°, a value representative of many Basin and Range faults and also of the fault on which Leach Hot Springs occur. Modeling results were obtained for fault dips of 60° and 90°. For comparison, both insulated and constant-temperature specifications were used along the vertical side boundaries of the model. In the latter case, a vertical temperature distribution corresponding to a conductive heat flow of 150 mW/m^2 was imposed.

For numerical solution, the model was subdivided into 10 layers of equal thickness and 23 vertical sections of varying width. Transient solutions for temperature and heat flow, with specified fluid-flow rates, were obtained using an integrated finite-difference computer code described by Sorey (1978).

Conduction-Only Solutions

A simulation of conductive heat flow in the absence of fluid flow was used to determine initial temperature distribution for subsequent simulation with fluid flow and for quantifying the effects of thermal refraction near faults separating the basement of the mountain ranges and the valley fill of the basins. The temperature distribution for the conduction-only solution with simulated side boundaries is shown in figure 31. The surficial heat-flow distribution shows a high heat-flow anomaly on the upthrown or basement side of the fault, with a corresponding heat-flow low on the fill side. This refraction effect was first proposed by Lachenbruch (1968) and developed further by Blackwell and Chapman (1977) and Blackwell (1983). For the parameters used in this model, the maximum heat flow is 220 mW/m^2 and the minimum is 120 mW/m^2. Surficial heat flow values are near the specified regional heat flow within a distance of about 5 km on either side of the fault.

The thermal-refraction effect noted above may influence heat-flow measurements made within the Basin and Range province, including those values used to delineate the Battle Mountain heat-flow high. The influence of adjacent ranges

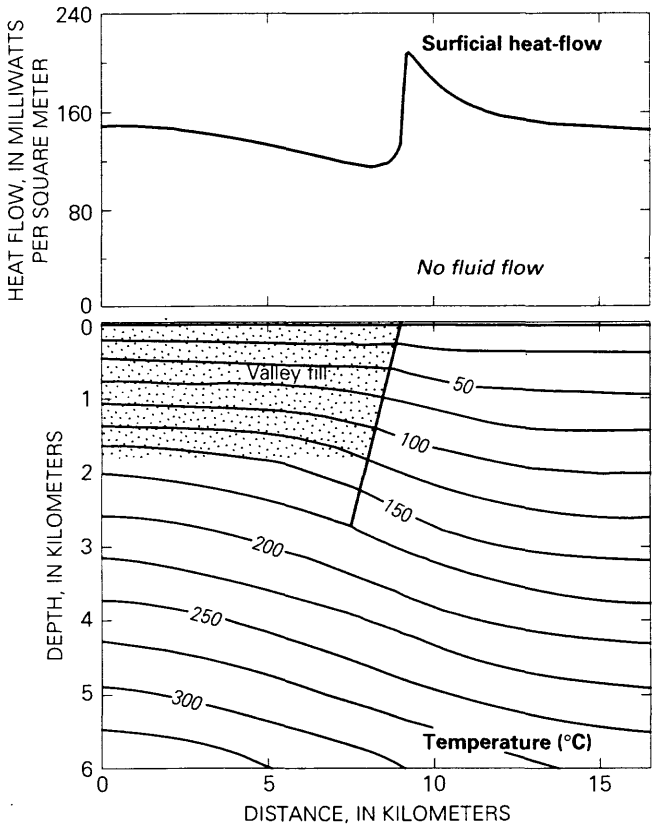

Figure 31. Steady-state temperature and surficial heat-flow distributions in fault-plane model with no fluid flow. Lines of equal temperature in degrees Celsius.

and valleys can cause larger refraction effects at greater distances from basin-bounding faults than indicated in figure 31 (Lee and Henyey, 1974; Blackwell, 1983). In the case of southern Grass Valley, the magnitude of the refraction effect would tend to be smaller than in our simulation if the thermal conductivity contrast were smaller than 2:1.

Although heat-flow values for some wells located within 1-2 km of basin-bounding faults in the vicinity of Leach Hot Springs and Panther Canyon may be significantly affected by refraction, no attempt was made to correct for this effect. Computed terrain corrections were negligibly small for the wells used in this study.

Larger effects on measured heat-flow values are caused by fluid circulation within the upper part of the basement, especially in areas of basement highs, and thermal-water upflow along the basin-bounding faults within the Leach Hot Springs and Panther Canyon thermal anomalies. Heat-flow values within the budget area outside the thermal anomalies, which average less than 80 mW/m^2, apparently are reduced by the effects of non-thermal ground-water circulation in the upper part of the basement and (or) by circulation of water that is recharging the deep hydrothermal system and absorbing a fraction of the regional heat flow.

Fluid-Downflow Cases

The effects of fluid downflow on temperatures within the fault-plane model are typified by the results in figure 32, for a case with 1.25 kg/s per kilometer of fault length flowing to a depth of 2.7 km. Comparison of steady-state temperatures in figures 31 and 32 shows that the primary effect of fluid flow is a downward bulge in the isotherms crossing the fault. The temperature of the fluid removed from the model at a depth of 2.7 km is 115 °C, whereas the initial temperature at this depth was 173 °C. At steady-state, almost all the heat added to the fluid as well as the conductive heat discharged at the land surface is supplied by the underlying regional heat flow. The constant-temperature (but vertically varying) side-boundary conditions used in this case allow a small amount of heat to enter the model along the left side. Corresponding simulations with insulated side boundaries yielded fluid outflow temperatures only about 2 percent below values for constant temperature side-boundary conditions.

Surficial heat flows shown in figure 32 are at

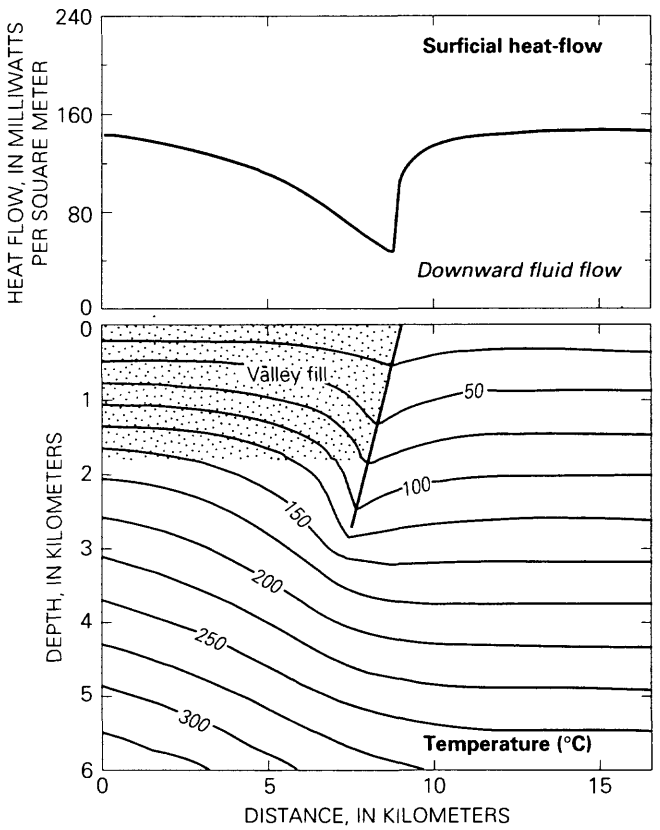

Figure 32. Steady-state temperature and surficial heat-flow distributions in fault-plane model with downward fluid flow to 2.7 km depth. Fluid flow rate equals 1.25 kg/s/km of fault length. Lines of equal temperature in degrees Celsius.

or below 150 mW/m^2. Beyond a distance of about 6 km on either side of the fault, heat flow is close to values under no-fluid flow conditions. In other words, the cooling effects of recharge down the fault do not extend beyond a distance of about twice the depth of fluid circulation. At the temperature attained by the downflowing fluid, the simulated surficial heat flow distribution should not be significantly different if the distance to the lateral boundaries was increased. For the system as a whole, the area of below-average heat flow near the recharge area would be balanced under steady-state conditions by areas of above-average heat flow in the vicinity of the discharge area(s).

Results from many different simulations with this model were combined to produce curves of exit temperature versus downflow per unit fault length (Q_w) for different depths of circulation (fig. 33). The result for the case depicted in figure 32 (Q_w = 1.25 kg/s/km and fault plane dipping 60°) is plotted in figure 33, along with one curve for a fault dipping at 90°. Differences in outflow temperature between the 60° and 90° dip cases are only about 10°C for any value of Q_w.

These curves show that circulation depths and fault lengths must be relatively large to obtain high fluid temperatures within the downflow part of the fault-plane model under steady-state conditions. For example, for Q_w = 9 kg/s/km along a fault dipping 60°, the curves in figure 33 indicate that D must be at about 4.5 km for an exit temper-

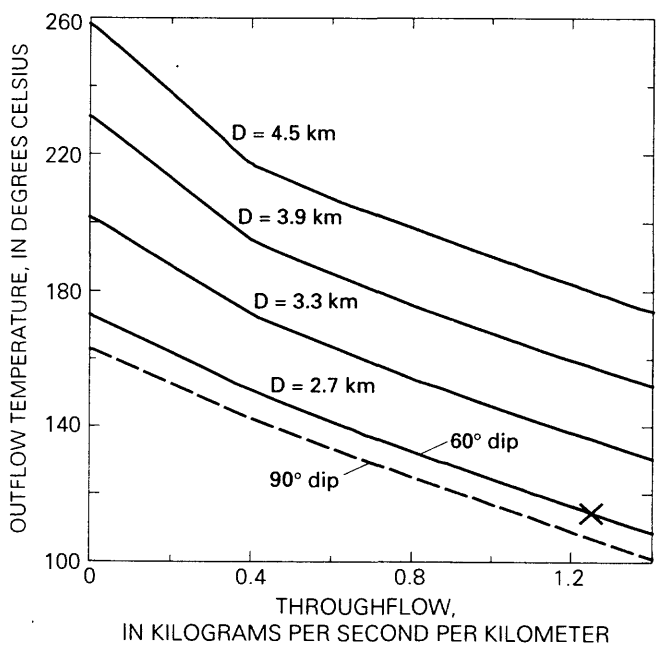

Figure 33. Fault-plane model results for outflow temperature as a function of throughflow per kilometer of fault length, L. Each solid curve is for a fault with 60° dip and a different depth of circulation, D. Result for a fault dipping at 90° with D=2.7 km is shown as a dashed curve, and the result from figure 32 is plotted as an x.

ature of 180°C. In this case, downflowing fluid lowers initial temperature at that depth by 65°C. The 180°C temperature is applicable to reservoir temperature for thermal water feeding Leach Hot Springs based on cation geothermometer calculations. Similarly, the value of Q_w = 1.25 kg/s/km could apply to the recharge zone supplying a deep reservoir if a total of 9 kg/s (equal to the surface discharge at Leach Hot Springs) flowed downward along a 7 km-long zone within the set of northwest- and north-trending faults between Leach Hot Springs and Sheepeater Canyon (fig. 2). Pottorff (1988) obtained similar results in terms of fluid temperature versus depth of circulation using the DSM model applied to the three-dimensional fault-plane model with a throughflow of 9 kg/s and recharge over an 8-km-long fault zone. If the total rate of thermal fluid flow in this system were as high as 15 kg/s, as suggested by Welch and others (1981) to account for both surface and subsurface discharge of thermal water, corresponding depths of fluid circulation and (or) fault lengths over which downflow occurs would need to be even greater for the fault-plane model to be applicable.

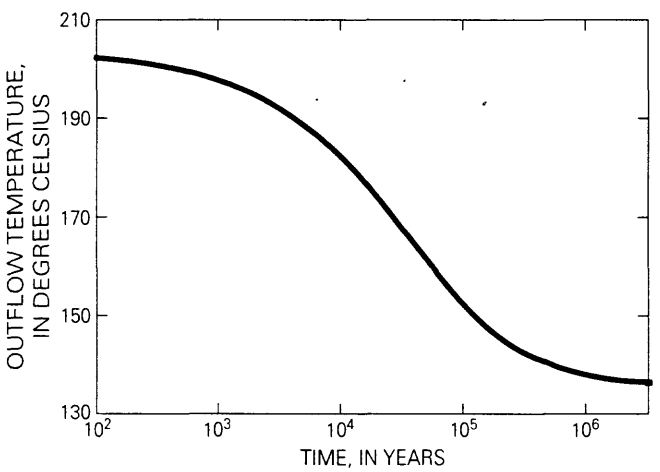

Figure 34. Transient response of outflow temperature at D=3.3 km from fault-plane model with fluid flow rate=1.25 kg/s/km and a fault dip of 60°.

Exit temperatures of 180°C are also possible with the fault-plane model for shallower depths of circulation under transient conditions when heat is being mined from storage. For example, the variation in exit temperature with time is shown in figure 34 for a case involving an initial exit temperature of 202°C at a depth of 3.3 km from the conduction-only solution. Steady-state conditions are reached after about 10^6 years, when the outflow temperature has fallen to 138°C.

Fluid-Upflow Cases

Temperature distributions associated with upflow along the fault conduit can also be simulated with the fault-plane model. In this case, the flow rate and temperature are specified at the base of the conduit. The steady-state result for Q_w = 6.0 kg/s/km, D = 2.7 km, and an input temperature of 180°C (fig. 35) shows a pronounced upward bulge in the isotherms across the fault and a fluid temperature of 100°C at the land surface. This flow rate may be representative of Leach Hot Springs, where the spring discharge is about 9 kg/s and the zone of high conductive heat flow measured around Leach Hot Springs is about 1.5 km long (fig. 27). This result suggests that conductive cooling, as opposed to mixing with nonthermal water, could account for much of the required temperature drop within the upflow conduit if the hot springs were supplied by a deep reservoir at 180°C. Simulated surficial heat flows (fig. 35) show an anomaly considerably larger than that due solely to thermal refraction and more similar to the observed heat-flow pattern around Leach Hot Springs. The additional complexity of the actual surficial heat-flow

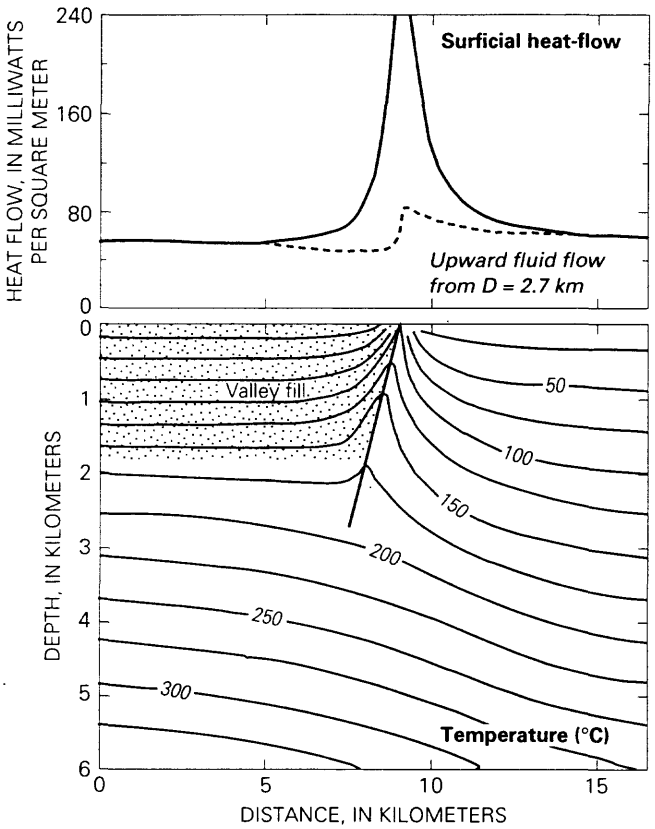

Figure 35. Steady-state temperature and surficial heat-flow distributions in fault-plane model with upward fluid flow from D=2.7 km. Fluid flow rate=6 kg/s/km. Lines of equal temperature in degrees Celsius.

pattern in this area (fig. 27) may be due to subsurface leakage of thermal water away from the main conduit and an additional zone of upflow southeast of the hot springs. A more detailed analysis of heat flow associated with hot-spring systems of different geometries was given by Sorey (1975, 1978).

Fluid Residence Time

Fluid residence time t_r for the fault-plane model can be calculated from

$$t_r = \phi \rho_w V/M \qquad (18)$$

where ϕ is porosity, ρ_w is fluid density, V is volume of permeable rock, and M is the total mass-flow rate through the model. For fault lengths and widths near 10 km and 50 m, respectively, t_r would be about 1,000 years for fluid flow rates of 10 kg/s circulating to depths of about 5 km (ϕ=0.1, ρ_w=0.95 kg/L). Such calculations apply to the combination of downflow and upflow regions within the fault zone; regions of lateral flow are assumed to be volumetrically small in comparison.

Lateral-Flow Model

An alternative conceptual model for hydrothermal circulation at Grass Valley and similar Basin and Range systems is referred to here as the lateral-flow model. As illustrated in figure 36, it involves recharge along a range-front fault and lateral flow through the basement toward the area of hot-spring discharge. Within some distance of the upflow region, reservoir temperatures should reach those estimated by chemical geothermometry. This model, in contrast with the fault-plane model, involves a reservoir of considerable areal

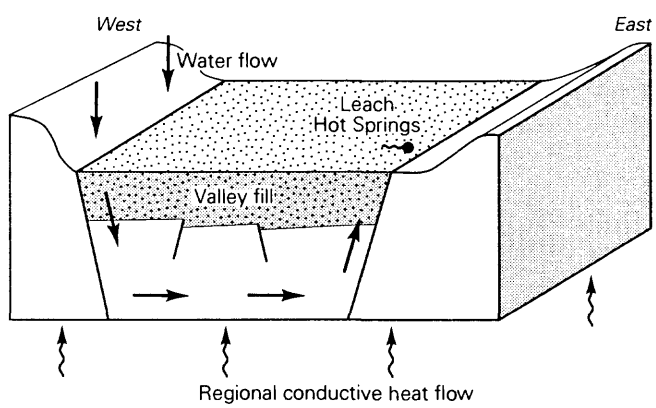

Figure 36. Lateral-flow conceptual model of a Basin and Range hydrothermal system.

extent, which tends to minimize the required depth of circulation because the regional heat flow is captured more efficiently. The minimum depth of circulation is controlled by the regional heat flow and fill-basement conductivities, as discussed by Welch and others (1981).

In southern Grass Valley, evidence of thermal-fluid circulation within basement aquifers at several locations away from Leach Hot Springs indicates a flow system larger in areal extent than one confined to a single fault zone. Stable-isotope data for this area, which support the concept of recharge from paleowater, are also consistent with lower fluid velocities and longer flow paths than those corresponding to a single fault zone. However, the directions of deep fluid flow toward Leach Hot Springs are as yet undetermined. Heat-flow contact area and fluid-travel-time considerations discussed below suggest lateral flow over distances of at least 10 km. Thus, recharge from the East Range or the Goldbanks Hills seems more likely than recharge from the adjacent Sonoma Range.

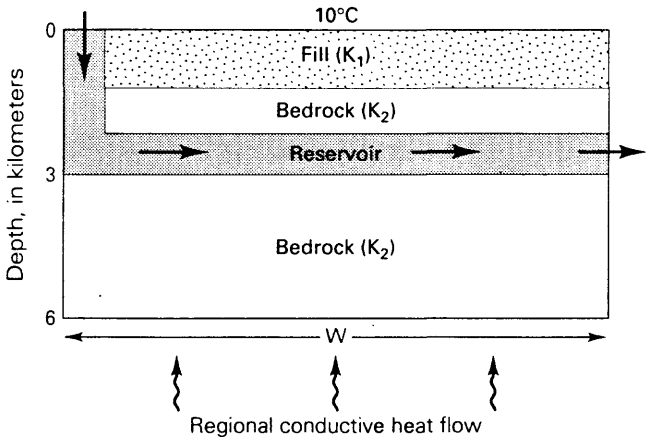

Figure 37. Lateral-flow model for numerical analysis of a Basin and Range hydrothermal system.

Computational Model

A simplified two-dimensional representation was used to generate numerical simulations for the lateral-flow model. A more detailed three-dimensional representation, which might also simulate the heat-flow anomalies at well QH3D and in the Panther Canyon area, was not attempted because of the lack of constraints from deep drilling data.

The two-dimensional computational model is shown in figure 37. The upflow portion of the circulation is not considered, under the assumption that reservoir temperatures at the exit on the right side of the model will be nearly equal to temperatures under the discharge area. Land-surface temperature and the temperature of the recharge water were fixed at 10°C and a uniform heat inflow of 150 mW/m^2 was specified at the base of the model at a depth of 6 km. Thermal conductivities of the fill and basement are the same as in the fault-plane model. Along the left-side boundary, heat is added over the depth of circulation D to simulate conduction from the adjacent basement. This lateral heat flow was specified on the basis of the fault-plane model results; the net effect is to raise the fluid temperature at depth D on the left side by about 40°C over that for an insulated boundary condition. The right-side boundary is assumed insulated; its effect is considered below.

Simulations were carried out for different model widths W, but with D = 3 km in each case. A 10 by 10 grid was used for each numerical simulation. The thicknesses of the fill layer and reservoir layer were 1.5 and 1 km, respectively. The conduction-only solution (not shown) provided initial temperature conditions for simulations with

fluid flow. This yielded an initial reservoir temperature which averaged 200°C.

Solutions with Fluid Flow

A flow rate of 1.2 kg/s/km was used in each simulation with the lateral-flow model, with the normalization done with respect to the dimension of the flow system normal to the 2-d cross-section. Steady-state results for the case where W = 10 km (fig. 38) show a reservoir temperature of 170°C at the of the model and a value of 117 mW/m^2 for surficial heat flow at the right side of the model. Reservoir temperatures at the right-side boundary increase as the width of the model increases, until W is about 15 outlet end km, at which point reservoir temperatures are in equilibrium with the vertical conductive flux of 150 mW/m^2 and the insulated boundary condition is strictly appropriate. Alternatively, higher exit temperatures could be obtained for W <15 km by increasing the depth of circulation. The duration of hydrothermal circulation is not as important in the results from this model because reservoir temperatures at the right-side boundary do not decrease significantly over the transient period for W ≥ 10 km.

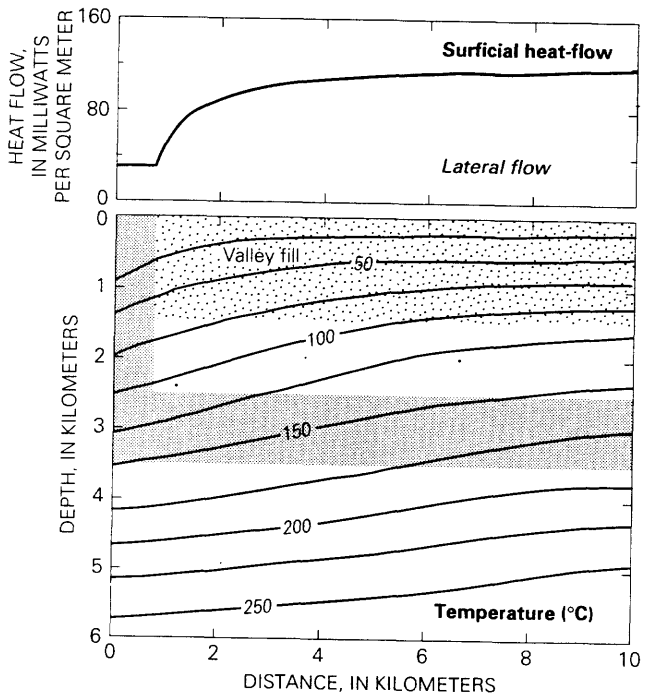

Figure 38. Steady-state temperature and surficial heat-flow distributions in lateral-flow model. Fluid flow rate=1.2 kg/s/km. Lines of equal temperature in degrees Celsius.

Simulated vertical temperature variations shown within the reservoir (fig. 38) would be smaller if a secondary convection-cell pattern were superimposed on the lateral-throughflow regime. This condition can be simulated in the model when the reservoir permeability is greater than about 5 x $10^{-14}m^2$ (50 millidarcies). However, the effects of this secondary convection on temperature variations and heat flow are less significant than was found by Sorey and others (1978) in model simulations of the Long Valley caldera, because the heat flux at the base of the model and at the bottom of the reservoir is much less than in the Long Valley model.

Fluid residence time calculated from equation 18 for the lateral-flow model results depicted in figure 37 is approximately 30,000 years with a reservoir porosity of 0.1. For a reservoir less than 1 km thick (or having a porosity less than 0.1), the corresponding residence time would be proportionately smaller because the fluid velocity would be higher. Relatively long residence times are consistent with the inference from the stable-isotope data that hot-spring water at Leach Hot Springs is late Pleistocene in age.

Pottorff (1988) and Lopez and others (1994) simulated the Leach Hot Springs flow system with 3-dimensional models that effectively

represent combinations of the fault-plane and lateral-flow models discussed above. In their models, ground water flows southward within the basin-bounding fault from which the springs discharge and westward from the Sonoma Range. The general pattern of fluid flow in these models is pictured in figure 39. Basal heat inputs and thermal-conductivity values for valley fill and basement were set to values close to those used in our simulations. In the model of Lopez and others (1994), circulatory free convection also occurs within the fault zone. Results from these 3-dimensional models fall between our results for the fault-plane and lateral-flow models in terms of depths of fluid circulation and areas of heat capture required to obtain temperatures near 180°C. Mean fluid residence times in the 3-dimensional models, for example 17,000 years in the model of Pottorff (1988), are also intermediate to our results for the limiting-case 2-dimensional models.

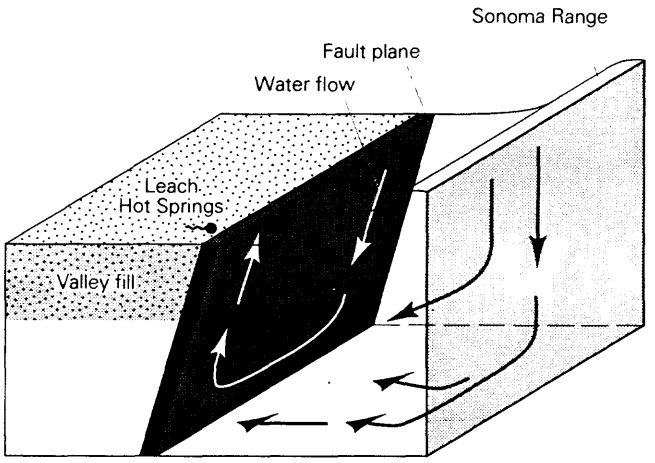

Figure 39. Conceptual model of a possible three-dimensional fluid-flow system supplying thermal water to Leach Hot Springs. (From Pottorff, 1989).

Generalizations and Constraints

The fault-plane and lateral-flow models introduce one level of complexity to the simplified constraint that the minimum depth of fluid circulation in Basin and Range hydrothermal systems can be approximated by the source-reservoir temperature divided by the background conductive temperature gradient. The 2-dimensional model results show that actual depths of fluid circulation required to obtain given reservoir temperate will exceed the estimated minimum depth unless the contact area for heating is relatively large or the flow system is relatively young and in a transient state. Results of simulations using 3-dimensional models involving fluid flow within a basin-bounding fault and the adjacent mountain block allow these constraints on reservoir temperature to be eased somewhat.

Additional constraints may be needed to decide which model actually applies to a particular system. For some systems, additional constraints on deep flow paths can be developed from stable isotope data, fluid-rock chemistry considerations, surficial heat-flow data, and hydraulic head and gradient data (Yeamans, 1983). For southern Grass Valley, stable-isotope and geochemical data suggest fluid residence times in pre-Tertiary basement rocks that are more in line with a deep flow system of basin-size dimensions than flow within a single fault conduit. Heat-flow measurements and chemical analyses suggest that thermal water from a common source reservoir contributes fluid to shallower zones over much of the southern Grass Valley region south of Leach Hot Springs. The available hydraulic-head data suggest that a potential may exist for thermal water to flow from the vicinity of wells QH3D and G105 toward

Leach Hot Springs. Temperature data from the 2.6-km deep Aminoil well indicate that thermal water (112°C) flows through a permeable zone near the top of the pre-Tertiary basement rocks northwest of Leach Hot Springs, but the data are inconclusive regarding the existence of a deeper, hotter reservoir.

The limiting factor in the occurrence of basin-sized high-temperature reservoirs within hydrothermal systems in the Basin and Range province is the need for laterally continuous permeability distributions. In the absence of geologic evidence for stratigraphic or lithologic control, as might be the case for Paleozoic carbonate rocks in some areas, deep fluid flow is most likely structurally controlled. Yeamans (1983) suggested that Basin and Range hydrothermal systems are not necessarily confined to the main range-bounding faults, but may occur within other structures where extensional tectonics have created permeable flow paths. Low-angle faults may in some cases provide conduits for fluid flow in basement rocks (Bartley and Glazner, 1985).

A common feature of these Basin and Range systems is a relatively low rate of fluid throughflow, as evidenced by rates of thermal-water discharge typically between 5 and 20 kg/s (Sorey, 1982; Olmsted and others, 1975). This factor suggests that the effective transmissivity of these flow systems is relatively low. Low or limiting transmissivity conditions could exist within the deep reservoir or within the upflow zone (or both). The actual distribution of high and low transmissivity determine whether and how a system can be exploited for geothermal energy, as shown by the analysis of Welch and others (1981).

SUMMARY AND CONCLUSIONS

Grass Valley is a typical structural basin in the northern part of the Basin and Range province. The basement that outlines the structural basin consists of slightly to moderately metamorphosed, intensively deformed sedimentary, volcanic, and plutonic rocks. These rocks have low primary porosity and permeability. More significant secondary porosity and permeability are related to fractures and to solution openings in carbonate rocks.

The valley fill within the basin consists of unconsolidated to semiconsolidated, undeformed to moderately deformed fluvial deposits, epiclastic and volcaniclastic deposits, tuff, and consolidated volcanic rocks--chiefly basalt flows and rhyolite. In the clastic deposits, porosity is chiefly primary and moderately high, permeability is moderate to low, and the ratio of horizontal to vertical permeability is high. In contrast, the physical characteristics of the Cenozoic basalt and rhyolite resemble those of the Paleozoic and Mesozoic basement.

Drilling-log data from shallow test wells indicate that 57 percent of the deposits penetrated in the near-surface part of the valley fill are coarse-grained, 38 percent are fine-grained, and 5 percent are tuffaceous. On this basis, core-sample data indicate that mean bulk density is 2,060 kg/m^3; mean porosity is about 37 percent; and mean bulk thermal conductivity is 1.56 W/m.K. However, gravity and deep-test-well data indicate that the mean density and mean thermal conductivity of the entire mass of valley fill may be substantially greater, possibly as much as 2,350 kg/m^3 and 2.19 W/m.K, respectively. The differences probably are due to lower porosity of

the major part of the valley fill in comparison with that of the near-surface part sampled by shallow test drilling. Measurements of grain properties indicate that, for the basement rocks, mean thermal conductivity is 2.72 W/m.K, and mean density is 2,670 kg/m^3.

Geophysical (chiefly gravity) data and limited deep test-well data indicate that the valley fill in southern Grass Valley is locally more than 1,800 m thick. The basement surface beneath the valley forms an asymmetrical trough with the axis located east of the center of the valley. Leach Hot Springs are in a northeast-trending fault zone near its intersection with a north-trending fault. At depth, however, the Bouguer gravity-anomaly pattern indicates that the hot springs fault zone has a north rather than a northeast trend. The fault zone, which has a throw of more than 800 m, separates the deep part of the southern Grass Valley basin from an alluvium-covered pediment on the east side of the valley. Throughout most of southern Grass Valley, faults along the east margin of the deep part of the basin appear to have larger aggregate throw than the faults along the west margin.

Ground water in southern Grass Valley comprises: (1) shallow ground water within the valley fill and the adjacent basement; and (2) deep, thermal water that circulates within the basement beneath the central part of the valley and rises along faults near the valley margins. Shallow ground water flows generally northward within the main, central part of southern Grass Valley. Information about patterns of deep ground-water flow is limited. Upward flow of thermal water from basement into valley fill is indicated at well site QH3, near the crest of a buried basement high 5 km south-southwest of Leach Hot Springs. The rising water is chemically and isotopically similar to the thermal water at Leach Hot Springs. Although the hydrostatic head of the water in the basement at site QH3 is greater than that at the orifices at Leach Hot Springs, heads at depth beneath the springs are unknown, and the flow of thermal water at depth is not necessarily from site QH3 toward the springs. The reversal of the temperature gradient within the basement at well QH3D seems to indicate flow of thermal water away from a heat source. Either this condition is transient or cooler water is flowing beneath the hotter water in order to maintain a heat sink. Hydrothermal upflow at Panther Canyon seems to be related to a fault or fault zone of large throw along the east margin of the basin. The upflow does not reach the land surface but instead appears to spread laterally at depths greater than 150 m.

Both thermal and nonthermal ground waters in southern Grass Valley have fairly low concentrations of dissolved solids. Except for samples from four nonthermal springs, in which dissolved-solids concentrations range from 600 to 910 mg/L, concentrations are lower in the nonthermal water (210-430 mg/L) than in most of the thermal water (500-620 mg/L). Thermal water differs from nonthermal water in having higher concentrations of sodium, potassium, fluoride, boron, and lithium and lower concentrations of calcium, magnesium, and chloride. Leach Hot Springs water has higher concentrations of silica than all the nonthermal water, but some thermal well water has lower concentrations than some nonthermal water.

Except for the acid-sulfate water at orifice 15 at Leach Hot Springs, which probably represents steam condensate in part, the hydrogen-isotope composition of thermal water in southern Grass Valley is lighter than that of all nonthermal waters

sampled. The lighter composition could result from (1) recharge of deep, thermal ground water from altitudes higher than those where recharge of shallow ground water occurs, (2) recharge from sometime in the past when the climate was colder than at present, or (3) both 1 and 2. The second or third possibilities, believed to be more likely than the first, suggest that thermal water in southern Grass Valley is at least 8,000 years old.

Excluding water from orifice 15, the ranges and averages for source temperatures of thermal water at Leach Hot Springs indicated by chemical geothermometry are 134-151 °C and 143 °C by the quartz-silica method, 200-223 °C and 209 °C by the sodium-potassium method, 94-143 °C and 106 °C by the potassium-magnesium method, 163-182 °C and 171 °C by the uncorrected sodium-potassium-calcium method, 126-162 °C and 146 °C by the magnesium-corrected sodium-potassium calcium method, and 151-163 °C and 158 °C by the sulfate-oxygen-isotope method. Because the water at Leach Hot Springs is not equilibrated according to the criterion proposed by Giggenbach (1988), the results from the sodium-potassium and potassium-magnesium methods are especially suspect. Considering all the evidence, the geothermometers indicate thermal-aquifer temperatures of 150-180 °C or possibly higher.

A predominantly conductive thermal regime and fairly uniform thermal conductivity within saturated valley fill is indicated by nearly constant temperature gradients at most places. However, increase in temperature gradient with depth, suggesting downward ground-water flow across bedding, was observed at two deep-well sites (QH3 and G106) in the south-central part of the valley. In contrast, upward flow at two other sites (the Aminoil well and G105) is indicated by a decrease in gradient with depth. The apparent decrease in gradient with depth at the Aminoil well may also reflect northwestward flow of thermal ground water from the Leach Hot Springs area in an aquifer or aquifers at depths greater than 49 m.

Unlike the valley fill, the basement and the consolidated volcanic rocks are characterized by nearly zero or reversed temperature gradients, indicating convection facilitated by vertical fracture permeability.

Southern Grass Valley contains at least three and possibly five near-surface heat-flow anomalies caused by rising thermal fluid: (1) The Leach Hot Springs anomaly, the largest and most intense anomaly and that associated with the only surface discharge of thermal fluid; (2) the south-central anomaly, a relatively small anomaly 6 km south of Leach Hot Springs; (3) the Panther Canyon anomaly, an extensive anomaly in the southeastern part of the valley; (4) the northwestern anomaly; and (5) the western anomaly. The last two anomalies have a maximum near-surface conductive heat flow of only 125-130 mW/m^2 and perhaps should not be considered anomalies. Whether the first three anomalies are manifestations of a single hydrothermal system or of separate systems is not known.

An average heat flow of 103-108 mW/m^2 was estimated from a heat budget for an area of 211 km^2 occupying most of southern Grass Valley. The estimate probably represents a minimum rather than a most likely value, chiefly because heat flow in the valley, which occupies only 37 percent of the tributary drainage basin, is likely to be less than in the mountains, and because lateral advective heat flux could not be estimated reliably and is not included in the total. Temperature-gradient

data in the Aminoil well northwest of Leach Hot Springs suggest a conductive heat flow of 150 ± 30 mW/m^2 in basement beneath the valley fill at that location. The mean heat flow in the southern Grass Valley area probably is within the range of 120-180 mW/m^2. A regional heat flow of 150 mW/m^2 is used in some of the modeling studies.

Two generalized conceptual models that apply as limiting cases to Basin and Range geothermal systems in areas of high regional heat flow were simulated numerically. The first, called the fault-plane model, consists of a steeply dipping fault zone that separates high-thermal-conductivity basement from low-thermal-conductivity valley fill at the edge of a basin. In this model, fluid flow at a specified rate per unit length of fault is restricted to a permeable fault plane. Conduction-only solutions with the fault-plane model show how thermal refraction can cause heat flows measured in valleys (basins) to be less than the regional average, and heat flows measured in the mountains to be higher than the regional average.

For reasonable estimates of fluid flow, the simulations for the fault-plane model indicated that circulation depths and fault lengths must be relatively large to obtain high fluid temperatures under steady-state conditions. Under transient conditions, circulation time becomes a critical factor in allowing shallower depths of circulation.

The alternative limiting-case model for Basin and Range hydrothermal systems is called the lateral-flow model. In contrast to the fault-plane model, this model involves a reservoir of considerable areal extent in which lateral flow occurs from beneath an area of recharge along a range-front fault toward an area of hot-spring discharge. This configuration captures regional heat flow more efficiently. Depths of circulation required to produce observed or inferred reservoir temperatures are correspondingly less, and duration of circulation is much less critical than in the fault-plane model. Evidence from the southern Grass Valley area, especially that indicating circulation of thermal fluid at several locations considerably removed from Leach Hot Springs, and also stable-isotope data, suggest the applicability of the lateral-flow model over the fault-plane model. A third model involving convective circulation in basin-bounding faults and advective flow through the adjacent Sonoma Range must also be considered as plausible for the Leach Hot Springs hydrothermal system.

REFERENCES CITED

Bartley, J.M., and Glazner, A.F., 1985, Hydrothermal systems and Tertiary low-angle normal faulting in the southwestern United States: Geology, v. 13, p. 562-564.

Benson, L.V., 1978, Fluctuation in the level of pluvial Lake Lahontan during the last 4900 years: Quaternary Research, v. 9, p. 300-318.

_____, 1994, Stable isotopes of oxygen and hydrogen in the Truckee River-Pyramid Lake surface-water system. 1. Data analysis and extraction of paleoclimatic information: Limnology and Oceanography, v. 39, no. 2, p. 344-355.

Beyer, J.H., 1977, Telluric and D.C. resistivity techniques applied to the geophysical investigation of Basin and Range geothermal systems, Part III. The analysis of data from Grass Valley, Nevada: Lawrence Berkeley Laboratory, Report LBL-6325 3/3, 115 p.

Beyer, J.H., Dey, Abhijit, Liaw, A.L.C., Majer, E.L., McEvilly, T.V., Morrison, H.F., and Wollenberg, H.A., 1976a, Geological and geophysical studies in Grass Valley, Nevada: Lawrence Berkeley Laboratory Preliminary Open-File Report LBL-5262, 144 p.

Beyer, J.H., Morrison, H.F., and Dey Abhijit, 1976b, Electrical exploration of geothermal systems in the Basin and Range valleys of Nevada, *in* Second U.N. Symposium on the development and use of geothermal resources, Proceedings: v. 2, p. 889-894.

Blackwell, D.D., 1983, Heat flow in the northern Basin and Range province: Geothermal Resources Council, Special Report No. 13, p. 81-92.

Blackwell, D.D., and Chapman, D.S., 1977, Interpretation of geothermal gradient and heat flow data for Basin and Range geothermal systems: Geothermal Resources Council, Transactions, v. 1, p. 19-20.

Bliss, J.D., 1983, NEVADA basic data for thermal springs and wells as recorded in GEOTHERM: U.S. Geological Survey Open-File Report 83-433, 707 p.

Bodvarsson, Gunnar, 1979, Convection and thermoelastic effects in narrow vertical fracture spaces with emphasis on analytical techniques: Final Report on U.S. Geological Survey Grant No. 14-08-001-6-398, 111 p.

Bredehoeft, J.D., and Papadopulos, I.S. 1965, Rates of vertical ground-water movement estimated from the earth's thermal profile: Water Resources Research, v. 1, no. 2, p. 325-328.

Brogan, G.E., and Birkhahn, P.C., 1981, Faults and occurrence of geothermal anomalies: Final report for contract No. 14-08-0001-16310 for the U.S. Geological Survey, 93 p.

Brook, C.A., Mariner, R.H., Mabey, D.R., Swanson, J.R., Guffanti, Marianne, and Muffler, L.J.P., Hydrothermal convection systems with reservoir temperatures >90°C, *in* Assessment of geothermal resources of the United States, L.J.P. Muffler, ed.: U.S. Geological Survey Circular 790, p. 18-85.

Buchanan, P.K., 1989, Recharge of geothermal fluids in the Great Basin: Geothermal Resources Council Transactions, v. 13, p. 117-123.

Christiansen, R.L., and McKee, E.H., 1978, Late Cenozoic volcanic and tectonic evolution of the Great Basin and Columbia? Intermontane regions, *in* Cenozoic tectonics and regional geophysics of the western Cordillera, R.B. Smith and G. P. Eaton, eds.: Geological Society of America Memoir 152, p. 283-311.

Cohen, Philip, 1964, A brief appraisal of the ground-water resources of the Grass Valley area, Humboldt and Pershing Counties, Nevada: Nevada Department of Conservation and Natural Resources, Ground Water Resources Reconnaissance Series Report 29, 40 p.

Coney, P.J., 1978, Mesozoic-Cenozoic Cordilleran plate tectonics, *in* Cenozoic tectonics and regional geophysics of the western Cordillera, R.B. Smith and G.P Eaton eds.: Geological Society of America Memoir 152, p. 33-50.

Cordell, Lindrith, and Henderson, R.G., 1968, Iterative three-dimensional selection of gravity anomaly data using digital computer: Geophysics, v.33, no. 4, p. 596-601.

Corwin, R.F., 1976, Self-potential exploration for geothermal resources: 2nd U.N. Symposium on the Development and Use of Geothermal Resources, v. 2, p. 937-945.

Craig, Harmon, 1961, Isotopic variations in meteoric waters: Science, v. 133, no. 3465, p. 1702-1703.

Criss, R.E., and Taylor, H.P., Jr., 1986, Meteoric-hydrothermal systems *in* Stable isotopes in high-temperature geological processes, Valley, J.W., Taylor, H.P., Jr., and O'Neil, J.R., eds.: Reviews of Mineralogy, v. 16, p. 373-424.

Dansgaard, W., 1964, Stable isotopes in precipitation: Tellus, v. 16, p. 436-464.

Dansgaard, W., Johnsen, S.J., Moller, J., and Langway, C.C., Jr., 1969, One thousand centuries of climatic record from Camp Century on the Greenland Ice Sheet: Science, v. 166, p. 377-381.

Davis, G.A., 1979, Problems of intraplate extensional tectonics, western United States, with special emphasis on the Great Basin, *in* 1979 Basin and Range symposium, G.W. Newman and H.D. Goode, eds.: Rocky Mountain Association of Geologists and Utah Geological Association, p. 41-54.

Davis, S.N., and DeWiest, R.J.M., 1966, Hydrogeology: New York, John Wiley & Sons, Inc., 463 p.

Dey, Abhijit, and Morrison, H.F., 1977, An analysis of the dipole-dipole resistivity method for geothermal exploration: Lawrence Berkeley Laboratory Report LBL-7332, 60 p.

Dreyer, R. M., 1940, Goldbanks mining district, Pershing County, Nevada: Nevada University Bulletin, v. 34, no. 1, 38 p.

Dutcher, L.C., and Garrett, A.A., 1963, Geologic and hydrologic features of the San Bernardino area, California: U.S. Geological Survey Water-Supply Paper 1419, 114 p.

Eaton, G.P., 1982, The Basin and Range province, origin and tectonic significance: Annual Review Earth Planetary Science, v. 10, p. 409-440.

Epstein, S.E., and Gow, A.J., 1970, Antarctic ice sheet: Stable isotope analysis of Byrd Station cores and interhemispheric climatic implications: Science, v. 168, p. 1570-1572.

Erwin, J.W., 1974, Bouguer gravity map of Nevada, Winnemucca sheet: Nevada Bureau of Mines and Geology Map 47, scale 1:250,000.

Faust, C.R., and Mercer, J.W., 1977, Finite-difference model of two-dimensional, single- and two-phase heat transport in a porous medium -- Version I: U.S. Geological Survey Open-File Report 77-234, 84 p.

Fenneman, N.M., 1931, Physiography of western United States: New York, McGraw-Hill, 534 p.

Flynn, Thomas, and Buchanan, P.K., 1993, Pleistocene origin of geothermal fluids in the Great Basin, western United States: Resource Geology Special Issue, No. 16, p. 60-68.

Fouillac, Christian, and Michard, Gil, 1981, Sodium-lithium ratio in water applied to the geothermometry of geothermal waters: Geothermics, v. 10, p. 55-70.

Fournier, R.O., 1981, Application of water geochemistry to geothermal exploration and reservoir engineering, *in* Rybach, Ladislaus, and Muffler, L.J.P., eds., Geothermal systems, Principles and case histories: New York, John Wiley & Sons, p. 109-143.

Fournier, R.O., and Potter, R.W. II, 1979, A magnesium correction for the Na-K-Ca chemical geothermometer: U.S. Geological Survey Open-File Report 78-796, 24 p.

Fournier, R.O. and Truesdell, A.H., 1974, Geochemical indicators of subsurface temperature--Part 1, Basic assumptions: U.S. Geological Survey Journal of Research, v. 2, no. 3, p. 259- 262.

Friedman, Irving, Redfield, A.C., Schoen, B., and Harris, J., 1964, The variation of the deuterium content of natural waters in the hydrologic cycle: Reviews of Geophysics. v. 2, p. 177-224.

Friedman, Irving, and O'Neil, J.R., 1977, Compilation of stable isotope fractionation factors of geochemistry interest: U.S. Geological Survey Professional Paper 440-K, 12 p.

Friedman, Irving, Smith, G.I., Gleason, J.D., Warden, Augusta, and Harris, J.M., 1992, Stable isotope composition of waters in southeastern California 1. Modern precipitation: Journal of Geophysical Research, v. 97, no. D5, p. 5795-5812.

Fritz, P., and Fontes, J.Ch., 1980, Handbook of environmental isotope geochemistry: volume 1, Elsevier Scientific Publishing Co., New York, 545 p.

Gamble, T.D., Goubau, W.M., and Clarke, J., 1977, Magnetotelluric data analysis: Tests of methods using data obtained at Grass Valley, Nevada: Lawrence Berkeley Laboratory Report LBL-6648

Gat, J.R., 1971, Comments on the stable isotope method in regional ground-water investigations: Water Resources Research, v. 7, no. 4, p. 980-993.

_____, 1980, The isotopes of hydrogen and oxygen in precipitation: Chapter 1 *in* Fritz, P., and Fontes, J.Ch., eds., Handbook of environmental isotope geochemistry: volume 1, Elsevier Scientific Publishing Co., New York, p. 20-47.

Giggenbach, W.F., 1988, Geothermal solute equilibria. Derivation of Na-K-Mg-Ca geoindicators: Geochimica et Cosmochimica Acta, v. 52, p.2749-2765.

Gilbert, C.M., and Reynolds, M.W., 1973, Character and chronology of basin development western margin of the Basin and Range province: Geological Society of America Bulletin, v. 84, no.8, p. 2489-2509.

Gilluly, James, 1963, The tectonic evolution of the western United States: Geological Society of London Quarterly Journal, v. 119, part 2, p.133-174.

Goldstein, N.E., and Paulsson, B., 1977, Interpretation of gravity surveys in Grass and Buena Vista Valleys, Nevada: Lawrence-Berkeley Laboratory Report LBL-7013, 43 p.

_____, 1978, Interpretation of gravity surveys in Grass and Buena Vista Valleys, Nevada: Geothermics, v. 7, no. 1, p. 29-50.

Hamilton, Warren, and Myers, W.B., 1966, Cenozoic tectonics of the western United States: Reviews of Geophysics, v. 4, p. 509-549.

Hansen, R.L., 1963, Surface water, *in* Cohen, Philip, ed., An evaluation of the water resources of the Humboldt River valley near Winnemucca, Nevada: Nevada Department of Conservation and Natural Resources Bulletin 24, p. 39-57.

Harbeck, G.E., Jr., 1962, A practical field technique for measuring reservoir evaporation utilizing mass-transfer theory: U.S. Geological Survey Professional Paper 272-E, p. 1-6.

Hardman, George, 1936, Nevada precipitation and acreages of land by rainfall zones: University of Nevada Agriculture Experimental Station mimeographed report and map, 10 p.

Hardman, George, 1965, Nevada precipitation map, adapted from map prepared by George Hardman and others, 1936: University of Nevada Agricultural Experiment Station, Bulletin 183, 57 p.

Heaton, T.H.E., Talma, A.S., and Vogel, J.C., 1986, Dissolved gas paleotemperatures and ^{18}O variations derived from ground water near Uitenhage, South Africa: Quaternary Research, v. 25, p. 79-88.

Hose, R.K., and Taylor, B.E., 1974, Geothermal systems of northern Nevada: U.S. Geological Survey Open-File Report 74-271, 27 p.

Ingraham, N.L., and Taylor, B.E., 1991, Light stable isotope systematics of large-scale hydrologic regimes in California and Nevada: Water Resources Research, v. 27, no. 1, p. 77-90.

Jacobson, R.L., Ingraham, N.L., and Campana, 1983, Isotope hydrology of a Basin and Range geothermal system: Water Resources Center, Desert Research Institute, University of Nevada System, Publication 41087, Reno, 18 p.

Johnson, M.G., 1977, Geology and mineral deposits of Pershing County, Nevada: Nevada Bureau of Mines and Geology Bulletin 89, 115 p.

Jones, C.J., 1915, The Pleasant Valley, Nevada, earthquake of October 2, 1915: Seismological Society of America Bulletin, v. 5, no. 4, p. 190.

Karst, G.B., Campana, M.E., and Jacobson, R.L., 1988, A mixing-cell model of the hydrothermal flow system, northern Dixie Valley, Nevada: Geothermal Resources Council Transactions, v. 12, p. 167-174.

Kharaka, Y.K., and Barnes, Ivan, 1973, SOLMNEQ-solution mineral equilibrium computations: Menlo Park, California, U.S. Geological Survey Computer Contribution, 81 p.; U.S. Department of Commerce, National Technical Information Service, Springfield, VA 22151 Report B-215 899.

Kharaka, Y.K., Specht, D.J., and Carothers, W.W., 1985, Low to intermediate subsurface temperatures calculated by chemical geothermometers: American Association of Petroleum Geologists Bulletin, v. 69/2, p. 273.

King, Clarence, 1878, Systematic geology: U.S. Geological exploration of the 40th parallel, v. 1, 803 p.

Kohler, M.A., Nordenson, T.J., and Baker, D.R., 1959, Evaporation maps for the United States: U.S. Department of Commerce, Weather Bureau Technical Paper 37, 13 p, 5 pls.

Köppen, W., 1931, Grundiss der Klimakunde: Walter de Gruyter & Co., Berlin.

Lachenbruch, A.H., 1968, Rapid estimation of the topographic disturbance to superficial thermal gradients: Reviews of Geophysics, v. 6, no. 3, p.365-400.

Lachenbruch, A.H., and Sass, J.H., 1977, Heat flow in the United States and the thermal regime of the crust, *in* Heacock, J.G., ed., The Earth's Crust: American Geophysical Union Monograph 20, p. 625-675.

Lee, T.C., and Henyey, T.L., 1974, Heat-flow refraction across dissimilar media: Geophysical Journal of the Royal Astronomical Society, v. 39, p.319-333.

Liaw, A.L.C., 1977, Microseisms in geothermal exploration; Studies in Grass Valley, Nevada: Lawrence Berkeley Laboratory Report LBL-7002, 181 p.

Lloyd, R.M., 1968, Oxygen isotope behavior in the sulfate-water system: Journal of Geophysical Research, v. 73, p. 6099-6110.

Lopez, D.L., Smith, Leslie, and Sorey, M.L., 1994, Modeling fluid flow and heat transfer at Basin and Range faults: Preliminary results for Leach Hot Springs, Nevada: Transactions of the Geothermal Resources Council, v. 18, p. 11-16.

Lopez, D.L., and Smith, Leslie, 1995, Fluid flow in fault zones: Analysis of the interplay of convective circulation and topographically driven ground-water flow: Water Resources Research, v. 31, p. 1489-1503.

Louderback, G.D., 1924, Period of scarp production in the Great Basin: University of California Publications in Geological Sciences, v. 15, p. 1-44.

Lowell, R.P., 1979, The onset of convection in a fault zone: Effect of anisotropic permeability: Geothermal Resources Council, Transactions, v. 3, p. 377-380.

Majer, E.L., 1978, Seismological investigations in geothermal regions: Lawrence Berkeley Laboratory Report LBL 7054, 225 p.

Mariner, R.H., Brook, C.A., Reed, M.J., Bliss, J.D., Rapport, A.L., and Lieb, R.J., 1983a, Low-temperature geothermal resources in the western United States, *in* Assessment of low-temperature geothermal resources of the United States--1982, M.J. Reed, ed.: U.S. Geological Survey Circular 892, p. 31-50.

Mariner, R.H., Presser, T.S., and Evans, W.C., 1983b, Geochemistry of active geothermal systems in the northern Basin and Range province: Geothermal Resources Council Special Report No. 13, p. 95-119.

Mariner, R.H., Presser, T.S., Rapp, J.B., and Willey, L.M., 1975, The minor and trace elements, gas, and isotope compositions of the principal hot springs of Nevada and Oregon: U.S. Geological Survey Open-File Report, 27 p.

Mariner, R.H., Rapp, J.B., Willey, L.M., and Presser, T.S., 1974, The chemical composition and estimated minimum thermal reservoir temperature of the principal hot springs of northern and central Nevada: U.S. Geological Survey Open-File Report, 32 p.

Maxey, G.B., and Eakin, T.E., 1949, Ground water in White River Valley, White Pine, Nye, and Lincoln Counties, Nevada: Nevada State Engineer Water Resources Bulletin 8, 59 p.

McKenzie, W.F., and Truesdell, A.H., 1977, Geothermal reservoir temperatures estimated from the oxygen-isotope compositions of dissolved sulfate in water from hot springs and shallow drill holes *in* Proceedings of the International Atomic Energy Agency Advisory Group on the Application of Nuclear Techniques to Geothermal Studies, Pisa, Italy: Geothermics, Special Issue.

Morrison, H.F., Lee, K.H., Opplinger, Gary, and Dey, Abhijit, 1979, Magnetotelluric studies in Grass Valley, Nevada: Berkeley, Lawrence Berkeley Laboratory Report 8643, 160 p.

Murphy, H.D., 1979, Flow near the outlet of a geothermal energy reservoir: Los Alamos Scientific Laboratory, NM, Report no. 7906-7, UC66a, July, 272 p.

National Oceanic and Atmospheric Administration, 1975, Climatological Data, Nevada, Annual Summary, 1975: U.S. Department of Commerce, NOAA (formerly U.S. Weather Bureau), v. 90, no. 13.

Nehring, N.L., and Mariner, R.H., 1979, Sulfate water isotopic equilibrium temperatures for thermal springs and wells of the Great Basin: Geothermal Resources Council, Transactions, v. 3, p. 485-488.

Nehring, N.L., Mariner, R.H., White, L.D., Huebner, M.A., Roberts, E.D., Harmon, Karen, Bowen, P.A., and Tanner, Lane, 1979, Sulfate geothermometry of thermal waters in the western United States: U.S. Geological Survey Open-File Report 79-1135, 11 p.

Nielsen, R.L., 1965, Right-lateral strike-slip faulting in the Walker Lane, west-central Nevada: Geological Society of America Bulletin, v. 76, p. 1301-1308.

Noble, D.C., 1975, Geologic history and geothermal potential of the Leach Hot Springs Area, Pershing County, Nevada: Preliminary report to the Lawrence Berkeley Laboratory.

Noble, D.C., Wollenberg, H.A., Silberman, M.L., and Archibald, Douglas, 1975, Late Cenozoic structural, volcanic, and hydrothermal evolution of the Leach Hot Springs geothermal area, Pershing County, Nevada [abs.]: Geological Society of America Abstracts with Programs, v. 7, p. 357.

Nolan, T.B., 1943, The Basin and Range province in Utah, Nevada, and California: U.S. Geological Survey Professional Paper 197-D, p. 141-196.

Nordstrom, D.K., and Jenne, E.A., 1977, Fluorite solubility equilibria in selected geothermal waters: Geochimica et Cosmochimica Acta, v. 41, no. 2, p. 175-188.

O'Connell, M.F., and Kaufmann, R.F., 1976, Radioactivity associated with geothermal waters in the western United States, basic data: Las Vegas, U.S. Environmental Protection Agency, Office of Radiation Programs, Technical Note ORP/LV-75-8A, 34 p.

Olmsted, F.H., Glancy, P.A., Harrill, J.R., Rush, F.E., and VanDenburgh, A.S., 1973, Sources of data for evaluation of selected geothermal areas in northern and central Nevada: U.S. Geological Survey Water-Resources Investigations Report 44-74, 78 p.

Olmsted, F.H., Glancy, P.A., Harrill, J.R., Rush, F.E., and VanDenburgh, A.S., 1975, Preliminary hydrogeologic appraisal of selected hydrothermal systems in northern and central Nevada: U.S. Geological Survey Open-File Report 75-56, 276 p.

Olmsted, F.H., Welch, A.H., VanDenburgh, A.S., and Ingebritsen, S.E., 1984, Geohydrology, aqueous geochemistry, and thermal regime of the Soda Lakes and Upsal Hogback geothermal systems, Churchill County, Nevada: U.S. Geological Survey Water-Resources Investigations Report 84-4054, 166 p.

Page, B.M., 1935, Basin-Range faulting of 1915 in Pleasant Valley, Nevada: Journal of Geology, v. 43, no. 7, p. 690-707.

Parasnis, D. S., 1971, Temperature extrapolation to infinite time in geothermal measurements: Geophysical Prospecting, v. 19, p. 612-614.

Phillips, F.M., Campbell, A.R., Smith, G.I., and Bischoff, J.L., 1994, Interstadial climatic cycles: A link between western North America and Greenland?: Geology, v. 22, p. 1115-1118.

Poland, J.F., Piper, A.M., and others, 1956, Ground-water geology of the coastal zone of the Long Beach-Santa Ana area, California: U.S. Geological Survey Water-Supply Paper 1109, 162 p.

Poland, J.F., Garrett, A.A., and Sinnott, Allen, 1959, Geology, hydrology, and chemical character of ground waters in the Torrance-Santa Monica area, California: U.S. Geological Survey Water-Supply Paper 1461, 425 p.

Pottorff, 1988, A new approach for simulating heat transfer and groundwater flow in the Leach Hot Springs hydrothermal system, Pershing County, Nevada: University of Nevada, Reno, Master's Thesis, 153 p.

Pritt, Jeffrey, and Jones, B.E., eds., 1989, 1990 National Water Quality Laboratory Services Catalog: U.S. Geological Survey Open-File Report 89-386, 119 p.

Proffett, J.M., Jr., 1977, Cenozoic geology of the Yerington district, Nevada, and implications for the nature and origin of Basin and Range faulting: Geological Society of America Bulletin, v. 88, p. 247-266.

Renner, J.L., White, D.E., and Williams, D.L., 1975, Hydrothermal convection systems, *in* Assessment of geothermal resources of the United States--1975, D.E. White and D.L. Williams, eds.: U.S. Geological Survey Circular 726, p. 5-57.

Roberts, R.J., 1951, Geology of the Antler Peak quadrangle, Nevada: U.S. Geological Survey Geologic Quadrangle Map GQ 10, scale 1:62,500.

Roberts, R.J., 1968, Tectonic framework of the Great Basin, *in* A coast to coast tectonic study of the United States (V.H. McNutt--Geology Department Colloquium Series 1): Missouri University, Rolla, Journal No. 1, p. 101-119.

Roberts, R.J., Hotz, P., Gilluly, James, and Ferguson, H.G., 1958, Paleozoic rocks of north-central Nevada: American Association of Petroleum Geologists Bulletin, v. 42, p. 2813-2857.

Rozanski, Kazimierz, Araguas-Araguas, Luis, and Gonfiantini, Roberto, 1992, Relation between long-term trends of oxygen-18 isotope composition of precipitation and climate: Science, v. 258, p. 981- 985.

Russell, I.C., 1885, Geological history of Lake Lahontan, a Quaternary lake of northwestern Nevada: U.S. Geological Survey Monograph 11, 288 p.

Sass, J.H., Lachenbruch, A.H., Munroe, R.G., Greene, G.W., and Moses, T. H., Jr., 1971, Heat flow in the western United States: Journal of Geophysical Research, v. 76, p. 6376-6413.

Sass, J.H., Olmsted, F.H., Sorey, M.L., Wollenberg, H.A., Lachenbruch, A.H., Munroe, R.J., and Galanis, S.P., Jr., 1976, Geothermal data from test wells drilled in Grass Valley and Buffalo Valley, Nevada: U.S. Geological Survey Open-File Report 76-85, 43 p.

Sass, J.H., Ziagos, J.P., Wollenberg, H.A., Munroe, R.J., diSomma, D.E., and Lachenbruch, A.H., 1977, Application of heat-flow techniques to geothermal energy exploration, Leach Hot Springs area, Grass Valley, Nevada: U.S. Geological Survey Open-File Report 77-762, 125 p.

Schaefer, D.H., and Maurer, D.K., 1981, Geophysical reconnaissance of Lemmon Valley,

Washoe County, Nevada: U.S. Geological Survey Open-File Report 80-1123, 29 p.

Sheppard, S.M.F., 1986, Characterization and isotopic variations in natural waters, chapter 6 *in* Valley, J.W., Taylor, HP., Jr., and O'Neil, J.R., eds., Stable isotopes in high temperature geological processes: Reviews in Mineralogy, v. 16, Mineralogical Society of America, p. 165-183.

Silberling, N.J., 1973, Geologic events during Permian-Triassic time along the Pacific margin of the United States, *in* Logan, A., and Hills, L.V., eds., The Permian and Triassic Systems and their mutual boundary: Alberta Society of Petroleum Geology, Calgary, Alberta, Canada, p. 345-362.

Silberling, N.J., and Roberts, R.J., 1962, Pre-Tertiary stratigraphy and structure of northwestern Nevada: Geological Society of America Special Paper 72, 58 p.

Smith, G.I., Friedman, Irving, Gleason, J.D., and Warden, Augusta, 1992, Stable isotope composition of waters in southeastern California: 2. Groundwaters and their relation to modern precipitation: Journal of Geophysical Research, v. 97, no. D5, p. 5813-5823.

Smith, J.F., Jr., and Ketner, K.B., 1977, Tectonic events since early Paleozoic in the Carlin-Pinon Range area, Nevada: U.S. Geological Survey Professional Paper 867-C, p. C1-C18.

Sorey, M.L., 1971, Measurement of vertical groundwater velocity from temperature profiles in wells: Water Resources Research, v. 7, no. 4, p. 963-970.

_____, 1975, Numerical modeling of liquid geothermal systems: U.S. Geological Survey Open-File Report 75-613, 66 p.

_____, 1978, Numerical modeling of liquid geothermal systems: U.S. Geological Survey Professional Paper 1044-D, 25 p.

_____, 1982, Geothermal reservoirs in hydrothermal convection systems: Proceedings of 8th Workshop Geothermal Reservoir Engineering, Stanford University, Stanford, CA, SGP-TR-60, p. 5-17.

Sorey, M.L., and Olmsted, F.H., 1994, The Leach Hot Springs hydrothermal system, Pershing County, Nevada: Transactions of the Geothermal Resources Council, v. 18, p. 31-36.

Spaulding, W.G., 1985, Vegetation and climates of the past 45,000 years in the vicinity of the Nevada Test Site, south-central Nevada: U.S. Geological Survey Professional Paper 1329, 83 p.

Speed, R.C., 1971, Golconda thrust, western Nevada--Regional extent: Geological Society of America Abstracts with Programs, v. 3, no. 2, p. 199-200.

Speed, R.C., and Sleep, N.H., 1982, Antler orogeny and foreland basin: A model: Geological Society of America Bulletin, v. 93, p. 815-828.

Stewart, J.H., 1983, Cenozoic structure and tectonics of the northern Basin and Range province, California, Nevada, and Utah: Geothermal Resources Council, Special Report no. 13, p. 25-40.

Stewart, J.H., and McKee, E.H., 1977, Geology and mineral deposits of Lander County, Nevada: Nevada Bureau of Mines and Geology Bulletin 88, 106 p.

Stewart, J.H., and Poole, F.G., 1974, Lower Paleozoic and uppermost Precambrian Cordilleran miogeocline, Great Basin, Western United States, *in* Dickinson, W.R.,

ed., Tectonics and Sedimentation: Society of Economic Paleontologists and Mineralogists Special Publication 22, p. 28-57.

Stute, Martin, and Deak, Jozsef, 1989, Environmental isotope study (^{14}C, ^{13}C, ^{18}O, noble gases) on deep groundwater circulation systems in Hungary with reference to paleoclimate: Radiocarbon, v. 31, no. 3, p. 902-918.

Stute, Martin, and Schlosser, P., 1993, Principles and applications of the noble gas paleothermometer *in* Climate change in continental isotopic records, Swart, P.K., Lohmann, K.C., McKenzie, J., and Savin, S., eds.: Geophysical Monograph 78, p. 89-111.

Stute, Martin, and Sonntag, C., 1992, Paleotemperatures derived from noble gases dissolved in groundwater and in relation to soil temperature in Isotopes of noble gases as tracers in environmental studies, Loosli, H.H., and Mazor, E., eds.: International Atomic Energy Agency, Vienna, p. 111-122.

Szabo, B.J., Kolesar, P.T., Riggs, A.C., Winograd, I.J., and Ludwig, K.R., 1994, Paleoclimatic inferences from a 120,000-yr calcite record of water-table fluctuation in Browns Room of Devils Hole, Nevada: Quaternary Research, v. 41, p. 59-69.

U.S. Geological Survey, 1973, Aeromagnetic map of the Leach Hot Springs and Cherry Creek quadrangles, Pershing, Humboldt, and Lander Counties, Nevada: U.S. Geological Survey Open-File map.

University of Utah Research Institute, 1981a, Water geochemistry and hydrothermal study: Salt Lake City, University of Utah Open-File item Leach Hot Springs (LCH)-1, 11 p.

_____, 1981b, Gravity survey data and interpretations: Salt Lake City, University of Utah Open-File item Leach Hot Spring (LCH)-2.

_____, 1981c, Geologic report and Kelsh plotter photomapping: Salt Lake City, University of Utah Open-File item Leach Hot Springs (LCH)-3, 21 p.

_____, 1981d, Temperature-gradient and heat-flow data for Grass Valley: Salt Lake City, University of Utah Open-File item Leach Hot Springs (LCH)-4, 142 p.

_____, 1981e, Magnetotelluric survey of the Leach Hot Springs area: Salt Lake City, University of Utah Open-File item Leach Hot Springs (LCH)-5, 23 p.

_____, 1981f, Seismic reflection survey of Grass Valley area: Salt Lake City, University of Utah Open-File item Leach Hot Springs (LCH)-6, 13 p.

University of Utah Research Institute, 1981g, Geology and geothermal regime, geothermal test well USA #11-36, Grass Valley: Salt Lake City, University of Utah Open-File item Leach Hot Springs (LCH)-7, 14 p.

_____, 1981h, Daily drilling reports and workover record, well USA #11-36: Salt Lake City, University of Utah Open-File item Leach Hot Springs (LCH)-8, 52 p.

van der Straaten, C.M., and Mook, W.G., 1983, Stable isotopic composition of precipitation and climatic variability in Paleoclimates and paleowaters, a collection of environmental isotope studies: International Atomic Energy Agency, Vienna, p. 53-64.

Wallace, R.E., 1977, Profiles and ages of young fault scarps, north-central Nevada: Geological Society of America Bulletin, v. 88, p. 1267-1281.

Wallace, R.E., 1980, Map of fault scarps formed during earthquake of October 2, 1915, Pleasant Valley, Nevada, and other young fault scarps: U.S. Geological Survey Open File Report 80-608.

Waring, G.A., 1965, Thermal springs of the United States and other countries of the world--A summary: U.S. Geological Survey Professional Paper 492, 383 p.

Welch, A.H., and Preissler, A.M., 1986, Aqueous geochemistry of the Bradys Hot Springs geothermal area, Churchill County, Nevada, *in* Subitzky, Seymour, ed., Selected papers in the hydrologic sciences 1986: U.S. Geological Survey Water-Supply Paper 2290, p. 17-36.

Welch, A.H., and Preissler, A.M., 1990, Geothermal resources of the western arm of the Black Rock Desert, northwestern Nevada--part II, Aqueous geochemistry and hydrology: U.S. Geological Survey Water-Resources Investigations Report 87-4062, 91 p.

Welch, A.H., Sorey, M.L., and Olmsted, F.H., 1981, The hydrothermal system in southern Grass Valley, Pershing County, Nevada: U.S. Geological Survey Open-File Report 81-915, 193 p.

Wells, P.J., 1983, Paleogeography of montane islands in the Great Basin since the last glaciopluvial: Ecological Monographs, v. 53, p. 341-382.

Wheatcraft, S.W., 1983, Numerical simulation of the geothermal reservoir in the Leach Hot Springs area, Grass Valley, Nevada: University of Nevada, Desert Research Institute, Water Resources Center, Publication No. 41089, 40 p.

White, D.E., 1970, Geochemistry applied to the discovery, evaluation, and exploitation of geothermal energy resources, *in* Proceedings of the United Nations symposium on the development and utilization of geothermal resources: Pisa, Geothermatics, Special Issue 2, part I.

White, D.E., Barnes, Ivan, and O'Neil, J.R., 1973, Thermal and mineral waters of nonmeteoric origin, California Coast Ranges: Geological Society of America Bulletin, v. 84, p. 547-560.

Wilt, M., Goldstein, N., Stark, M., and Haught, R., 1980, An electromagnetic (EM-60) survey in the Panther Canyon area, Grass Valley, Nevada: Lawrence Berkeley, Report LBL-10993, UC-66b, 97 p.

Winograd, I.J., and Friedman, Irving, 1972, Deuterium as a tracer of regional ground-water flow, south Great Basin, Nevada and California: Geological Society of America Bulletin, v. 83, p. 3691-3708.

Winograd, I.J., and Pearson, F.J., Jr., 1976, Major carbon-14 anomaly in a regional carbonate aquifer: Possible evidence for megascale channeling, south-central Great Basin: Water Resources Research, v. 12, no. 6, p. 1125-1143.

Wollenberg, H.A., 1974, Radioactivity of Nevada hot-spring systems: Geophysical Research Letters, v. 1, p. 359-362.

Wollenberg, H.A., Bowman, H.R., and Asaro, Frank, 1977, Geochemical studies at four northern Nevada hot spring areas: Lawrence Berkeley Laboratory Report LBL-6808, 69 p.

Wood, W.W., 1976, Guidelines for collection and field analysis of ground-water samples for selected unstable constituents: U.S. Geologi-

cal Survey Techniques of Water-Resources Investigations, Book 1, Chapter D2, 24 p.

Yapp, C.J., and Epstein, S., 1977, Climatic implications of D/H ratios of meteoric water over North America (9,500-22,000 B.P.) as inferred from ancient wood cellulose C-H hydrogen: Earth and Planetary Science Letters, v. 34, p. 333-350.

Yeamans, Frank, 1983, Basin and Range geothermal hydrology: An empirical approach: Geothermal Resources Council, Special Report No. 13, p. 159-175.

Zaporozec, Alexander, 1972, Graphical interpretation of water-quality data: Ground Water, v. 10, no. 2, p. 32-43.

Zietz, Isidore, Gilbert, F.P., and Kirby, J.R., 1978, Aeromagnetic map of Nevada color-coded intensities: U.S. Geological Survey Geophysical Investigations Map GP-922, scale 1:1,000,000.

Zoback, M.L., and Anderson, R.E., 1983, Style of basin-range faulting as inferred from seismic reflection data in the Great Basin, Nevada and Utah: Geothermal Resources Council, Special Report No. 13, p. 363-381.

APPENDIX--INVENTORY OF WELLS AND SPRINGS IN SOUTHERN GRASS VALLEY

Explanation of Table A1

Basic data for the wells and springs inventoried in the present study are given in table A1. The information in the columns in the table, in order from left to right, is explained in the following paragraphs.

Numbers of Test Wells, Private Wells, and Springs

Test wells, private wells, and springs have been assigned a combination of a letter or letters and a number, as listed in the first column of table A1. Several sets of test wells have been drilled by the U.S. Geological Survey, Lawrence Berkeley Laboratory, and GeothermEx, Inc., with different letter designations being used to distinguish the various sets. The wells assigned the capital letters DH were drilled for the Geological Survey and were drilled by the hydraulic-rotary method. Some of these wells were fitted with screens and were used to obtain water-level and hydrogeochemical data as well as temperature and geologic information; others were capped at the bottom and filled with water and were used primarily to measure temperature gradient. Some of the capped wells were later perforated by explosive charge (gun-perforated) to permit water-level measurements and (or) sampling of water for chemical analysis.

The wells designated by the prefixes QH, Q, and T were drilled for the Lawrence Berkeley Laboratory (LBL) and were also drilled by the hydraulic-rotary method. Two to four QH wells were drilled at each site, of which the first (the A well) was capped and filled with water for temperature-gradient measurement; the other(s) were fitted with screens or well points at the bottom. All the Q wells were capped and filled, although Q1, Q6, Q23, and Q24 were gun-perforated later to permit geochemical sampling and water-level measurement. The T wells, also capped and filled, were shallow (15-18 m) and were placed to help define the detail around known thermal anomalies and isolated deeper wells.

The wells having a G prefix were drilled for Sunoco Energy Development Co. by GeothermEx, Inc. as part of a geothermal exploration program in order to obtain geologic information. All these wells were capped and filled and were also used to measure temperature gradient. Wells G5a, G105, and G108 were gun-perforated after original completion in order to obtain water-level measurements.

Private wells are designated by the prefix PW and are numbered in the order they were inventoried during the present study. Springs and one stream-flow sampling site are designated by the prefix S and are also numbered in the approximate order of inventory.

Names of Wells or Springs

Many private wells and springs are also identified by formal or informal names; where names are lacking, the site is designated by a description of the location.

Location Numbers

Wells and springs are assigned numbers according to the rectangular system of subdividing

public lands, referred to the Mount Diablo baseline and meridian, as indicated in the second or third column in table A1. As shown in figure A1, the first two elements of the number, separated by a slash, are, respectively, the township (north) and range (east); the third element, separated from the second by a hyphen, indicates the section number; and the lowercase letters following the section number indicate the successive quadrant subdivisions of the section. The letters a, b, c, and d designate, respectively, the northeast, northwest, southwest, and southeast quadrants as shown in the diagram. Where more than one well or spring is catalogued within the smallest designated quadrant, the last lowercase letter is followed by a numeral that designates the order in which the feature was catalogued during the investigation. For example, well number 32/23-25bdb1 designates the first well recorded in the NW 1/4 SE 1/4 NW 1/4 section 25, T. 32 N., R. 23 E., Mount Diablo baseline and meridian.

Most of the wells in table A1 were also listed by Welch and others (1981, table 1), but some of the location numbers differ from those of the earlier report. There are two principal reasons for the differences: (1) correction of inaccurate locations plotted on the older, 15' maps at 1:62,500 scale used in the earlier report; and

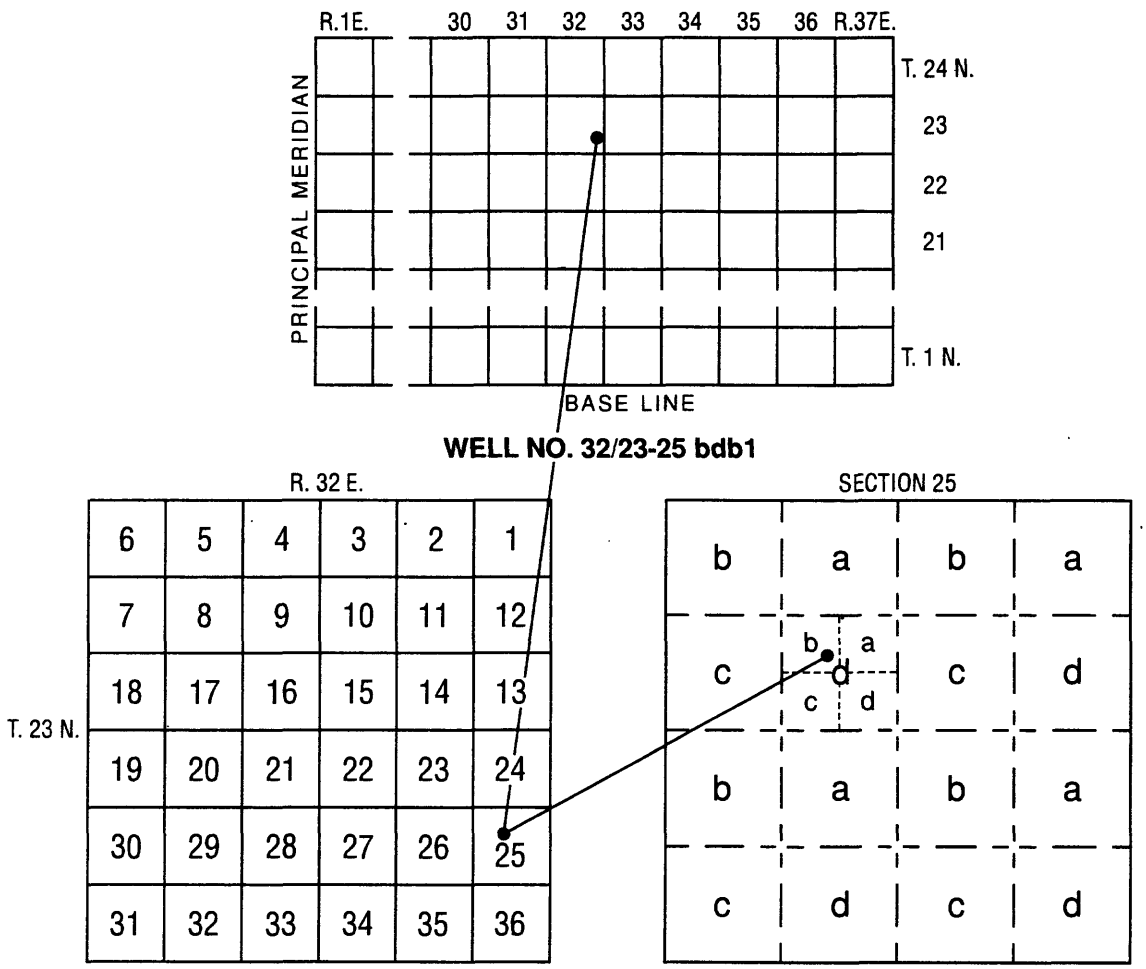

Figure A1. Numbering system for wells, springs, and samples.

(2) small changes in the locations of the U.S. land-net section lines from the 15' maps to the newer 7.5' maps at 1:24,000 scale used to plot locations of many wells in the present report. Latitude and longitude coordinates are correspondingly affected slightly, as discussed below.

Latitude and Longitude

In order to facilitate plotting with computer programs, and also finding the wells in the field using the new global-positioning-system (GPS) devices, latitude and longitude coordinates are listed for all the wells and springs in table A1. These coordinates were determined from the positions plotted on U.S. Geological Survey topographic maps. Locations of wells plotted on the 7.5'-series maps at a scale of 1:24,000 (all but two of the DH wells, the Aminoil USA 11-36 well, most of the QH wells, and some of the other wells and springs) are believed to be accurate to within about 30 m, or about 1" of latitude and 1.3" of longitude. Location numbers for these wells and springs are preceded by the symbol + in table A1. Other wells and springs, which were plotted on the 15'-series maps, are believed to be accurate to within about 100 m, or about 3" of latitude and 4" of longitude. The horizontal datum of 1927, rather than the horizontal datum of 1983, was used for all latitudes and longitudes. In order to adjust the figures to the 1983 datum, latitudes should be decreased by about 0.5" and longitudes increased by about 3.4".

Altitude of Land-Surface Datum

Altitude of land-surface datum at each well and spring was determined in most cases by (1) spirit leveling from an established U.S. Geological Survey or U.S. Geodetic Survey bench mark, or (2) interpolation from land-surface contours on U.S. Geological Survey 15' or 7.5' topographic maps. Altitudes determined by leveling are listed to the nearest 0.001 or 0.01 m; those by interpolation from contours are listed to the nearest 1 m except for a few sites in the mountains, which are listed to the nearest 10 m. At a few sites, altitudes are given to tenths of a meter; these are from altitudes given to the nearest foot (about 0.3 m) on the topographic maps.

Height of Measuring Point

The height of measuring point listed in the sixth column in table A1 is the height of the top of well casing above the land-surface datum. Negative numbers indicate measuring points *below* the land surface.

Depth of Screen or Cap at Bottom

These depths are referred to land-surface datum; the height of measuring point is added in order to obtain the total length of casing and screen or well point. Single numbers generally refer to the depth of the cap at the bottom, although, in a few cases, the numbers refer to the mid-point depth of the screen, well point, or perforations.

Nominal Inside Diameter of Casing

The numbers in this column refer to the *nominal*, rather than the *actual*, inside diameter of the casing; the actual diameter usually is some-

what greater than the nominal diameter.

Type of Completion

Almost all the test wells were cased with either galvanized steel or plastic (polyvinyl chloride--PVC) pipe. Private wells were finished with steel or black-iron casing. The symbol Sc is used where the test wells were screened, fitted with well points, or perforated, and the symbol C is used where the wells capped at the bottom and filled with water for temperature measurement. The lowercase symbol c indicates that the annulus between the casing and the walls of the drill hole was filled with cement in order to prevent upward or downward movement of water outside the casing and to ensure isolation of the screened or perforated interval from shallower aquifers.

Geophysical Logs Available

Borehole geophysical logs were run in most of the DH, QH, and Q wells in order to define depth to the saturated zone and temperature gradient, and to assist in interpretation of the lithology of the materials penetrated. Gamma (natural gamma) and resistivity logs were used primarily in lithologic interpretation. Gamma-gamma and neutron (density) logs were used in lithologic interpretation but were also extremely useful in indicating the position of the top of the saturated zone (water table). Temperature logs were made with continuous-recording devices and were a useful adjunct to temperature measurements made at discrete depths, which were also made in most wells.

Other Data Available

Other data available include lithologic logs made at the time the wells were drilled, commonly supplemented by interpretation of the borehole geophysical logs, water-level measurements, chemical analyses of samples pumped from the wells or obtained from springs, temperature profiles made from measurements at discrete depths (as mentioned above), and core samples from which several parameters, including grain density, dry bulk density, saturated bulk density, and porosity were measured in the laboratory.

TABLE A1. Data for wells and springs in southern Grass Valley.

[Explanation of symbols: +, location from 7.5' series map; St, galvanized-steel pipe; P, polyvinyl chloride (PVC) pipe; Sc, screen or wellpoint at bottom; C, capped at bottom and filled with water; c, cement seal in annulus (all other holes sealed with drill cuttings or surface materials); G, natural gamma log; G2, gamma-gamma (density) log; N, neutron log; T, temperature log; R, resistivity log; L, lithologic log; W, water-level measurements; Tp, temperature profile; Ch, chemical analysis of water; Cs, core sample(s). Numbers in parentheses indicate depth at which well casing was perforated by explosive charges in order to obtain water-level measurements. Height of measuring point is above land-surface datum.]

Number of test well	Location number	Latitude (° ' " N)	Longitude (° ' " W)	Altitude of land-surface datum (m)	Height of measuring point (m)	Depth of screen or cap at bottom (m)	Nominal inside diameter of casing (mm)	Type of completion	Geophysical logs available	Other data available
DH1 +	31/38- 1cab	40 35 16	117 39 10	1,406.835	0.152	44.62-44.88	51	P,Sc	G,G2,N,T	L,W,Ch,Tp
DH2	32/39-30acc	40 37 11	117 38 02	1,469	.457	50.05	51	P,C	G,G2,N,T	L,Tp
DH3 +	32/39-31cbb	40 36 12	117 38 28	1,455.252	.610	49.98	51	P,C	G,G2(2),N(2),T	L,W,Tp
DH4 +	32/38/25dcc	40 36 44	117 38 45	1,429.4	.610	49.83	51	P,C	G,G2,N,T	L,W,Ch,Tp
DH5 +	32/39-31cad	40 36 08	117 38 02	1,482	.914	27.13	51	P,C	G,G2,N,T	L,Tp
DH6 +	31/38- 1aac	40 35 42	117 38 53	1,425.946	.914	44.38-44.84	38	St,Sc	G,G2,N,T	L,W.Tp
DH7 +	32/38-25ccd	40 36 42	117 39 34	1,395.932	.524	49.98-50.44	51	P,Sc	G,G2,N,T	L,W,Tp
DH8 +	32/38-35dab	40 36 09	117 40 01	1,394.067	.914	44.10-44.56	38	St,Sc	G,G2,N,T	L,W,Tp
DH9 +	32/38-36dcb	40 36 00	117 39 04	1,417.146	.914	44.56-45.20	38	St,Sc	G,G2,N,T	L,W,Tp
DH10 +	32/38-36ada	40 36 26	117 38 44	1,429.573	.610	16.38-16.79	38	St,Sc	G,T	L,W,Ch,Tp
DH11 +	32/38-36bdc	40 36 21	117 39 20	1,400.608	.853	44.35-44.81	38	St,Sc	G,G2,N,R,T	L,W,Tp
DH12 +	31/38- 1bbd	40 35 40	117 39 28	1,401.172	.518	44.18-44.64	51	P,Sc	G,G2,N,T	L,W,Tp
DH13A +	32/38-36daa1	40 36 14	117 38 42	1,440.244	.610	51.37-52.28	51	P,Sc	T	W,Ch,Tp
DH13B +	32/38-36daa2	40 36 14	117 38 42	1,440.244	.607	41.43	32	St,C,c	T	----------
DH14A +	32/38-36abc1	40 36 35	117 39 02	1,415.186	.305	45.00-45.91	51	P,Sc	G,G2,N,T	L,W,Ch,Tp
DH14B +	32/38-36abc2	40 36 35	117 39 02	1,415.186	.302	32.07	51	P,C	T	----------
DH15	32/39-31cce	40 35 53	117 38 26	1,455	.594	44.39	51	P,C	G,G2,N,T	L,W,Tp

TABLE A1. Data for wells and springs in southern Grass Valley--**continued.**

[Explanation of symbols: +, location from 7.5' series map; St, galvanized-steel pipe; P, polyvinyl chloride (PVC) pipe; Sc, screen or wellpoint at bottom; C, capped at bottom and filled with water; c, cement seal in annulus (all other holes sealed with drill cuttings or surface materials); G, natural gamma log; G2, gamma-gamma (density) log; N, neutron log; T, temperature log; R, resistivity log; L, lithologic log; W, water-level measurements; Tp, temperature profile; Ch, chemical analysis of water; Cs, core sample(s). Numbers in parentheses indicate depth at which well casing was perforated by explosive charges in order to obtain water-level measurements. Height of measuring point is above land-surface datum.]

Number of test well	Location number	Latitude (° ' " N)	Longitude (° ' " W)	Altitude of land-surface datum (m)	Height of measuring point (m)	Depth of screen or cap at bottom (m)	Nominal inside diameter of casing (mm)	Type of completion	Geophysical logs available	Other data available
QH1A	32/39-31bbb1	40 36 38	117 38 26	1,446.023	.101	137.15	32	St,C,c	R,T,G,G2,N,T	L,Cs
QH1B	32/39-31bbb2	40 36 38	117 38 26	1,446.023	.152	152.4-152.8	38	St,Sc,c	----------	W
QH1C	32/39-31bbb3	40 36 38	117 38 26	1,446.023	.128	25.20-25.66	38	St,Sc	----------	L,Cs
QH2A +	32/39-19dba1	40 37 36	117 37 49	1,490	-0.085	134.0	32	St,C,c	R,T,G,G2,N	L,Cs
QH2B +	32/39-19dba2	40 37 36	117 37 49	1,490	-0.2	152.92-153.38	38	St,Sc,c	----------	----------
QH3A +	31/38-14acd1	40 33 43	117 40 07	1,434.38	.305	140.12	32	St,C,c	R.T,G,G2,N	L,Cs
QH3B +	31/38-14acd2	40 33 43	117 40 07	1,434.38	.845	153.36-153.82	38	St,C,c	R,T,G,G2,N	W,Ch
QH3C +	31/38-14acd3	40 33 43	117 40 07	1,434.38	1.316	63.54-63.91	38	St,Sc	----------	W
QH3D +	31/38-14acd4	40 33 43	117 40 07	1,434.38	1.307	408.7-410.2	?	St	R,T,G,G2,N	L,Cs,W,Ch
QH4A	31/38-22cab1	40 32 39	117 41 33	1,519	.168	123.58	32	St,C,c	R,T,G,G2,N	L,Cs
QH4B	31/38-22cab2	40 32 39	117 41 33	1,519	.290	127.27-127.73	38	St,Sc,c	----------	W
QH5A +	32/38-14acc1	40 38 54	117 40 14	1,390.933	.396	130	32	St,C,c	R,T,G	L,Cs
QH5B +	32/38-14acc2	40 38 54	117 40 14	1,390.933	1.103	130	51	P,Sc,c	----------	W
QH6A +	32/38-21bcb1	40 38 07	117 42 00	1,378.234	.457	55	32	St,Sc,c	R,T,G	L,Cs
QH6B +	32/38-21bcb2	40 38 07	117 42 00	1,378.234	.351	55	51	P,Sc,c	----------	W

TABLE A1. Data for wells and springs in southern Grass Valley--**continued.**

[Explanation of symbols: +, location from 7.5' series map; St, galvanized-steel pipe; P, polyvinyl chloride (PVC) pipe; Sc, screen or wellpoint at bottom; C, capped at bottom and filled with water; c, cement seal in annulus (all other holes sealed with drill cuttings or surface materials); G, natural gamma log; G2, gamma-gamma (density) log; N, neutron log; T, temperature log; R, resistivity log; L, lithologic log; W, water-level measurements; Tp, temperature profile; Ch, chemical analysis of water; Cs, core sample(s). Numbers in parentheses indicate depth at which well casing was perforated by explosive charges in order to obtain water-level measurements. Height of measuring point is above land-surface datum.]

Number of test well	Location number	Latitude (° ' " N)	Longitude (° ' " W)	Altitude of land-surface datum (m)	Height of measur-ing point (m)	Depth of screen or cap at bottom (m)	Nominal inside diameter of casing (mm)	Type of compl e-tion	Geophysical logs available	Other data available
QH7A +	31/38- 3aac1	40 35 42	117 41 07	1,396.530	.427	75	32	St,C,c	R,T,G	L,Cs
QH7B +	31/38- 3aac2	40 35 42	117 41 07	1,396.530	.792	75	51	P,Sc,c	----------	W,Ch
QH8A +	31/39- 5ccc1	40 34 58	117 37 24	1,478.264	.762	50	32	St,Sc,c,	R,T,G	L,Cs
QH8B +	31/39- 5ccc2	40 34 58	117 37 24	1,478.264	.088	50	51	P,Sc,c	----------	W
QH9A +	31/39-17abd1	40 33 56	117 36 41	1,478.554	.702	91	32	St,C,c	R,T,G	L,Cs
QH9B +	31/39-17abd2	40 33 56	117 36 41	1,478.554	.972	91	51	P,Sc,c	R,T,G	L,Cs,W
QH11A +	31/38-16abd1	40 33 52	117 42 44	1,484	.582	55	32	St,C,c	R,T,G	L,Cs
QH11B +	31/38-16abd2	40 33 52	117 42 44	1,484	.396	55	51	P,Sc,c	----------	W
QH12A +	31/39-34bab1	40 31 24	117 34 49	1,512	.396	53	32	St,C,c	R,T,G	L,Cs
QH12B +	31/39-34bab2	40 31 24	117 34 49	1,512	.600	53	51	P,Sc,c	----------	W
QH13A +	31/39-22abc1	40 32 59	117 34 25	1,548	.503	55	32	St,C,c	R,T,G	L,Cs
QH13B +	31/39-22abc2	40 32 59	117 34 25	1,548	.488	55	51	{.Sc.c	----------	W,Ch
QH14A +	32/38-32dbb1	40 36 16	117 43 44	1,407	.213	85	32	St,C,c	R,T,G	L,Cs
QH14B +	32/38-32dbb2	40 36 16	117 43 44	1,407	.216	85	51	P,Sc,c	----------	W
Q1 +	32/38-26bba	40 37 30	117 40 42	1,385.6	.30	188 (61.0)	32	St,C,c	G,G2,N,T,R	L,Cs,W
Q2	31/39-12daa	40 34 25	117 38 25	1,419	----	162	32	St,C,c	G,G2,N,T,R	L,Cs

TABLE A1. Data for wells and springs in southern Grass Valley--**continued.**

[Explanation of symbols: +, location from 7.5' series map; St, galvanized-steel pipe; P, polyvinyl chloride (PVC) pipe; Sc, screen or wellpoint at bottom; C, capped at bottom and filled with water; c, cement seal in annulus (all other holes sealed with drill cuttings or surface materials); G, natural gamma log; G2, gamma-gamma (density) log; N, neutron log; T, temperature log; R, resistivity log; L, lithologic log; W, water-level measurements; Tp, temperature profile; Ch, chemical analysis of water; Cs, core sample(s). Numbers in parentheses indicate depth at which well casing was perforated by explosive charges in order to obtain water-level measurements. Height of measuring point is above land-surface datum.]

Number of test well	Location number	Latitude (° ' " N)	Longitude (° ' " W)	Altitude of land-surface datum (m)	Height of measuring point (m)	Depth of screen or cap at bottom (m)	Nominal inside diameter of casing (mm)	Type of completion	Geophysical logs available	Other data available
Q3	31/39-28aad	40 32 16	117 35 15	1,491	----	175	32	St,C,c	G,G2,N,T,R	L,Cs
Q4 +	31/38-24ccd	40 37 35	117 39 34	1,403	----	66	51	P,C	R,T,G	L,Cs
Q5 +	32/39-30bba	40 37 31	117 38 19	1,454	----	107	51	P,C	R,T,G	L,Cs
Q6	32/38-29bba	40 37 27	117 44 12	1,393	.61	59 (45.7)	51	P,C	R,T,G	L,Cs,W
Q7	31/38- 4daa	40 35 16	117 42 09	1,402	----	75	51	P,C	R,T,G	L,Cs
Q8 +	31/38- 8aad	40 34 47	117 43 19	1,437	----	75	51	P,C	R,T,G	L,Cs
Q9 +	31/38-10dcb	40 34 12	117 41 22	1,438	----	58	51	P,C	R,T,G	L,Cs
Q10	31/38-12cdc	40 34 07	117 39 28	1,643?	----	56	51	P,C	R,T,G	L,Cs
Q11	31/38-14ccc	40 33 18	117 40 34	1,466	----	83	51	P,C	R,T,G	L,Cs
Q12	31/38-23dca	40 32 32	117 40 05	1,463	----	67	51	P,C	R,T,G	L,Cs
Q13	31/39-24ddd	40 32 22	117 38 38i	1,436	----	101	51	P,C	R,T,G	L,Cs
Q14	31/39-29bbb	40 32 15	117 37 19	1,447	----	87	51	P,C	R,T,G	L,Cs
Q15	31/39-28bcb	40 32 09	117 36 23	1,465	----	53	51	P,C	R,T,G	L,Cs
Q16	31/39-21dcb	40 32 34	117 35 43	1,496	----	82	51	P,C	R,T,G	L,Cs
Q17	31/39-27acc	40 31 55	117 34 28	1,527	----	76	51	P,C	R,T,G	L,Cs
Q18 +	32/38-18aba	40 39 11	117 44 37	1,375	----	64	51	P,C	R,T,G	L,Cs
Q19	32/38-34bbd	40 36 34	117 41 36	1,389	----	59	51	P,C	R,T,G	L,Cs

TABLE A1. Data for wells and springs in southern Grass Valley--**continued.**

[Explanation of symbols: +, location from 7.5' series map; St, galvanized-steel pipe; P, polyvinyl chloride (PVC) pipe; Sc, screen or wellpoint at bottom; C, capped at bottom and filled with water; c, cement seal in annulus (all other holes sealed with drill cuttings or surface materials); G, natural gamma log; G2, gamma-gamma (density) log; N, neutron log; T, temperature log; R, resistivity log; L, lithologic log; W, water-level measurements; Tp, temperature profile; Ch, chemical analysis of water; Cs, core sample(s). Numbers in parentheses indicate depth at which well casing was perforated by explosive charges in order to obtain water-level measurements. Height of measuring point is above land-surface datum.]

Number of test well	Location number	Latitude (° ' " N)	Longitude (° ' " W)	Altitude of land-surface datum (m)	Height of measuring point (m)	Depth of screen or cap at bottom (m)	Nominal inside diameter of casing (mm)	Type of completion	Geophysical logs available	Other data available
Q20	31/38- 2dcc	40 34 56	117 40 12	1,405	----	72	51	P,C	R,T,G	L
Q21	31/38-13cdd	40 33 12	117 39 12	1,433	----	64	51	P,C	R,T,G	L,Cs
Q22	31/39-20ccc	40 33 14	117 37 24	1,441	----	49	51	P,C	R,T,G	L,Cs
Q23 +	31/39- 6cca	40 35 10	117 38 19	1,433.5	----	152 ( )	51	St,C,c	T	L,W,Tp
Q24 +	31/39-35caa	40 30 59	117 33 28	1,581	----	152 ( )	51	St,C,c	T	L,W
T1	31/38-15aaa	40 33 59	117 40 52	1,440.2	----	18.0	51	P,C	T	----------
T2	31/38-14bda	40 33 48	117 40 19	1,433.5	----	18.0	51	P,C	T	----------
T3	31/38-14bdd	40 33 40	117 40 19	1,439.3	----	18.0	51	P,C	T	----------
T4	31/38-14dbb	40 33 33	117 40 13	1,442.3	----	18.0	51	P,C	T	----------
T5	31/38-14dab	40 33 35	117 39 52	1,435.0	----	18.0	51	P,C	T	----------
T6	31=38-14aac	40 33 53	117 39 59	1,428.3	----	18.0	51	P,C	T	----------
T7	31/38-13cca	40 33 22	117 39 28	1,434.7	----	18.0	51	P,C	T	----------
T8	31/39-29bad	40 32 12	117 36 58	1,451.8	----	18.0	51	P,C	T	----------
T9	31/39-29abd	40 32 10	117 36 36	1,463.4	----	18.0	51	P,C	T	----------
T10	31/39-28bda	40 32 05	117 35 49	1,487.8	----	18.3	51	P,C	T	----------
T11	31/39-28adc	40 32 01	117 35 15	1,500.9	----	18.0	51	P,C	T	----------
T12	31/39-27bcd	40 31 57	117 34 51	1,512.8	----	17.8	51	P,C	T	----------

TABLE A1. Data for wells and springs in southern Grass Valley--**continued.**

[Explanation of symbols: +, location from 7.5' series map; St, galvanized-steel pipe; P, polyvinyl chloride (PVC) pipe; Sc, screen or wellpoint at bottom; C, capped at bottom and filled with water; c, cement seal in annulus (all other holes sealed with drill cuttings or surface materials); G, natural gamma log; G2, gamma-gamma (density) log; N, neutron log; T, temperature log; R, resistivity log; L, lithologic log; W, water-level measurements; Tp, temperature profile; Ch, chemical analysis of water; Cs, core sample(s). Numbers in parentheses indicate depth at which well casing was perforated by explosive charges in order to obtain water-level measurements. Height of measuring point is above land-surface datum.]

Number of test well	Location number	Latitude (° ' " N)	Longitude (° ' " W)	Altitude of land-surface datum (m)	Height of measuring point (m)	Depth of screen or cap at bottom (m)	Nominal inside diameter of casing (mm)	Type of completion	Geophysical logs available	Other data available
T13	31/39-27dab	40 31 53	117 34 08	1,546.4	----	18.0	51	P,C	T	----------
T14 +	31/39-15ddd	40 33 15	117 34 00	1,573.2	----	18.0	51	P,C	T	----------
T15	31/39-22 bcc	40 32 50	117 35 01	1,523.5	----	18.0	51	P,C	T	----------
T16	31-39-21bcb	40 32 53	117 36 09	1,487.2	----	15.5	51	P,C	T	----------
T17	31/39-21dcd	40 32 25	117 35 29	1,498.2	----	18.0	51	P,C	T	----------
T18	31/39-27dbc	40 31 43	117 34 30	1,524.6	----	18.0	51	P,C	T	----------
T19	31/39-27 dcd	40 31 31	117 34 14	1,537.5	----	18.0	51	P,C	T	----------
T20	31/39-27cdd	40 31 30	117 34 35	1,519.8	----	18.0	51	P,C	T	----------
T21	31/39-27abc	40 32 11	117 34 24	1,540.3	----	28.0	51	P,C	T	----------
T22	31/39-34bcb	40 31 08	117 35 03	1,510.4	----	14.6	51	P,C	T	----------
T23	31/38-12bab	40 34 51	117 39 24	1,408.5	----	18.0	51	P,C	T	----------
T24	31/38-12cbc	40 34 22	117 39 42	1,415.2	----	18.0	51	P,C	T	----------
T25	31/38-23bab	40 33 09	117 40 29	1,461.9	----	18.0	51	P,C	T	----------
T26	31-38-14ddd	40 33 18	117 39 52	1,441.7	----	18.0	51	P,C	T	----------
T27 +	32/38-19adc	40 38 00	117 44 28	1,387.8	----	16.8	51	P,C	T	----------
T28 +	32/38-18dbb	40 38 45	117 44 45	1,380.4	----	18.0	51	P,C	T	----------
T29 +	32/37-13dad	40 38 43	117 45 27	1,381.4	----	18.0	51	P,C	T	----------

TABLE A1. Data for wells and springs in southern Grass Valley--**continued.**

[Explanation of symbols: +, location from 7.5' series map; St, galvanized-steel pipe; P, polyvinyl chloride (PVC) pipe; Sc, screen or wellpoint at bottom; C, capped at bottom and filled with water; c, cement seal in annulus (all other holes sealed with drill cuttings or surface materials); G, natural gamma log; G2, gamma-gamma (density) log; N, neutron log; T, temperature log; R, resistivity log; L, lithologic log; W, water-level measurements; Tp, temperature profile; Ch, chemical analysis of water; Cs, core sample(s). Numbers in parentheses indicate depth at which well casing was perforated by explosive charges in order to obtain water-level measurements. Height of measuring point is above land-surface datum.]

Number and name of well	Location number	Latitude (° ' " N)	Longitude (° ' "W)	Altitude of land-surface datum (m)	Depth of well or perforations (m)	Nominal inside diameter of casing (mm)	Other data available	Description of well
T30 +	32/37-13aaa	40 39 13	117 45 28	1,376.2	----	18.0	51	P,C
T31 +	32/38-17bac	40 39 05	117 44 01	1,374.0	----	18.0	51	P,C
G2 +	32/38-26adc	40 37 13	117 39 57	1,396.3	----	152.4	38	St,C
G3	32/39-29bcc	40 37 08	117 37 25	1,521.3	----	152.4	38	St,C
G4 +	32/38-35cda	40 35 58	117 40 20	1,397.8	----	152.4	38	St,C
G5	32/39-32bdb	40 36 27	117 37 05	1,570	----	--------	----	------
G5a	32/39-32bca	40 36 25	117 37 11	1,536.8	----	152.4	25	St,C
G7	31/39- 5bca	40 35 24	117 37 17	1,524	----	152.4	25	St,C
G8 +	31/39- 8bbd	40 34 52	117 37 17	1,493.9	----	152.4	38	St,C
G9 +	31/39-14cba	40 33 52	117 33 46	1,603.6	----	134.1	38	St,C
G10	31/39-20qqe	40 33 03	117 36 25	1,469.5	----	152.4	38	St,C
G11	31/39-29cda	40 32 01	117 36 49	1,457.3	----	152.4	38	St,C
G12	31/39-28cda	40 31 36	117 35 42	1,487.8	----	152.4	38	St,C
G13	31/39-33ddb	40 30 50	117 35 19	1,503.0	----	146.3	38	St,C
G14	30/39- 4bcc	40 30 11	117 36 16	1,481.7	----	152.4	38	St,C
G15	30/39- 3caa	40 30 02	117 34 45	1,512.1	----	152.4	38	St,C
G105	31/39- 6bcc	40 35 30	117 38 31	1,436.9	----	352.1 (139.3)	51	St,C
G106 +	31/39-18caa	40 33 33	117 38 02	1,434.4	----	454.8	51	St,C

TABLE A1. Data for wells and springs in southern Grass Valley--**continued.**

[Explanation of symbols: +, location from 7.5' series map; St, galvanized-steel pipe; P, polyvinyl chloride (PVC) pipe; Sc, screen or wellpoint at bottom; C, capped at bottom and filled with water; c, cement seal in annulus (all other holes sealed with drill cuttings or surface materials); G, natural gamma log; G2, gamma-gamma (density) log; N, neutron log; T, temperature log; R, resistivity log; L, lithologic log; W, water-level measurements; Tp, temperature profile; Ch, chemical analysis of water; Cs, core sample(s). Numbers in parentheses indicate depth at which well casing was perforated by explosive charges in order to obtain water-level measurements. Height of measuring point is above land-surface datum.]

Number and name of spring	Location number	Latitude (° ' " N)	Longitude (° ' " W)	Altitude of land-surface datum (m)	Description of spring	Other data available
G108	31/39-27caa	40 31 48	117 34 32	1,525.0	----	448.2 ( )
PW1 Gold Banks windmill	30/39-16acb	40 28 21	117 35 37	1,475.695 *	----------	------
PW2 Well near Mud Spring	31/39-33cba	40 30 56	117 36 03	1,481	----------	------
PW3 +	31/38-26abb	40 32 14	117 40 13	1,473	52-56	153
PW4 Quicksilver windmill	31/38-34ada	40 31 08	117 40 53	1,547	----------	------
PW5 + New mine well	31/39-27bbb	40 32 19	117 34 57	1,510	----------	------
PW6 + New Mud Springs Ranch well	31/39-32dcc	40 31 28	117 36 46	1,460.781 *	90.2	406
PW7 + Old Mud Springs Ranch well	31/39-32abc	40 31 18	117 36 49	1,460.403 *	53-88	------
PW8 + Turner well	32/38-18acc	40 38 53	117 44 46	1,378.0	43-76	153
PW9 +	32/38-33bcc	40 36 16	117 43 09	1,400	----------	------
PW10 + Aminoil USA 11-36 well	32/38-36bbb	40 36 37	117 39 37	1,393.9	2,611	508
PW11 + Hot Springs Ranch well	32/38-36cba	40 36 12	117 39 28	1,397.766 *	30.5-40.1	305
PW12 + Old mine well	31/39-14ccc	40 33 13	117 33 59	1,571	----------	------
S1 Coyote Spring	30/39-30ddd	40 26 11	117 37 33	1,430		T,Ch
S2 Summit Spring	30/40-32cdb	40 25 42	117 30 10	2,580		T,Ch

TABLE A1. Data for wells and springs in southern Grass Valley--**continued.**

[Explanation of symbols: +, location from 7.5' series map; St, galvanized-steel pipe; P, polyvinyl chloride (PVC) pipe; Sc, screen or wellpoint at bottom; C, capped at bottom and filled with water; c, cement seal in annulus (all other holes sealed with drill cuttings or surface materials); G, natural gamma log; G2, gamma-gamma (density) log; N, neutron log; T, temperature log; R, resistivity log; L, lithologic log; W, water-level measurements; Tp, temperature profile; Ch, chemical analysis of water; Cs, core sample(s). Numbers in parentheses indicate depth at which well casing was perforated by explosive charges in order to obtain water-level measurements. Height of measuring point is above land-surface datum.]

Number and name of spring	Location number	Latitude (° ' " N)	Longitude (° ' " W)	Altitude of land-surface datum (m)	Description of spring	Other data available
S3 Spring in Spaulding Canyon	31/37-27dac	40 31 37	117 48 13	1,620		T,Ch
S4 + Spring in southwestern Grass Valley	31/38- 9bca	40 34 38	117 42 54	1,435		T,Ch
S5 + Mud Spring	31/39-33ccc	40 30 40	117 36 09	1,481.6		T,Ch
S6 + Spring in Pollard Canyon	31/39-36ccd	40 30 39	117 32 35	1,610		T,Ch
S7 + Petain Spring	31/40-18dab	40 33 37	117 30 46	1,780		T,Ch
S8 Point Spring	32/37-23bbd	40 38 15	117 47 29	1,460		T,Ch
S9 + Sheep Ranch Spring	32/39-17add	40 38 54	117 36 20	1,530		T,Ch
S10 + Grand Trunk Spring	33/39-30dcc	40 42 01	117 37 41	1,680		T,Ch
S11 Clear Creek near west edge of Sonoma Range	33/38-13cac	40 43 51	117 39 22	1,460		T,Ch
S12 + Leach Hot Springs	32/38-36dba	40 36 12	117 38 53	1,421-1,424	28 orifices along fault	T,Ch
S13 + Warm spring southwest of Leach Hot Springs	32/38-36dcc	40 35 52	117 39 07	1,415.8	Single pool 5 m in diameter	T

* Altitude of measuring point at top of casing
# Compensated formation density-neutron and dual induction-sonic logs

TABLE A2. Water levels in southern Grass Valley.

Well number	Altitude of land-surface datum (m)	Depth of mid-point of screen or perforations (m)	Date of measurement (yr mo da)	Depth to water below land-surface datum (m)	Altitude of water level (m)
DH1	1,406.835	44.75	73 11 14	12.372	1,394.463
			73 11 15	12.5g,n	1,394.3
			75 06 21	12.530	1,394.305
			77 06 07	12.674	1,394.161
DH2	1,469	50.05c	73 11 14	42.5g,n	1,417
DH3	1,455.252	49.98c	73 11 13	26.1g,n	1,429.2
			75 09 18	26.1g,n	1,429.2
DH4	1,429.4	49.83c	73 11 14	23.6g,n	1,405.8
			75 09 18	24.0g,n	1,405.4
DH5	1,482	27.13c	73 11 13	>27.13 g	<1,455
DH6	1,425.946	44.61	73 11 15	16.7	1,409.2
			73 12 14	16.368	1,409.578
			75 06 21	16.435	1,409.541
			77 06 07	16.404	1,409.552
DH7	1,395.932	50.21	73 11 09	26.3g,n	1,369.6
			73 12 15	26.335	1,369.597
			75 06 21	26.475	1,369.457
			77 06 06	26.530	1,369.402
DH8	1,394.067	44.33	73 11 09	22.6g,n	1,371.5
			73 12 13	23.156	1,370.911
			75 06 21	23.287	1,370.780
			77 06 08	23.354	1,370.713
DH9	1,417.146	44.88	73 11	36.0g,n	1,381.1
			77 06 07	36.436	1,380.710
DH10	1,429.573	16.58	73 12 15	5.767	1,423.806
			75 06 22	5.782	1,423.791
			77 06 15	5.870	1,423.703
DH11	1,400.608	44.58	73 11 13	29.2g,n	1,370.4
			73 12 15	29.316	1,371.292

TABLE A2. Water levels in southern Grass Valley**--continued**

Well number	Altitude of land-surface datum (m)	Depth of mid-point of screen or perforations (m)	Date of measurement (yr mo da)	Depth to water below land-surface datum (m)	Altitude of water level (m)
DH11			75 06 21	29.224	1,371.384
			77 06 07	29.331	1,371.277
DH12	1,401.172	44.41	75 06 21	25.106	1,376.066
			75 09 17	24.7g,n	1,376.5
DH12	1,401.172	44.41	77 06 07	25.127	1,376.045
DH13A	1,440.244	51.82	75 07 20	17.334	1,422.910
			77 06 15	17.317	1,422.927
DH14A	1,415.186	45.46	75 06 22	31.410	1,383.776
			77 06 15	32.004	1,383.182
DH15	1,455	44.39c	75 07 19	22.2n	1,433
QH1B	1,446.023	152.73	76 10 01	12.674	1,433.349
			77 05 28	25.1n	1,420.9
QH1C	1,446.023	25.43	76 10 01	25.582	1,420.441
			76 06 15	25.492	1,420.531
QH2B	1,490	153.15	76 10 01	74.809	1,415
			77 06 07	74.917	1,415
QH3B	1,434.38	153.59	76 09 30	61.883	1,372.50
			77 05 27	62.2g	1,372.1
			77 06 06	61.967	1,372.41
QH3C	1,434.38	63.72	76 09 30	61.259	1,373.12
			77 06 06	61.271	1,373.11
QH3D	1,434.38	409.4	77 06 28	4.98	1,429.40
QH4B	1,519	127.50	76 09 30	45.758	1,473
			77 06 07	45.870	1,473
QH5B	1,390.933	130	76 09 30	30.352	1,360.581
			77 06 06	30.397	1,360.536
QH6B	1,378.234	55	76 10 01	16.954	1,361.280
			77 06 06	16.990	1,361.244

TABLE A2. Water levels in southern Grass Valley**--continued**

Well number	Altitude of land-surface datum (m)	Depth of mid-point of screen or perforations (m)	Date of measurement (yr mo da)	Depth to water below land-surface datum (m)	Altitude of water level (m)
QH7B	1,396.530	75	76 09 30	29.986	1,366.544
			77 06 06	30.144	1,366.386
QH8B	1,478.264	50	76 09 30	40.739	1,437.525
			77 06 07	45.557	1,432.707
QH9B	1,478.554	91	76 09 30	65.654	1,412.900
			77 06 07	65.718	1,412.836
QH11B	1,484	55	76 09 30	38.092	1,446
			77 06 06	38.106	1,446
QH12B	1,512	53	76 10 01	31.235	1,481
QH12B	1,512	53	77 06 07	31.429	1,481
QH13B	1,548	55	76 10 01	45.606	1,502
			77 06 07	45.635	1,502
QH14B	1,407	85	76 10 01	45.653	1,361
			77 06 06	45.717	1,361
Q1	1,385.6	61.0 pe	80 06 18	21.3	1,364.3
Q6	1,393	45.7 pe	80 07 31	31.6	1,361
Q23	1,433.5	pe	77 07 18	21.0	1,412.5
Q24	1,581	pe	77 07 18	65.5	1,516
Q5a	1,536.6	?	79 10 15	79.3*	1,457.3
G105	1,436.9	139.3 pe	80 07 31	-2.4	1,439.3
G108	1,525.0	?	80 07 31	32.4	1,493
PW1	1,475.695mp	---------	77 03 07	4.795	1,470.900
			77 05 26	4.749	1,470.946
PW2	1,481	----------	77 06 07	Flowing	>1,481
PW3	1,473	54	47 07 12	46.*	1,427
			77 03 10	49.372	1,424
			77 06 06	49.618	1,423
PW4	1,547	----------	77 04 29	27.373	1,520
PW5	1,510	----------	77 04 27	40.35 p	1,470 p

TABLE A2. Water levels in southern Grass Valley—**continued**

Well number	Altitude of land-surface datum (m)	Depth of mid-point of screen or perforations (m)	Date of measurement (yr mo da)	Depth to water below land-surface datum (m)	Altitude of water level (m)
			80 05 17	20.1	1,490
PW6	1,460.781mp	90.2	77 03 08	45.038	1,415.743
			77 04 27	44.935	1,415.846
			77 06 07	46.137	1,414.644p
PW7	1,460.403mp	70.5	58 05 22	42.*	1,418
			77 03 08	44.194	1,416.209
			77 04 27	44.125	1,416.278
			77 06 07	45.705	1,414.698p
PW8	1,378.0	40.5	55 09 22	24.*	1,354
			77 04 26	25.25	1,352.8
			77 06 05	27.388	1,350.61
PW9	1,400	59.5	77 04 26	39.84	1,360
PW11	1,397.139	37.8	56 08 27	24.430	1,372.709
PW11	1,397.139	37.8	73 06 14	25	1,372
			77 03 11	29.219	1,367.920
PW12	1,571	----------	77 03 08	16.627	1,554p?

mp Altitude of measuring point
g Depth to water estimated from gamma-gamma log
n Depth to water estimated from neutron log
pe Perforated by explosive charge after completion
p Pumping or pumped recently
c Capped at bottom; perforated by explosive charge after completion
* Data from Cohen (1964, table 8) and files of Nevada State Engineer

TABLE A3. Chemical and isotopic analyses of water samples from southern Grass Valley and vicinity.

[Chemical analyses were performed by the U.S. Geological Survey Central Laboratory, Arvada, Colorado, except where otherwise specified. All analyses are reported as milligrams per liter, except as noted. Locations of sample sites for samples 1-11 are shown in figure 7; those for samples 12-41 in figure 10; that for sample 42 in figure 1. See notes at end of table for additional information.]

Sample number	Sample site	Date of sample (yr mo da)	Water temperature (°C)	Specific conductance (microsiemens per cm)	pH (units)	Delta deuterium (‰)	Delta oxygen-18 (‰)	Calcium (Ca)	Magnesium (Mg)	Sodium (Na)	Potassium (K)	Bicarbonate (HCO_3)	Carbonate (CO_3)	Chloride (Cl)	Sulfate (SO_4)	Fluoride (F)	Silica (SiO_2)	Boron (B)	Lithium (L)	Dissolved solids
Leach Hot Springs																				
1	Orif. 1	77 06 ...	85	830	7.2	(-129)	-15.7	9.7	0.8	170	12	390	0	26	53	8.2	115	1.3	0.87	590
2	Do	78 09 14	86	810	6.7	-129	-16.0	11	1.1	180	13	385	0	26	56	9.0	105	1.3	.87	590
3	Do	83 12 28	86.5	780	6.9	(-129)	(-16.3)	9.5	0.87	160	11	370	0	31	52	8.5	125	1.2	.78	560
4	Orif. 12	79 03 20	92	840	9.0	-127	-15.4	9.6	0.1	180	16	324	3	32	57	2.7	115	1.3	.94	580
5	Orif. 13	72 06 17	92	810	7.4	(-129)	-15.7	8.8	0.5	160	13	366	0	29	53	7.8	135	1.2	1.7	590
6	Do	83 12 28	95.5	770	7.1	-129	-16.2	8.5	0.6	160	12	---	---	30	53	8.5	145	1.2	.78	---
7	Orif. 15	78 12 13	92	580	5.9	-124	-14.0	8.6	0.2	85	12	3	0	13	200	2.7	180	.48	.45	500
8	Orif. 22	77 06 ...	81	830	7.0	-130	-16.4	10	1.0	170	12	390	0	28	50	8.5	100	1.3	.86	570
9	Do	78 09 14	81	800	6.6	-131	-16.9	11	1.2	170	11	369	0	25	52	9.0	95	1.3	.83	560
10	Do	83 12 29	84.5	790	7.0	-129	-16.3	9.7	1.0	160	12	360	0	24	48	8.7	115	1.2	.78	550
11	Orif. ?	57 05 16	97	810	8.8	---	---	---	---	---	---	---	---	---	---	---	---	---	---	----
Thermal wells																				
12	DH6	86 11 29	23	880	8.7	-131	-16.4	8.6	1.8	200	7.6	---	---	26	19	5.6	7.5	1.1	---	---
13	QH3B	78 08 29	24.5	390	6.2	-129	-16.1	14	2.0	57	3.5	82	0	59	41	1.5	16	.44	.11	270
14	QH3D	78 08 29	58	800	8.2	-133	-16.8	11	1.8	180	11	456	4	24	30	3.9	16	.6	.24	510
15	Do	78 09 15	58	820	8.1	---	---	13	2.1	180	12	457	3	23	26	4.3	8.3	.54	.24	500
16	G105	86 11 28	52.5	960	8.1	-132	-16.4	8.0	0.3	210	2.4	470	0	26	47	7.7	93	1.2	.36	620
17	DH4	86 11 29	30	1,320	---	-130	-16.2	---	---	---	---	---	---	29	---	7.9	---	1.0	---	---
18	DH14A	78 08 30	29	810	8.5	---	---	12	2.3	180	11	399	6	24	49	8.1	79	1.3	.91	570

TABLE A3. Chemical and isotopic analyses of water samples from southern Grass Valley and vicinity**--continued.**

[Chemical analyses were performed by the U.S. Geological Survey Central Laboratory, Arvada, Colorado, except where otherwise specified. All analyses are reported as milligrams per liter, except as noted. Locations of sample sites for samples 1-11 are shown in figure 7; those for samples 12-41 in figure 10; that for sample 42 in figure 1. See notes at end of table for additional information.]

Sample number	Sample site	Date of sample (yr mo da)	Water temperature (°C)	Specific conductance (microsiemens per cm)	pH (units)	Delta deuterium (‰)	Delta oxygen-18 (‰)	Calcium (Ca)	Magnesium (Mg)	Sodium (Na)	Potassium (K)	Bicarbonate (HCO_3)	Carbonate (CO_3)	Chloride (Cl)	Sulfate (SO_4)	Fluoride (F)	Silica (SiO_2)	Boron (B)	Lithium (L)	Dissolved solids
Thermal wells--continued																				
19	DH14A	86 11 28	29	810	8.6	-130	-16.4	12	2.1	170	10	360	22	25	47	6.8	68	1.2	0.8	540
20	DH10	78 09 14	86	820	8.6	-131	-16.6	11	1.5	180	12	383	7	27	43	8.8	49	1.3	0.81	530
21	Do	86 11 29	86	900	8.0	-129	-16.1	9.5	1.1	170	13	390	0	27	52	8.2	97	1.2	0.8	560
22	DH13A	78 08 23	52.5	1,240	8.6	-134	-16.4	8.5	2.0	270	14	365	8	140	110	6.2	17	1.8	0.81	760
23	Do	86 11 29	52.5	1,300	8.6	-132	-16.0	15	2.6	240	14	---	0	20	34	1.3	36	0.44	0.76	---
Nonthermal springs																				
24	S1	77 06 ...	22	960	7.0	---	---	73	17	130	8.2	480	0	70	65	1.4	40	0.63	0.22	640
25	S2	82 08 02	4	---	6.6	(-127)	-16.8	4.4	1.2	6.6	0.41	25	0	4.0	4	<0.1	7.4	---	---	40
26	S3	77 06 ...	13	960	7.2	-124	-15.8	99	32	65	3.8	290	0	86	150	1.0	19	0.23	0.06	600
27	S4	77 06 ...	20	1,220	7.6	-124 (-125)	-15.2	91	32	110	4.7	180	0	180	190	7	26	0.36	0.06	720
28	S5	77 06 ...	14	620	7.3	(-122)	-16.0	66	18	32	1.8	200	0	56	59	0.2	22	0.10	0.008	350
29	S6	... ...	---	---	---	(-120)	---	---	---	---	---	---	---	---	---	---	---	---	---	---
30	S7	77 06 ...	12	540	7.6	-124	-16.4	67	9.1	29	4.6	210	0	39	38	0.3	58	0.08	0.004	350
31	Do	78 08 22	16	520	7.8	-124 -123	-15.8	65	9.6	29	4.2	217	0	36	39	0.2	54	0.19	0.009	340
32	S8	77 06 ...	10	1,250	7.6	(-124)	---	150	61	65	6.5	300	0	110	350	0.5	19	0.17	0.03	910
34	Do	78 08 22	17	740	7.5	---	---	72	34	31	3.5	----	---	62	110	0.3	20	0.12	0.02	---
33	S9	77 06 ...	13	720	7.7	(-124)	---	72	32	29	2.5	210	0	59	110	0.2	21	0.11	0.01	430

TABLE A3. Chemical and isotopic analyses of water samples from southern Grass Valley and vicinity**--continued.**

[Chemical analyses were performed by the U.S. Geological Survey Central Laboratory, Arvada, Colorado, except where otherwise specified. All analyses are reported as milligrams per liter, except as noted. Locations of sample sites for samples 1-11 are shown in figure 7; those for samples 12-41 in figure 10; that for sample 42 in figure 1. See notes at end of table for additonal information.]

Sample number	Sample site	Date of sample (yr mo da)	Water temperature (°C)	Specific conductance (microsiemens per cm)	pH (units)	Delta deuterium (‰)	Delta oxygen-18 (‰)	Calcium (Ca)	Magnesium (Mg)	Sodium (Na)	Potassium (K)	Bicarbonate (HCO_3)	Carbonate (CO_3)	Chloride (Cl)	Sulfate (SO_4)	Fluoride (F)	Silica (SiO_2)	Boron (B)	Lithium (L)	Dissolved solids
Nonthermal springs--continued																				
35	S10	... ...	---	---	---	(-126)	-16.5	---	---	---	---	---	---	---	---	---	---	---	---	---
Nonthermal wells																				
36	PW1	81 04 23	12	430	---	-121	-15.7	---	---	---	---	---	---	---	---	---	---	---	---	---
37	DH1	78 08 24	15.5	470	8.4	-125	-16.9	45	12	38	3.2	172	2	39	43	0.4	25	0.14	0.03	290
38	QH7B	78 08 23	16.5	380	8.6	-125	-16.6	18	6.2	53	4.5	137	3	39	48	0.8	21	0.26	0.03	330
39	QH13B	78 08 30	18.5	540	8.3	-124	-16.4	47	12	52	3.0	208	2	39	48	0.8	21	0.26	0.03	330
40	PW2	77 06 ...	15	680	7.7	-122	-15.9	68	19	38	2.3	190	0	81	53	0.1	20	0.11	0.008	370
41	DH8	78 08 23	15	540	8.3	-124	-16.6	56	12	39	3.1	202	2	36	53	0.3	19	0.30	0.03	320
Surface water																				
42	S11	79 03 20	5	370	8.2	-122	-15.8	42	13	15	2.0	153	1	14	35	0.4	17	0.07	0.003	215

Notes:

Well-water temperatures are bottom-hole or depth-of-perforations values from down-hole temperature measurements.

Bicarbonate and carbonate species were mathematically distributed, using field pH and titration data.

Dissolved solids = computed sum (with bicarbonate multiplied by 0.492 to make the result comparable with residue-upon-evaporation values).

Samples of June 1977 were collected by R.H. Mariner, U.S. Geological Survey, Menlo Park, California.

Isotopic analysis of samples collected by R.H. Mariner were performed by two laboratories. The values not in parentheses are from a commercial laboratory that also performed the analysis of other samples. The values in parentheses were performed under the supervision of Carol Kendall, U.S. Geological Survey, Reston, Virginia.

Oxygen-isotope analyses were performed by a commercial laboratory, except for the samples collected by R.H. Mariner, which were performed under the supervision of JR. O'Neil, U.S. Geological Survey, Menlo Park, California.

Data from Leach Hot Springs orifice 13 are from Mariner and others (1974; 1975).

TABLE A4. Temperature gradient, thermal conductivity, and conductive heat flow in test wells.

Test-well site	Depth to saturated zone (m)	Depth interval (m)	Temperature gradient °C/km	Thermal conductivity (W/m.K)	**q1 Heat flow (mW/m^2)**	Depth interval (m)	Temperature gradient °C/km	Thermal conductivity (W/m.K)	**q2 Heat flow (mW/m^2)**	Depth interval (m)	Temperature gradient °C/km	Thermal conductivity (W/m.K)	**q3 Heat flow (mW/m^2)**
DH 1	12.7	15-20	39	1.4	**54**	30-44	74	1.5	**110**	-------	--------	----	------
2	>50	14-20	68	1.0	**68**	42-50	36	1.5	**54**	-------	--------	----	------
3	26	14-20	621	1.1	**680**	26-38	488	1.6	**780**	-------	--------	----	------
4	24	14-20	378	1.1	**420**	24-48	251	1.7	**430**	-------	------	----	------
5	>27	14-20	194	1.1	**210**	24-27	128	1.5	**190**	-------	------	----	------
6	16.4	18-28	130	2.1	**270**	31-41	170	1.8	**310**	-------	------	----	------
7	26.5	--------	-------	----	------	29-49	112	1.6	**180**	-------	------	----	------
8	23.3	28-33	43	1.5	**64**	31-44	72	1.3	**94**	-------	------	----	------
9	>34	--------	------	----	------	37-41	641	1.4	**900**	-------	------	----	------
10	5.8	10-17	2,010	1.4	**2,800**	-------	------	----	------	-------	------	----	------
11	29.2	--------	-------	----	------	35-44	233	1.3	**300**	-------	------	----	------
12	25.1	--------	-------	----	------	28-42	81	1.7	**140**	-------	------	----	------
13	17.3	14-18	629	1.7	**1,100**	42-50	663	1.7	**1,100**	-------	------	----	------
14	32.0	14-18	377	1.2	**450**	34-42	257	1.9	**480**	-------	------	----	------
15	34	14-20	372	1.3	**480**	40-44	296	1.7	**500**	-------	------	----	------
QH 1	26	14-20	315	1.2	**380**	-------	------	----	------	80-155	224	1.69	**379**
2	74.9	--------	-------	----	------	25-130	52	1.20	**62**	-------	------	----	------
3	61.3	14-20	80	1.3	**100**	?	118	1.81	**214**	-------	------	----	------
4	45.9	14-20	25	0.96	**24**	-------	------	----	------	125-155	42	1.36	**57**
5	30.4	14-20	65	1.3	**84**	-------	------	----	------	55-128	37	1.78	**66**
6	17.0	14-20	86	1.2	**100**	17-50	51	1.73	**88**	-------	------	----	------
7	30.0	14-20	98	.96	**94**	30-73	45	1.54	**69**	-------	------	----	------

TABLE A4. Temperature gradient, thermal conductivity, and conductive heat flow in test wells--**continued**

Test-well site	Depth to saturated zone (m)	Depth interval (m)	Temperature gradient °C/km	Thermal conductivity (W/m.K)	**q1 Heat flow (mW/m^2)**	Depth interval (m)	Temperature gradient °C/km	Thermal conductivity (W/m.K)	**q2 Heat flow (mW/m^2)**	Depth interval (m)	Temperature gradient °C/km	Thermal conductivity (W/m.K)	**q3 Heat flow (mW/m^2)**
8	40.7	14-20	81	1.0	**81**	41-49	69	1.44	**99**	-------	------	----	------
QH 9	65.7	14-20	83	1.2	**100**	67-75	40	1.66	**66**	-------	-------	----	------
11	38.1	14-20	------	----	------	40-55	52	1.19	**62**	-------	------	----	------
12	31.2	14-20	109	1.1	**120**	38-48	110	1.46	**161**	-------	------	----	------
13	45.6	14-20	131	1.2	**160**	46-52	116	1.67	**194**	-------	------	----	------
14	45.7	14-20	42	1.1	**46**	46-73	30	1.64	**49**	-------	------	----	------
Q 1	21e	15-25	63	1.2	**76**	-------	------	----	------	50-200	65.5	1.43	**94**
2	25e	15-25	32	1.1	**35**	-------	------	----	------	50-160	55.5	1.54	**86**
3	33e	14-20	124	1.2	**150**	-------	------	----	------	50-170	120	1.70	**204**
4	33e	14-20	55	1.1	**60**	33-56	51	1.62	**83**	-------	------	----	------
5	54e	14-20	65	1.2	**78**	-------	------	----	------	-------	------	----	------
6	39e	12-27	90	1.3	**120**	39-55	45	1.74	**78**	-------	------	----	------
7	32e	14-20	65	1.1	**72**	35-73	35	1.57	**55**	-------	------	----	------
8	-----	17-38	139	.84	**120**	44-66	59	1.71	**101**	-------	------	----	------
9	49e	14-20	47	1.3	**61**	49-57	30	1.85	**56**	-------	------	----	------
10	38e	14-20	-24	1.2	**-30**	38-55	52	1.64	**85**	-------	------	----	------
11	55e	14-20	-89	1.2	**-100**	46-78	37	1.76	**65**	-------	------	----	------
12	51e	14-20	9	1.2	**11**	51-62	45	1.64	**74**	-------	------	----	------
13	38e	14-20	58	1.3	**75**	38-82	39	1.85	**72**	-------	------	----	------
14	42e	14-20	45	1.3	**58**	-------	------	----	------	51-116	21	1.90	**40**
15	40e	26-40	95	1.0	**97**	-------	------	----	------	-------	------	----	------
16	54e	14-20	114	1.1	**130**	54-81	78	1.62	**126**	-------	------	----	------

TABLE A4. Temperature gradient, thermal conductivity, and conductive heat flow in test wells--**continued**

Test-well site	Depth to saturated zone (m)	Depth interval (m)	Temperature gradient °C/km	Thermal conductivity (W/m.K)	**q1 Heat flow (mW/m^2)**	Depth interval (m)	Temperature gradient °C/km	Thermal conductivity (W/m.K)	**q2 Heat flow (mW/m^2)**	Depth interval (m)	Temperature gradient °C/km	Thermal conductivity (W/m.K)	**q3 Heat flow (mW/m^2)**
17	43e	14-20	193	1.3	**250**	44-75	134	1.80	**241**	-------	------	----	------
18	25e	14-23	98	1.0	**98**	38-53	71	1.46	**104**	-------	------	----	------
19	27e	13-27	67	1.0	**67**	32-55	45	1.48	**67**	-------	------	----	------
Q 20	37e	12-30	72	1.3	**94**	38-69	42	1.88	**79**	-------	------	----	------
21	49e	14-20	50	1.3	**65**	49=61	37	1.85	**68**	-------	------	----	------
22	39e	12-24	34	1.0	**34**	39-49	20	1.79	**36**	-------	------	----	------
23	-----	16-32	61	1.2	**73**	-------	------	----	------	57-124	144	1.7	**240**
24	-----	--------	------	----	------	-------	------	----	------	87-151	45	1.7	**76**
T 1	64e	14-18	79	1.3	**100**	-------	------	----	------	-------	------	----	------
2	63e	14-18.3	144	1.3	**190**	-------	------	----	------	-------	------	----	------
3	65e	14-18.3	118	1.3	**150**	-------	------	----	------	-------	------	----	------
4	65e	14-18	131	1.3	**170**	-------	------	----	------	-------	------	----	------
5	60e	14-18	102	1.3	**130**	-------	------	----	------	-------	------	----	------
6	56e	14-18	93	1.3	**120**	-------	------	----	------	-------	------	----	------
7	54e	14-18.3	77	1.3	**100**	-------	------	----	------	-------	------	----	------
8	43e	14-18.3	59	1.3	**77**	-------	------	----	------	-------	------	----	------
9	44e	14-18	62	1.1	**68**	-------	------	----	------	-------	------	----	------
10	47e	14-18.4	102	1.1	**110**	-------	------	----	------	-------	------	----	------
11	40e	14-18	138	1.2	**170**	-------	------	----	------	-------	------	----	------
12	37e	14-17.8	207	1.2	**250**	-------	------	----	------	-------	------	----	------
13	55e	14-18	246	1.3	**320**	-------	------	----	------	-------	------	----	------
14	215e	14-18	100	1.2	**120**	-------	------	----	------	-------	------	----	------

TABLE A4. Temperature gradient, thermal conductivity, and conductive heat flow in test wells--**continued**

Test-well site	Depth to saturated zone (m)	Depth interval (m)	Temperature gradient °C/km	Thermal conductivity (W/m.K)	**q1 Heat flow (mW/m^2)**	Depth interval (m)	Temperature gradient °C/km	Thermal conductivity (W/m.K)	**q2 Heat flow (mW/m^2)**	Depth interval (m)	Temperature gradient °C/km	Thermal conductivity (W/m.K)	**q3 Heat flow (mW/m^2)**
15	51e	14-18	106	1.2	**130**	-------	------	----	------	-------	------	----	------
16	57e	14-15.5	115	1.1	**130**	-------	------	----	------	-------	------	----	------
17	47e	14-18	106	1.2	**130**	-------	------	----	------	-------	------	----	------
18	41e	14-18	188	1.2	**230**	-------	------	----	------	-------	------	----	------
19	48e	14-18	122	1.2	**150**	-------	------	----	------	-------	------	----	------
T 20	36e	14-18	171	1.1	**190**	-------	------	----	------	-------	------	----	------
21	51e	14-18	234	1.3	**300**	-------	------	----	------	-------	------	----	------
22	29e	14-14.9	97	1.1	**110**	-------	------	----	------	-------	------	----	------
23	28e	14-18	61	1.3	**79**	-------	------	----	------	-------	------	----	------
24	42e	14-18	68	1.3	**88**	-------	------	----	------	-------	------	----	------
25	61e	14-18.3	56	1.2	**67**	-------	------	----	------	-------	------	----	------
26	61e	14-18.3	77	1.3	**100**	-------	------	----	------	-------	------	----	------
27	33e	14-16.8	102	1.2	**120**	-------	------	----	------	-------	------	----	------
28	30e	14-18	126	1.0	**130**	-------	------	----	------	-------	------	----	------
29	-----	14-18	118	1.0	**120**	-------	------	----	------	-------	------	----	------
30	-----	14-18.3	100	1.0	**100**	-------	------	----	------	-------	------	----	------
31	21e	14-18.2	104	1.0	**100**	-------	------	----	------	-------	------	----	------
G 2	25e	--------	------	----	------	30-50	66.3	1.77	**119**	110-150	80.7	1.67	**135**
3	-----	--------	------	----	------	30-60	52	1.57	**82**	100-150	59	1.67	**93**
4	24e	--------	------	----	------	30-70	52.5	1.74	**91**	70-150	66.2	1.72	**114**
5a	-----	--------	------	----	------	30-80	142.2	1.93	**274**	80-150	111.0	1.86	**206**
7	-----	--------	------	----	------	40-70	3.6	2.07	**7.5**	70-85	37	1.39	**52**

TABLE A4. Temperature gradient, thermal conductivity, and conductive heat flow in test wells--**continued**

Test-well site	Depth to saturated zone (m)	Depth interval (m)	Temperature gradient °C/km	Thermal conductivity (W/m.K)	**q1 Heat flow (mW/m^2)**	Depth interval (m)	Temperature gradient °C/km	Thermal conductivity (W/m.K)	**q2 Heat flow (mW/m^2)**	Depth interval (m)	Temperature gradient °C/km	Thermal conductivity (W/m.K)	**q3 Heat flow (mW/m^2)**
8	38e	--------	------	----	------	60-90	40	1.63	**65**	90-150	42	1.63	**69**
9	40e	--------	------	----	------	45-52	43	1.76	**76**	100-120	0	----	**0**
10	30e	--------	------	----	------	35-45	60	1.86	**112**	100-150	49	1.86	**91**
11	43e	--------	------	----	------	45-58	3.8	1.95	**7.4**	105-150	46.8	1.77	**83**
12	13e	--------	------	----	------	45-100	102.3	1.55	**159**	100-150	116.7	1.62	**189**
13	-----	--------	------	----	------	30-52	57	1.78	**101**	100-145	74.4	1.76	**131**
14	-----	--------	------	----	------	30-60	25.7	1.82	**47**	60-150	54.3	1.47	**80**
15	-----	--------	------	----	------	30-54	38	1.83	**70**	100-150	40	1.83	**73**
105	21e	--------	-------	----	------	20-50	290	1.4	**410**	100-150	264	1.4	**370**
106	43e	--------	-------	----	------	50-100	28	1.5	**42**	100-150	22	1.55	**34**
108	41e	-------	-------	----	------	50-120	114	1.7	**194**	120-150	100	1.7	**170**
Aminoil USA 11-36	26e	--------	------	----	------	-------	------	----	------	1530-1650	40	2.0	**80**